Title

Dynamic IR Peak Coalescence and Ultrafast Chemical Exchange Reactions Studied by Two Dimensional Infrared Spectroscopy

Author

Zoerb, Matthew Cody

Publication Date

2012

Peer reviewed|Thesis/dissertation

Dynamic IR Peak Coalescence and Ultrafast Chemical Exchange Reactions Studied by Two Dimensional Infrared Spectroscopy

By

Matthew Cody Zoerb

A dissertation submitted in partial satisfaction of the

requirements for the degree of

Doctor of Philosophy

in

Chemistry

in the

Graduate Division

of the

University of California, Berkeley

Committee in charge:

Professor Charles B. Harris, Chair
Professor Graham R. Fleming
Professor Robert W. Dibble

Fall 2012

Dynamic IR Peak Coalescence and Ultrafast Chemical Exchange Reactions Studied by Two Dimensional Infrared Spectroscopy

By

Matthew Cody Zoerb

Abstract

Dynamic IR Peak Coalescence and Ultrafast Chemical Exchange Reactions Studied by Two Dimensional Infrared Spectroscopy

By

Matthew Cody Zoerb

Doctor of Philosophy in Chemistry

University of California, Berkeley

Professor Charles B. Harris, Chair

Vibrational spectroscopy is one of the most powerful techniques in chemistry due to its ability to report direct information on the geometries and nuclear motions of complex molecules. At thermal equilibrium, rearrangements between different, or equivalent, molecular structures help to define the reactivity of the system. On the ultrafast timescale, these chemical exchange reactions may cause features in the vibrational spectrum to become averaged. The Bloch equations have been used previously to quantitatively predict the rates of such reactions. This approach has been quite successful in NMR spectroscopy where exchange on the microsecond timescale is often sufficient to cause peak coalescence. The application of the Bloch equations to IR spectroscopy has been debated due to the presence of other contributions to the vibrational lineshape that may prevent an accurate description of the relevant dynamics. Two dimensional infrared spectroscopy (2D-IR) is a time resolved ultrafast technique that is capable of directly measuring the kinetics of chemical exchange at thermal equilibrium where there is no net change in the populations of reactants and products. This work examines two model systems that display dynamic IR peak coalescence. A group of mixed valence dimers of trinuclear ruthenium clusters have exhibited a wide range of IR coalescence that is sensitive to solvent, temperature, and ligand substitution. No electron exchange was observed by 2D-IR during the timescale required for peak coalescence. The two isomers of a square pyramidal ruthenium dithiolene compound also result in highly coalesced spectra. The equilibrium populations, as well as the extent of peak coalescence, are strongly dependent on temperature and solvent. The experimental results of this second project were largely inconconclusive; however, future work with density functional theory calculations looks promising for revealing more information on these dynamics. Ultimately, the application of the Bloch equations to IR spectra is not generally reliable. While this type of analysis may still yield accurate results in some special cases, it is very difficult to distinguish legitimate exchange induced coalescence from similar broadened lineshape features, and this approach should be avoided.

To my friend,
Bill the Cat

Contents

Acknowledgements iv

1 Introduction 1

1.1 Two Dimensional Infrared Spectrocopy 3

2 Methods 7

2.1 Two Dimensional Infrared Spectrocopy 7
2.2 Density Functional Theory 10

3 Simulation of Dynamic IR Lineshapes 11

3.1 Introduction 11
3.2 Dynamic IR Spectroscopy 12
3.2.1 Generalization to Larger Systems 14

4 Electron Dynamics in Mixed Valence Ruthenium Dimers 16

4.1 Introduction 16
4.2 Previous IR Spectral Analysis 17
4.3 Two Dimensional Infrared Spectroscopy Results 19
4.3.1 Sample Preparation 20
4.4 Density Functional Theory Results 45
4.5 Discussion 57
4.5.1 Lack of Cross Peaks 59
4.5.2 On the Origin of Biexponential Kinetics 60
4.5.3 Possible Sources of Peak Coalescence 62
4.5.4 Argument Against Exchange Intensity 64
4.6 Conclusions 65

5 Ground State Isomerization of $Ru(S_2(CCF_3)_2)(PPh_3)_2CO$ 67

5.1 Introduction 67
5.2 Isomerization Mechanism 68
5.3 Two Dimensional Infrared Spectroscopy Results 69
5.4 Density Functional Theory Results 72
5.5 Discussion and Conclusions 72

6 Conclusions 74

References 76

Appendix A: DFT Geometry Optimization Results: Cartesian Coordinates 83

Appendix B: Matlab Programs: Source Code 104

Acknowledgements

Graduate school has been quite the adventure. I am left indebted to many people who have helped me along the way. My advisor, Charles Harris, has always been very supportive and patient. I will miss the freedom he allows, and encourages, in his group. Vijaya Narasimhan was the group's administrative assistant for my first several years at Berkeley. Things always ran a little more smoothly when she was around. This work was supported primarily by the National Science Foundation. Some specialized equipment was made available by the U.S. Department of Energy, Office of Basic Energy Science, Chemical Sciences Division under contract DE-AC02-05CH11231. I also acknowledge the National Energy Research Scientific Computing Center and the UC Berkeley Molecular Graphics and Computation Facility for computational resources.

My fellow graduate students have been a source of knowledge, support, and inspiration over the last several years. Many of them have become great friends. When I joined the liquid side of the Harris group, James Cahoon and Karma Sawyer quickly took me under their wings. I could always count on James to get coffee and share his insight. I don't think Karma ever got over the time I wore a plastic bag around lab. Jacob Schlegel was also there from the beginning and never ceases to amaze me with all of his random knowledge. He can make a pretty mean cocktail, too. I only overlapped with Libby Glascoe for a couple months, but I will always remember her as the type of colleague that will share her instant oatmeal after you've stayed up all night doing quantum problems. Several younger students have come along since I've been here. Son Nguyen, Justin Lomont, and Adam Hill have helped to define my graduate school experience. Son's knowledge of Vietnamese drinking games was always good for some fun. Justin's skills at cartography have perplexed us all.

On the surface side, Aram Yang, Matt Strader, and James Johns also welcomed me into the lab as a first year. Their high expectations were always a motivation. Ben Caplins could stand to chew his vegetables a little bit more. David Suich has impressed me by being one of the few people I've known in California that is perhaps more Southern than I am. I can always count on Alex Shearer to sing some Alan Jackson songs with me. Finally, I'd like to thank Eric Muller, my work spouse. Eric and I joined the Harris lab at the same time and shared many of the trials and tribulations of graduate school. I will really miss being across the hall from that guy.

Above the D-Level, Luke Valin and Phil Kalisman always kept life exciting. My collaborators at UCSD, Starla Glover and Jane Henderson, were fun temporary additions to the group. Sarah Hanson and Sylvi Cohn were pleasant reminders that there is life outside of the chemistry department.

I would also like to thank the San Francisco Mandolin Orchestra for encouraging me to pursue interests outside of graduate school. Achille Bocus was a wonderful mandolin instructor; I learned a lot from him. As the head of the SFMO, I was impressed with how Nicola Bocus kept things running smoothly from season to season. All of the others in the group made rehearsals and concerts a fun weekend distraction from the stresses of grad school.

It took several people to get me here in the first place. My family deserves a great deal of gratitude. Without my parents' love and support, I never would have made it all the way to 24th grade. Steve Symes, my undergraduate advisor, remains one of my close friends. He is responsible for getting me involved in research and inspiring me to follow his footsteps in academia. Furthermore, he was pretty instrumental in my decision to switch to acoustic music and pick up the mandolin. Moth Henderson, Michael Hart, and Steve Pitts also deserve some credit for helping me get through my days before Berkeley.

Last and most importantly, I’d like to thank my fiancé, Genevieve Lidoff. She is the strongest, most dedicated, and most determined person I know. Her joy is contagious, and it is hard not to have fun around her. She makes every day a little better. I would never have made it without her.

Chapter 1

Introduction

Stated most simply, physical chemistry is the study of how molecules work. Ultrafast laser spectroscopy has revolutionized the ways through which we access the molecular level details of chemical reactions. Not all chemical reactions proceed in the femto- to picosecond timescale, but many of the fundamental transformations leading to this reactivity involve ultrafast changes in the electronic and nuclear coordinates. In the condensed phase, structural changes, solvent fluctuations, and charge redistribution on the ultrafast timescale define how molecules interact with one another and ultimately form chemical products.

Vibrational spectroscopy is one of the most powerful techniques in chemistry. Molecular vibrations give us direct information on the nuclear coordinates of the system. Time-resolved vibrational spectroscopy allows us to monitor these structural details as they change over time. At thermal equilibrium, molecules are far from static. Intramolecular rearrangements and intermolecular interactions dynamically alter their properties and determine the behavior of the molecule. These equilibrium dynamics are the focus of this work.

Progress in physical chemistry is driven both by the desire to understand basic chemical phenomena and the technological advances necessary to make new types of observations. I have followed this reasoning by pursuing experiments designed to elucidate the fundamental physics and chemistry of several metal complexes that exhibit IR spectral coalescence. Using ultrafast two dimensional infrared spectroscopy (2D-IR) and density functional theory calculations (DFT), I have studied the dynamics of charge redistribution and structural exchange in several ruthenium compounds. These experiments also allow me to address the origin and interpretation of peak coalescence in vibrational spectroscopy.

Peak coalescence is a phenomenon in which two or more spectral features become averaged as a result of exchange. To cause peak coalescence, the exchange dynamics must occur at a rate similar to the frequency splitting between the spectral features. Peak coalescence is fairly common in NMR spectroscopy where peak splittings are in the hertz to megahertz range. Dynamics on the order of seconds to microseconds may cause coalescence.[1-4] It is much less common in vibrational spectroscopy where peak splittings in the terahertz range require picosecond dynamics to affect the spectra. In this way, any steady state spectroscopic measurement has an inherent element of time resolution.

The prototypical example of peak coalescence is the spectra of iron pentacarbonyl. Iron pentacarbonyl is fluxional, meaning it is constantly exchanging between equivalent structures. The carbonyl ligands are exchanged via the Berry pseudorotation mechanism in ca. 8 ps.[5] The IR spectrum of iron pentacarbonyl has two carbonyl stretches, one for the axial CO based normal mode and one for the degenerate equatorial CO based normal modes. The ^{13}C NMR spectra of iron pentacarbonyl have only one peak; the five carbonyl ligands exchange much too quickly to be resolved by this “slower” technique.[6,7]

In many cases, the degree of peak coalescence can be varied, typically by changes in sample temperature. The Bloch equations provide a mathematical formalism to describe the spectral features associated with exchange and facilitate quantitative predictions of the barrier height and timescales of the exchange reaction. This approach is relatively common in NMR, and many fluxional and isomerization reactions happen on the timescales associated with this technique.[1-4] IR peak coalescence is much less common due to the requirement that dynamics must be ultrafast to affect the spectrum. Further, the analysis of coalesced IR spectra with the Bloch equations has been debated because of the sensitivity of IR lineshapes to interfering dynamics.[8-21] The first goal of this work is to employ time-resolved IR spectroscopy to assess the ability of the Bloch equations to accurately determine quantitative kinetic information from coalesced IR spectra.

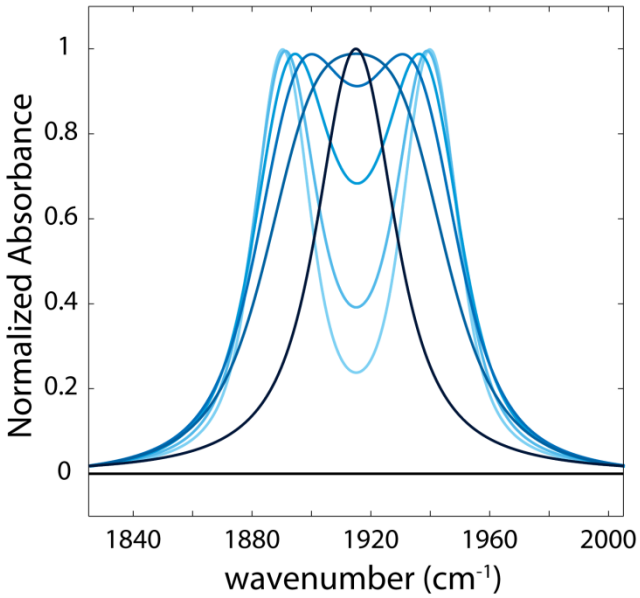

Figure 1.1: Simulated spectra with a peak separation of 50 cm^{-1} and exchange time constants 0.1-10 ps (dark to light).

Electron transfer is one of the most basic transformations in chemistry and is important to many fields including biology and materials science.[22-26] In particular, intramolecular electron transfer has received significant interest due to its relevance to molecular scale devices and their function.[27-29] Despite this interest, many details of charge transport through molecules are poorly understood. In cases of high electronic coupling, electron transfer between sites can be very rapid and the extent of charge distribution can be ambiguous. This border between localized and delocalized electronic behavior is the subject of many theoretical treatments.[30-34] This regime also presents some unique challenges experimentally. Near delocalization, electron transfer approaches the ultrafast timescale and can begin to alter vibrational lineshapes.

Bridged ruthenium dimers, such as the compound in Figure 1.2, have been studied extensively by the group of Clifford Kubiak at UC San Diego.[35-54] Upon reduction to the -1 mixed valence state, these compounds exhibit a wide variety of interesting behavior including highly tunable coalescence of the carbonyl vibration peaks. This peak coalescence was previously interpreted as a signature of ultrafast transfer of the extra electron between the two metal sites. Lineshape analysis with the Bloch equations yielded exchange time constants under

1 ps for several of the dimers. The broad tunability of peak coalescence in these systems offers a unique opportunity to test the ability of the Bloch equations to make accurate quantitative predictions of the mechanism and timescale of ground state exchange.

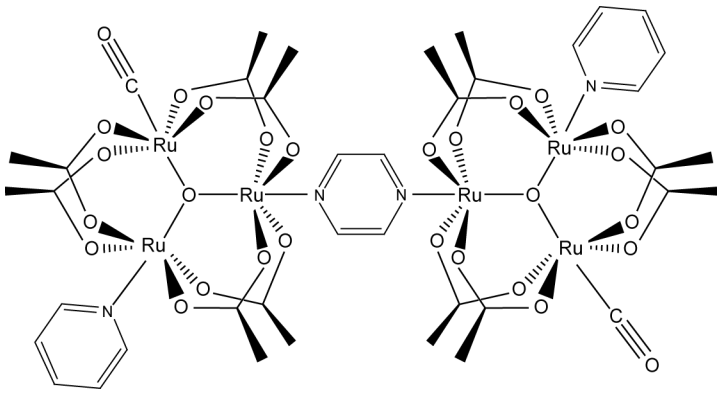

Figure 1.2: One example of the dimers of ruthenium trimers detailed in Chapter 4.

In collaboration with the Kubiak group, I have comprehensively studied the IR spectra and electronic behavior of the dimers of ruthenium trimers with 2D-IR and DFT calculations. Surprisingly, I measured *no site exchange* in any of the ruthenium dimers. The experimental window was limited by average vibrational relaxation times of ca. 12 ps in these systems. While I was not able to directly measure electron transfer in these systems, I can place a lower limit on the exchange rate. Any electron transfer likely takes place on a longer timescale than this relaxation time. The Bloch equations predict that exchange must be faster than ca. 10 ps to cause *any* change to the IR spectrum.[36] If no exchange takes place in the first 10 ps in these systems, peak coalescence must have some other origin. These experiments span the full range of timescales relevant to peak coalescence. Although I was unable to measure electron site exchange, I can directly address the viability of the Bloch equations for the analysis of coalesced IR lineshapes.

Also in collaboration with the Kubiak group, I have studied the isomerization of $Ru(S_2(CCF_3)_2)(PPh_3)_2CO$. The IR spectra of this compound are another example of dynamic IR peak coalescence. Unlike the electron transfer reactions, this is not a self-exchange reaction. The coalescence involves the CO peaks from two different isomers. An interesting feature of the isomerization reaction is that the degree of peak coalescence and relative isomer populations both vary with changes in solvent and temperature. Unfortunately, 2D-IR was unable to conclusively determine the isomerization rate. The peaks were either too highly coalesced to resolve the exchange or too weak to measure enough signal. The results of DFT calculations do, however, give some insight on possible mechanisms and timescales of isomerization. More theoretical work is needed to fully understand the dynamic equilibrium in these systems.

1.1 Two Dimensional Infrared Spectroscopy

Few techniques are capable of directly measuring dynamics at thermal equilibrium where there is no net change in populations and no formation of new products. Fluctuations in structure and electron distribution on the ultrafast timescale often have a large impact on reactivity, but the associated spectral features can appear averaged and may obscure important details about the

system properties. Two dimensional infrared spectroscopy (2D-IR) is a relatively new technique that is well suited to investigate such ultrafast ground state dynamics.

2D-IR is a nonlinear vibrational spectroscopy that combines ultrafast time resolution with the ability to measure the ground state interactions and transformations of molecular vibrations. There are two primary implementations of the technique. The full four-wave mixing Fourier transform approach involves sending three broadband mid-IR pulses to the sample and interfering the generated vibrational echo with another mid-IR pulse.[55-57] This approach offers temporal resolution only limited by the laser bandwidth, and full phase information is maintained by controlling each interaction of the electric field with the sample. Nearly equivalent information can be collected with the double resonance frequency domain technique used in this work.[58,59] This approach requires just two mid-IR beams in a pump-probe geometry. Only one beam time delay, rather than three, needs to be controlled. A spectrally narrow band pump pulse scans the frequency range of interest, selectively exciting the vibrations of the system. This is followed in time by a broadband probe pulse. This implementation has several advantages. The apparatus and alignment are simplified, and detailed kinetics traces can be taken quickly by holding the frequency of the pump pulse fixed and varying the time delay. These horizontal slices of the two dimensional spectrum are taken as simple pump-probe spectra. For the same kinetic information from the Fourier transform technique, one of the time delays must be scanned and Fourier transformed for each kinetic time point. The primary disadvantage to the frequency domain technique is that the spectrally narrow band pump pulse has a larger temporal width and the time resolution is reduced to approximately 1 ps. More recently, many of the advantages of both of these 2D-IR variants have been combined by the introduction of mid-IR pulse shapers.[60,61] These experiments combine the high time resolution and phase information of the Fourier transform technique with the fast data acquisition associated with the frequency domain technique.

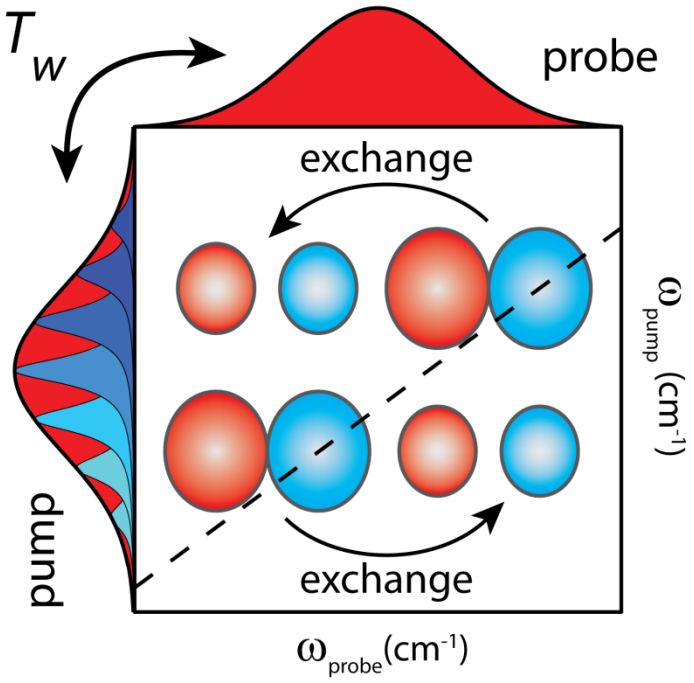

Figure 1.3: Schematic 2D-IR spectrum.

In frequency domain 2D-IR, a narrowband IR pump pulse creates a population in the first excited level of a vibration. This excitation can be thought of as a vibrational label. A second pulse follows after a variable delay time and monitors the evolution of the vibrational label. This is shown schematically in Figure 1.3. The pump pulse is generated by passing a broadband mid-IR pulse through a Fabry-Perot interferometer. This is an optical cavity with two highly reflective end mirrors placed very close to one another. The mirror spacing determines what wavelengths are transmitted and can be varied to change the frequency of the narrow band pulse and scan across the frequency range of interest. The spectrum is collected as a difference spectrum; only the spectral changes associated with the introduction of the pump pulse are displayed in the spectrum. Features in the spectrum are usually present as peak pairs. The blue peaks are negative and represent the depletion of vibrations in the v=0 state. Since the pump pulse creates a population in the v=1 state, transitions from v=1→ v=2 are al so accessible and appear as the positive red peaks. These peaks are shifted to lower frequency due to the anharmonicity of the vibrational potential. If no dynamics affect the vibrational label, the frequency will not change during the time delay and the frequency will be the same along both axes, resulting in a diagonal peak. Along the diagonal, these peaks give analogous information to linear absorption spectra. In exchanging systems, the environment around the labeled vibration may change, causing a frequency shift. As the waiting time increases, this will result in a decrease in peak amplitude along the diagonal with new peaks growing in the off diagonal region. These cross peaks are shifted along the horizontal, allowing them to be correlated to the original excitation frequency. The rate of cross peak growth and diagonal peak decay correspond to the rate of equilibrium exchange.

The major limitation to this technique is that the dynamics of interest must occur faster than, or on a similar timescale to, vibrational energy relaxation (VER). VER will eventually cause any solution phase vibrational excitation to decay by energy transfer to the surrounding bath. The vibrational label must persist for long enough to observe the dynamics. For organometallics, VER can be anywhere from a few picoseconds to hundreds of picoseconds. Other vibrational dynamics can also interfere with the 2D-IR measurement. For example, intramolecular vibrational redistribution (IVR) can cause the energy of the vibrational label to be redistributed among other vibrations in the absence of exchange. This can even include uphill energy flow by coupling to the solvent.

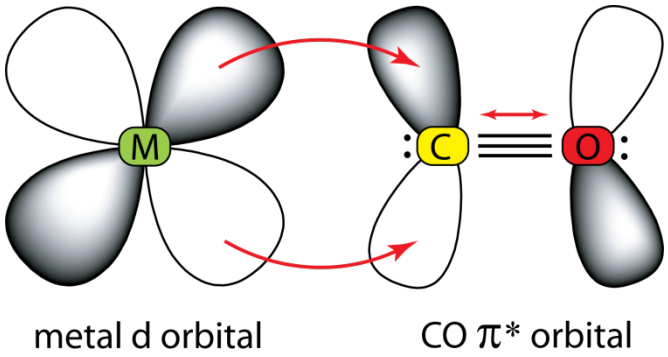

Figure 1.4: π backbonding from a metal d orbital to a carbonyl ligand.

Metal carbonyls are excellent probes of dynamics in infrared spectroscopy. Conveniently, they typically exhibit sharper and stronger peaks than most other vibrations. Perhaps more important is their interaction with the metal d orbitals (Figure 1.4). In organometallic

compounds, the frontier molecular orbitals are usually based primarily in the metal atom based d orbitals. Carbonyl ligands donate density to the metal through a σ interaction, but withdraw density through π interactions known as π backbonding.[62] Changes in geometry or electron distribution can have significant effects on the orbital overlap and density. The π backbonding occurs between the d orbitals of the metal and a π* orbital of the CO ligand. Small changes in the population of this orbital directly affect the strength of the CO bond and, therefore, the frequency of the vibration. This sensitivity to changes in the environment at the metal center make CO ligands uniquely suited as probes of both electron distribution and geometry in vibrational spectroscopy.

Chapter 2

Methods

2.1 Two Dimensional Infrared Spectroscopy

The apparatus used for these experiments is capable of a variety of ultrafast vibrational spectroscopic techniques. It is convertible between UV pump-IR probe transient spectroscopy, broadband IR pump-IR probe spectroscopy, two dimensional infrared spectroscopy (2D-IR), two-color 2D-IR, and transient 2D-IR setups. The experiments in this thesis all use the two-color 2D-IR setup tuned to one color for reasons mentioned below.

The apparatus begins with a commercial laser system from Spectra-Physics comprising four separate lasers. The first is a diode pumped Nd:YVO_4 continuous wave laser (*Millennia Vs J*) with an output of 5W at 532 nm. This laser pumps the ultrafast Ti:Sapphire oscillator (*Tsunami*) whose pulsed output at 800 nm, 80 MHz, and average power ~650 mW seeds the regenerative amplifier. The amplifier is pumped by a 527 nm Q-switched Nd:YLF pump laser (*Empower*) with a maximum average power of 10 W at 1 kHz. The Ti:Sapphire regenerative amplifier (*Spitfire*) produces ultrafast pulses at 800 nm, 1 kHz, and average power ~1.2 W. After the amplifer, the rest of the apparatus is home built.

The output of the amplifier is split by a 50/50 800 nm beam splitter into two mid-IR optical parametric amplifiers (OPAs). The OPAs are tunable from 3-6 μm with a FWHM of ca. 150 cm^{-1}. The general design has been reported previously in the theses of multiple graduate students[63,64] and is based on the design of Hamm[65]. I personally built the second OPA as a duplicate of the first. The two OPAs are nearly identical and need no comment beyond the previous descriptions. The two-color 2D-IR setup with both OPAs, however, requires some noteworthy modifications. The modified apparatus is depicted schematically in Figure 2.1 and the major optics and equipment are listed in Table 2.1. Some of the optics have been in place for many years and the manufacturer is unknown. These optics are fairly generic and can be purchased from many suppliers. The wedged window (WW) has recently been replaced by a series of two beamsplitters. The original wedged window reflected ca. 15% from both the front and back surfaces to separate the probe and reference lines. The remaining ca. 70% was transmitted to the pump line. The new pair of optics consists of an 85/15 beamsplitter (BS1) to split the pump/(probe and reference) followed by a 50/50 beamsplitter (BS2) to split probe/reference. BS1 and BS2 are not pictured in Figure 2.1.

The output of the pump OPA first passes through a Fabry-Perot interferometer. Since it was originally reported,[66] I replaced the mirrors with higher quality optics that have 85 ± 3% reflectivity. The old mirrors worked over the full spectral range of the OPAs, but varied significantly from the average 85% reflectivity. The new mirrors are designed for use over a narrower frequency range, requiring multiple sets to span the full output range of the OPAs. For the work described here, the operating range was 5.0-5.6 μm or approximately 1786-2000 cm^{-1}.

Compared to the old Fabry-Perot mirrors, the reflectivity is significantly higher over much of the spectral range.

Multiple modes are supported in any resonator. There is a relationship between the output peak width and the separation between adjacent modes. The ratio of peak separation to peak width is called the finesse of the cavity. Increasing the mirror reflectivity increases the finesse of the cavity by the following relationship[67]:

$$\mathcal{F} = \frac{\Delta\lambda}{\delta\lambda} = \frac{\pi R^{1/2}}{1-R} \tag{2.1}$$

where R is the mirror reflectivity, and is wavelength dependent. The peak separation is $\Delta\lambda$ and the peak width is $\delta\lambda$. The overall spectral bandwidth of the input mid-IR beam is ca. 150 cm^{-1}. I usually kept the pump pulse spectral width at 12-15 cm^{-1}. For a cavity with low finesse, multiple narrowband peaks can be supported for 12-15 cm^{-1} peak widths over a 150 cm^{-1} range. This is undesirable since we want a single narrowband pump pulse at the sample to excite a single vibration. Multiple pump frequencies can cause multiple vibrations to be pumped accidentally and ruin the specificity of the vibrational label. Maintaining high mirror reflectivity reduces the chance of unwanted pump intensity at the wrong frequency. In practice, with the new mirrors, I rarely saw multiple peaks supported within the 150 cm^{-1} spectral envelope of the pump OPA.

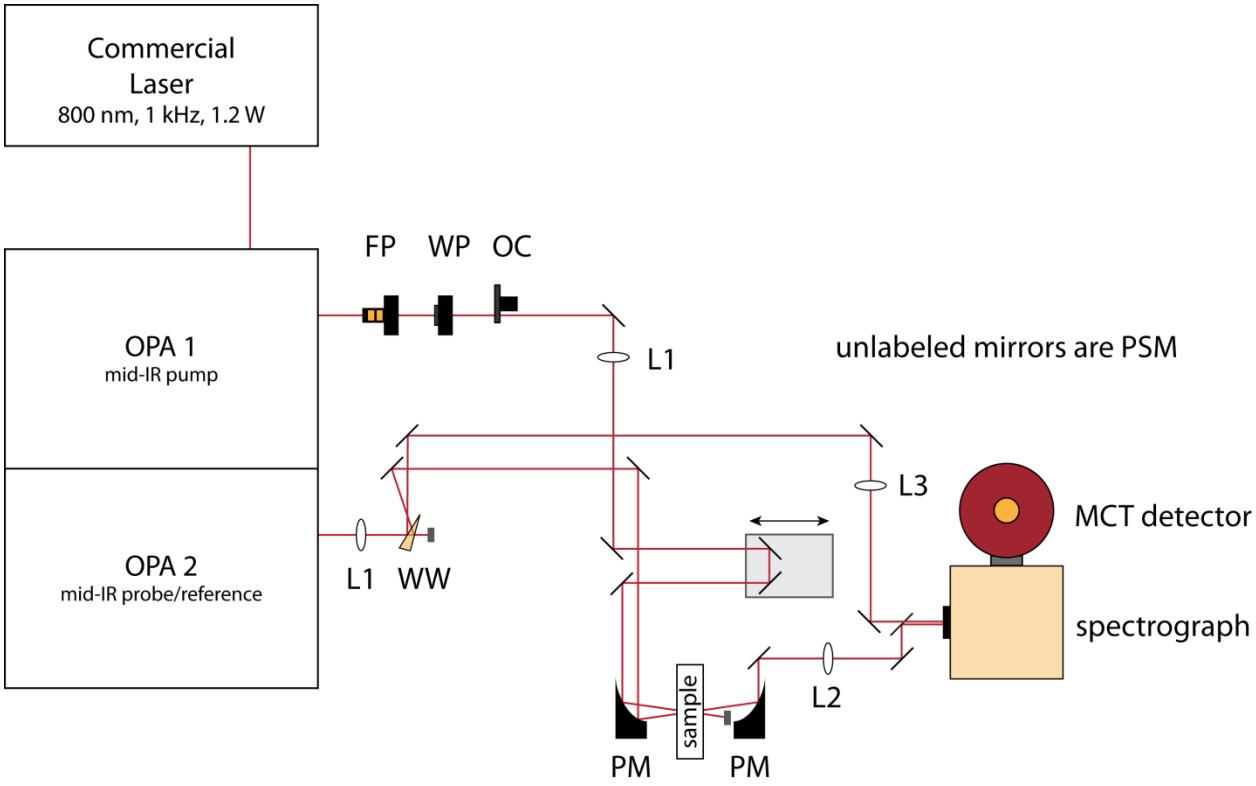

Figure 2.1: Schematic of the two OPA 2D-IR apparatus. The equipment and optics labels are described in Table 2.1.

Before reaching the sample, the narrow band pump pulse also passes through a half wave plate and an optical chopper. The wave plate allows me to change the polarization of the pump pulse relative to the probe pulse. For all of the experiments reported here, I held the two beams at magic angle, 54.7°, relative to one another to remove the effects of orientational diffusion. The optical chopper runs at a frequency of 500 Hz, half of the repetition rate of the laser system. This blocks every other pump pulse from hitting the sample. A difference spectrum can be collected by subtracting spectra of (pump on) – (pump off), allowing me to take a data point with 1000 averages every 2 seconds. The time delay between the two pulses is controlled by passing the pump pulse through a mechanical delay stage. The stage changes the time delay between the two pulses by changing the distance that the pump pulse travels relative to the probe beam path. Finally, the pump and probe pulses are focused onto the sample with an off-axis parabolic mirror. Parallel beams impinging on a parabolic mirror will have the same focal point. During beam alignment, I only need to assure that the two beams are parallel entering the first parabolic mirror. The probe pulse passes through no moving parts so that proper alignment into the detector is maintained.

Label	Description	Source
PM	Off-Axis Parbolic mirror, Protected Gold Coating, FL = 10 cm	Janos Technology
PSM	Protected Silver Mirror	Thorlabs Inc.
WW	ZnSe Wedge Window, 1° wedge, uncoated	Rocky Mountain Instrument Co.
BS1	85/15 Beamsplitter, 3-7 μm, ZnSe, 3° wedge	Rocky Mountain Instrument Co.
BS2	50/50 Beamsplitter, 3-7 μm, CaF_2	Infrared Optical Products, Inc.
OC	Optical Chopper, Model 3501	New Focus
FP	Fabry-Perot Interferometer	-
	Piezoelectric Kinematic Mount, P/N KC1-T-PZ	Thorlabs Inc.
	ZnSe Mirror, $R_{avg} = 85 \pm 3\%$ @ 5.0 -5.6 um	Rocky Mountain Instrument Co.
WP	Waveplate	-
	Motorized Rotation Stage, Model RGV100	Newport Corp.
	Dual Element (CdS/CdSe) Waveplate, 180° retardance, 4.5-6.0 μm	Cleveland Crystals
L1	CaF_2 Lens, FL = 100 cm	unknown
L2	CaF_2 Lens, FL = 15 cm	unknown
L3	CaF_2 Lens, FL = 30 cm	unknown

Table 2.1: Description of optics and equipment from Figure 2.1.

The probe and reference beams are focused into a spectrograph (*Acton Research Corp., SpectraPro-150*) where the beams are dispersed by a tunable grating onto a 2x32 pixel mercury cadmium telluride detector (*Infrared Associates, Inc., MCT-7-64*). The raw signals are passed through a data processing unit (*Infrared Systems Development Corp., IR-6416*) before being transferred to our data collection computer. The data collection program (LabView) and data processing programs (Matlab) were written in house by previous graduate students and have only had small modifications since their previous description.[66]

The primary advantage of the 2 OPA setup is that it is capable of collecting two-color 2D-IR spectra. The two OPAs can be tuned independently to different spectral regions. A secondary benefit is that each OPA in the 2 OPA setup has a *higher* output power with *lower* input power relative to the normal 1 OPA setup. The usual 1 OPA setup includes separate line for the UV generation. The amplifier output is split 30/70 between UV and IR, respectively, by an 800 nm beamsplitter. For the 2 OPA setup, the UV/IR beamsplitter is removed, and the amplifier output is split into the two OPAs. As a result, each OPA only gets 50% of the amplifier output instead of 70% in the 1 OPA setup. The 1 OPA setup usually requires filters in both the first and second pass pump lines to avoid optical damage to the BBO crystal. With the lower input power of the 2 OPA setup, these filters can be removed. Removing the filters should compensate somewhat for the lower OPA input power. Perhaps the lower power allows us to focus harder into the BBO crystal and have higher conversion efficiency. While we do not currently have a mid-IR power meter that can detect our OPA output, the signal at the detector appears approximately 2-3x greater in the 2 OPA configuration. Although the mid-IR power increase in the 2 OPA configuration is rather modest, it has made a significant impact on my ability to take high quality data. In particular, I could not get the signal high enough above the noise for any of the samples in Chapter 4 with the 1 OPA setup.

2.2 Density Functional Theory

All of the density functional theory (DFT) calculations in this work were performed in Gaussian 09 with the BP86 functional.[68-70] Unrestricted BP86 was used for calculations on all -1 charged compounds. BP86 is a generalized gradient approximation (GGA) functional and is considered one of the best functionals for transition metal and transition metal carbonyl complexes. It has been shown to outperform the widely popular hybrid functional B3LYP.[71,72] Another functional TPSS, a meta-GGA functional, has been shown slightly more accurate than BP86 with a similar price to performance ratio.[71,72] The transition metal complexes in this work are very large, and meeting the standard convergence criteria was difficult for most of the geometry optimizations. I attempted several calculations with TPSS, but the calculations did not converge.

For the metal atoms (ruthenium) in all of the compounds in this work, I used the LANL2DZ basis.[73-76] This basis set uses an effective core potential (ECP) that reduces the number of electrons in the calculations by replacing the core electrons with an effective potential. The basis sets on all other atoms depend on the system. For the compounds in Chapter 4, I used 6-31G. For the compounds in Chapter 5, I used 6-31G++(d,p) for all calculations.[77-86]

Chapter 3

Simulation of Dynamic IR Lineshapes

3.1 Introduction

A primary focus of this thesis is the phenomenon of dynamic infrared peak coalescence. Two of the most well documented cases of IR peak coalescence are the mixed valence dimers also featured in this work (Chapter 4)[35-54] and the class $Fe(CO)_3(\eta^4$-diene) compounds[16-21]. For both sets of compounds, analysis of the IR lineshapes was performed by comparison of the experimental spectra with simulations based on the Bloch equations. The program used for these projects previously, VIBEXGL, was written by R.E.D. McClung, a coauthor on one of the iron diene tricarbonyl papers.[20] While McClung did not share authorship on any papers involving the mixed valence dimers, he did provide a version of his program to the Kubiak lab for their lineshape analysis.

The VIBEXGL program was written in FORTRAN and compiled for use on a Macintosh computer. The program was written before Mac switched to a Linux based operating system for their OS X in 2002. To run the program on a modern computer requires the user to emulate an older Mac operating system or to simply use a 10+ year old computer. The paper by Grevels et al.[20] describes most of the math involved in the simulations, but I had several questions about the implementation of the math in the program. Some of the math is system dependent and since the program was not originally written for, or described in the context of, the ruthenium dimers, I wanted to know specifically how the code was written for the dimers. McClung is no longer an active professor, and I could not contact him to ask specific questions about the code. As a coding language, FORTRAN is difficult to read, and I was unable to answer my questions based on the source code.

To better understand these simulations, I wrote a new and improved version of the program in Matlab. The new program, Zoerbex, is based on the same optical Bloch equations math as the previous program and can produce identical outputs to VIBEXGL, although my program has some noteworthy improvements. First, Zoerbex can be run on any modern computer with Matlab installed. Three versions of the standard Zoerbex program are available and have been published in the Journal of Chemical Education as a technical report. One version is a standard Matlab script and can be run from the command line in Matlab. Two other versions run from a graphical user interface (GUI); one within Matlab and the other as an executable standalone file. The executable file version of the program can be run on any PC, even without Matlab, by installing a free file library. All three versions of the program are available in the Supporting Information to reference 87. The source code for both Matlab versions is given in

Appendix B of this thesis. The Matlab environment also allowed me to add some simple figure options, such as figure zoom, into Zoerbex program, and the user can save the simulated spectra as a Matlab figure file and further edit the figure properties within Matlab. Another large improvement is the free availability of the source code. Mathematical code in Matlab is very easy to read and understand. Small modifications to the existing code enable the user to simulate dynamic IR lineshapes for a variety of systems. By default the program simulates two peaks, but can be easily modified to simulate as many peaks as the user cares to include.

3.2 Dynamic IR Spectroscopy

Peak coalescence is much more common in NMR than in IR spectroscopy. The requirement that exchange in IR spectra be on the picosecond timescale restricts the phenomenon to the observation of only the fastest rearrangements. Further, the ability to extract quantitative information from coalesced IR spectra is limited by the presence of other ultrafast processes that can alter line shapes and peak frequencies. I do expect that the Bloch equations can accurately describe the spectral effects due to a known exchange rate; however, separating these effects from other contributions to an experimental spectrum is not generally possible. Simulations made with the program are useful for better understanding the spectral changes accompanying ultrafast site exchange and seeing the qualitative features associated with different mechanisms and rates of exchange.

The dynamic IR lineshapes in this program are simulated using the optical Bloch equations formalism to describe exchange between two sites. This math is closely based on the presentation by Grevels et al.[20] with some notable differences. I will present a brief summary of the math here. We follow the naming conventions from the previous paper as closely as possible to allow for easy comparison.

Voigt lineshapes are used to simulate the IR peaks in each spectrum. These lineshapes are separated into Lorentzian and Gaussian components. The full width at half maximum (FWHM) values for each contribution to the individual peaks as well as their center frequencies and relative populations are input parameters to the simulation.

The other inputs to the program determine the exchange rate of the simulation. The user has two input options, the exchange time constant (k_{ex}^{-1}) or a reaction barrier height and temperature. The barrier height and temperature are converted to a rate using simple transition state theory[88]:

$$k_{ex} = \frac{k_B T}{h} \exp\left(-\frac{\Delta G^{\ddagger}}{k_B T}\right) \tag{3.1}$$

where k_B is Boltzmann's constant, h is Planck's constant, $\Delta G^{\ddagger}$ is equivalent to the transition state or barrier height (assuming the partition functions of the reactants and transition state are approximately equal), and T is temperature. To simulate a spectrum without exchange effects, the user can specify a large time consant (e.g 10,000 ps), high barrier (e.g. 5 kcal/mol), or a low temperature (e.g. 5 K). Exchange under these conditions is sufficiently slow so as to make no contribution to the vibrational lineshape.

The effects of exchange on the system are contained in the exchange matrix **K**. The form of this square matrix is entirely system dependent. The order of the matrix is equivalent to the

number of exchanging sites. The simplest example (and program default) is that of a two site system exchanging with equivalent forward and backward reaction rates as in Reaction 3.1.

Reaction 3.1

$$A \underset{}{\overset{k_{ex}}{\rightleftharpoons}} B$$

Grevels et al. offers a detailed account on dipole moment transfer and the details required to determine the general form of this exchange matrix.[20] Here, we take a much simpler approach and consider only the case of unit dipole moment transfer. Two equal intensity vibrational modes of a molecule exchange 100% of their intensity with a rate, k_{ex}. The resulting matrix is:

$$\mathbf{K} = k_{ex}\begin{bmatrix} -1 & 1 \\ 1 & -1 \end{bmatrix} \tag{3.2}$$

Any number of peaks can be simulated by increasing the matrix dimensions..

For each peak, α, the matrix **A** contains the information on peak center frequencies (ω_α) and Lorentzian FWHM ($\Gamma_\alpha^{(L)}$). The diagonal entries are:

$$A_{\alpha\alpha} = -i\omega_\alpha + \Gamma_\alpha^{(L)} - \mathrm{K}_{\alpha\alpha} \tag{3.3}$$

And the off diagonal entries are:

$$A_{\alpha\alpha'} = -K_{\alpha\alpha'} \tag{3.4}$$

The matrix **G** is diagonal and contains the information on Gaussian contributions to the peak width, ($\Gamma_\alpha^{(G)}$). It is noteworthy that the Grevels paper incorrectly defines this matrix; the proper form is:

$$G_{\alpha\alpha} = [\Gamma_\alpha^{(G)}]^2 \tag{3.5}$$

The program is designed to simulate the lineshapes of dynamically exchanging species. This is best achieved by directly altering the time domain signal. Here, we directly calculate the vibrational time correlation function. This signal can be Fourier transformed to the frequency domain with the fast Fourier transform (fft) method. While the correlation function is not output by default, the program can be easily modified to plot the result. The program provides an opportunity to compare signals from the two domains and better understand the relationship between Fourier transform pairs.

The **A** and **G** matrices enter the correlation functions as **Λ** and **G'**. The matrix **A** is first solved for its eigenvalues and eigenvectors.

$$\mathbf{AS} = \mathbf{\Lambda S} \tag{3.6}$$

where **Λ** is a diagonal matrix of the eigenvalues of **A** with elements Λ_j, and **S** is a matrix of the eigenvectors of **A** with elements $S_{\alpha j}$. **G'** is the similarity transform of **G** with the eigenvectors of **A**:

$$G'_j = [\mathbf{S}^{-1} \cdot \mathbf{G} \cdot \mathbf{S}]_{jj} \tag{3.7}$$

The vibrational correlation function may then be defined as:

$$G_{\text{vib}}(t) = \vec{\mathbf{p}}^{\dagger} \cdot \mathbf{S} \cdot \exp(-\mathbf{\Lambda} t - \mathbf{G}' \mathrm{t}^2/2) \cdot \mathbf{S}^{-1} \cdot \vec{\mathbf{1}} \tag{3.8}$$

where $\vec{\mathbf{1}}$ is a column vector with all entries are equal to 1 and $\vec{\mathbf{p}}^{\dagger}$ is the complex transpose of the column vector $\vec{\mathbf{p}}$:

$$\vec{\mathbf{p}} = P_{\alpha}(2\omega_{\text{average}} / \hbar) \tag{3.9}$$

P_{α} is a scaling factor for the relative intensity of each peak (equal to the population variable in the program). The vibrational correlation function can be converted to the absorption spectrum by a Fourier transform, performed with the fft method in Matlab.

3.2.1 Generalization to Larger Systems

This approach is entirely generalizable to larger systems or different reactions by only changing the elements of the **K** matrix. Any additional peaks merely increase the size of the other matrices, but their form as defined here is identical. Assuming, as we have here, that any exchange results in unit dipole transfer, appropriate choice of an alternate **K** matrix is based on the simple kinetic equation:

$$\frac{d\mathbf{V}}{dt} = \mathbf{K} \cdot \mathbf{V} \tag{3.10}$$

where **V** is a column vector with elements v_{α} that describe the amplitude of each vibration. For example, Reaction 3.1 has equal forward and backward reaction rates, k_{ex}. The two vibrations, v_{a} and v_{b} are transformed by the exchange matrix as follows.

$$\frac{d\mathbf{V}}{dt} = k_{ex} \begin{bmatrix} -1 & 1 \\ 1 & -1 \end{bmatrix} \cdot \begin{bmatrix} \mathrm{v}_{\mathrm{a}} \\ \mathrm{v}_{\mathrm{b}} \end{bmatrix} \tag{3.11}$$

$$= \begin{bmatrix} -k_{ex}\mathrm{v}_{\mathrm{a}} + k_{ex}\mathrm{v}_{\mathrm{b}} \\ k_{ex}\mathrm{v}_{\mathrm{a}} - k_{ex}\mathrm{v}_{\mathrm{b}} \end{bmatrix} \tag{3.12}$$

Now, consider a three species equilibrium where the forward and backward reaction rates are independent, as in Reaction 3.2.

Reaction 3.2.

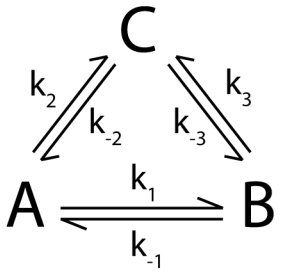

The kinetic rate equation allows us to construct a new **K** matrix for this system. Increasing the order of the other matrices contributing to the vibrational correlation function is the only other change necessary to simulate this new reaction type.

$$\frac{d\mathbf{V}}{dt} = \begin{bmatrix} -(k_1 + k_2) & k_{-1} & k_{-2} \\ k_1 & -(k_{-1} + k_3) & k_{-3} \\ k_2 & k_3 & -(k_{-2} + k_{-3}) \end{bmatrix} \cdot \begin{bmatrix} \mathrm{v_a} \\ \mathrm{v_b} \\ \mathrm{v_c} \end{bmatrix} \tag{3.13}$$

$$= \begin{bmatrix} -(k_1 + k_2)\mathrm{v_a} + k_{-1}\mathrm{v_b} + k_{-2}\mathrm{v_c} \\ k_1\mathrm{v_a} - (k_{-1} + k_3)\mathrm{v_b} + k_{-3}\mathrm{v_c} \\ k_2\mathrm{v_a} + k_3\mathrm{v_b} - (k_{-2} + k_{-3})\mathrm{v_c} \end{bmatrix} \tag{3.14}$$

Chapter 4

Electron Dynamics in Mixed Valence Ruthenium Dimers

4.1 Introduction

Electron transfer is one of the most basic transformations in chemistry and physics. Despite their ubiquitous nature, there is much left to learn about these processes. The focus of this chapter is electron transfer in bridged dimers of trinuclear ruthenium compounds. This is particularly relevant to more applied research on topics such as molecular electronics, whose understanding requires detailed knowledge of the timescales and mechanisms of charge transport between two or more sites through molecular groups.

I have performed a detailed spectroscopic and computational study of the bridged dimers of trimers shown in Figure 4.1. This work has been performed in collaboration with the Kubiak group at UC San Diego. Previous work in the Kubiak lab has focused on the highly tunable IR peak coalescence of CO vibrations in the -1 mixed valence species.[35-50] The degree of coalescence observed in these spectra varies with temperature, solvent, and ligand substitution. The tunable peak coalescence has been used as an indication of ultrafast electron transfer between the two metal sites in the dimer. Analysis of these spectra with simulations based on the Bloch equations was used previously to extract exchange rate constants ranging from 0.35 ps to several picoseconds at room temperature. Further work has examined the optical and Raman spectra of these compounds.[42,46,51]

With the combination of highly tunable IR peak coalescence and the spectroscopic convenience of strong carbonyl absorptions, we viewed these systems as ideal candidates for study with ultrafast two dimensional infrared spectroscopy (2D-IR). The use of the Bloch equations to extract quantitative information from IR spectra has been debated due to the presence of other ultrafast dynamics that can alter the IR lineshapes.[8-21] 2D-IR allows me to make a direct measurement of the time dependence of the CO vibrational frequency and assess the validity of the previous method. I collected 2D-IR spectra for several dimers with different bridging and ancillary ligands in three different solvents. In all cases, no exchange between the two CO vibrations was observed within the experimentally accessible time window (ca. 15 ps).

The lack of electron transfer in under 15 ps indicates that the origin of IR peak coalescence is likely not ultrafast electron transfer between the two metal sites.[36] I have examined several alternate mechanisms to explain the interesting spectral features in the absence of exchange. Analysis of the vibrational relaxation rates from 2D-IR measurements, combined with new density functional theory (DFT) calculations, indicate that a second isomer may be contributing to the IR spectra of some dimers. Further work is underway to elucidate the electronic dynamics and definitively determine the origin of IR peak coalescence for these compounds.

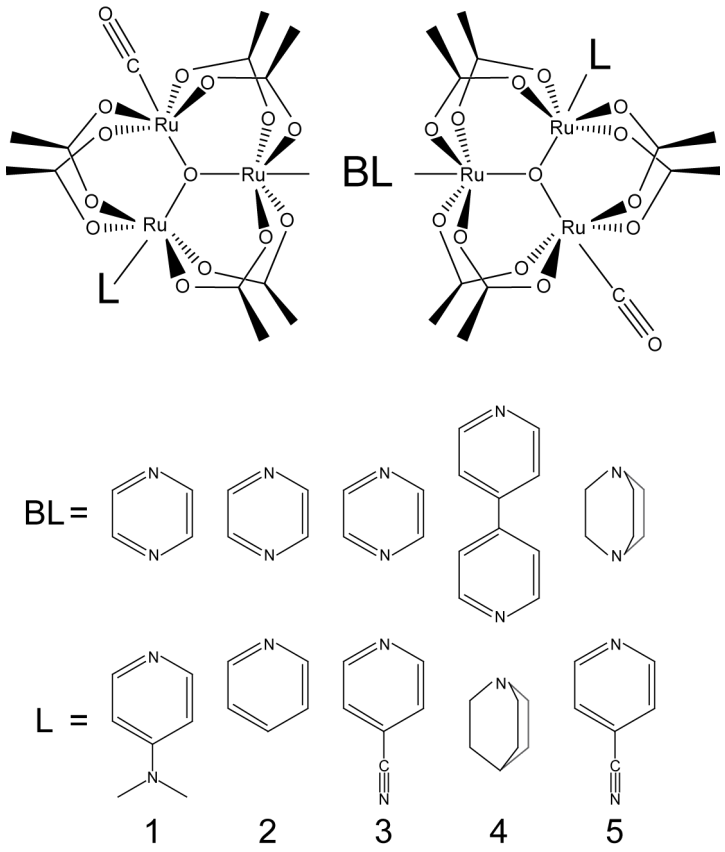

Figure 4.1: Bridging ligand (BL) and ancillary ligand (L) combinations for compounds 1-5 examined in this work. The bridging ligand for compounds 1-3 is pyrazine, 4 is 4,4'-bipyridine, and 5 is 1,4-diazabicyclo[2,2,2]octane. The ancillary ligands for compounds 1-5 are 4-dimethylaminopyridine, pyridine, 4-cyanopyridine, 1-azabicyclo[2,2,2]octane, and 4-cyanopyridine.

4.2 Previous IR Spectral Analysis

The general structure of the ruthenium dimers is given in Figure 4.1. Cyclic voltammograms of the dimers typically show two single electron reduction waves corresponding to sequential reduction of the two trinuclear metal sites.[36,37] For some dimers with bipyridine and diazabicyclooctane bridges, only one reduction wave is observed, indicating that the -1 state is not stable. All of the compounds in the current study have stable singly reduced states. In most cases, both reduced states are spectroscopically accessible through either spectroelectrochemical techniques or by chemical reduction. As mentioned previously, CO ligands are excellent reporters for these systems due to the high sensitivity of the vibrational frequency to changes in electron density. The neutral and -2 compounds are symmetric and have only a single CO peak in the IR spectrum; the electron density at each ligand is identical. In the -1 compounds, two CO peaks are observed at approximately half the height of the CO peaks of the isovalent species. In cases where the electronic coupling between sites is low, such as bipyridine or diazabicyclooctane bridged dimers, the two CO peaks are at approximately the same frequency, and have similar lineshapes, as the corresponding isovalent peaks. The asymmetric charge

distribution is achieved when the extra electron is localized at one of the two metal sites so that in the mixed valence state, one monomer resembles the neutral compound and one monomer resembles the -2 compound (where both sites have a -1 charge).

In the -1 pyrazine bridged dimers, the FTIR spectra are qualitatively very different. The two CO peaks are shifted significantly toward the average of the frequencies for the isovalent compounds. These frequency shifts are accompanied by significant increases in peak widths. The peak shifts and broadening are typical of the peak coalescence predicted by the Bloch equations for ultrafast site exchange between the 0/-1 and -1/0 charge distributions. The degree of this peak coalescence is sensitive to changes in the solvent, temperature, and ancillary ligand. In extreme cases, the two CO peaks collapse completely into a single, broad feature with only one maximum.

Rates for site exchange in these systems have been predicted based on comparison of experimental spectra with simulations using the Bloch equations. To date, all of the published simulations have been based on a version of the program VIBEXGL written by R.E.D. McClung.[20] Beyond the absolute rates predicted with this method, several important correlations have been made. First, the qualitative increase in peak coalescence, or the quantitative increase in predicted rate, correlates with an increase in the electron donating nature of the ancillary ligand.[47,89] The cyanopyridine ligand is an electron withdrawing group and compounds with this ligand show the least coalescence in the series.[35] The electron donating character of the ligands increases with pyridine and further with dimethylaminopyridine, and compounds with these ligands show the highest degree of coalescence.[47] In other words, as the electron donating ability of the ancillary ligands increases, the electronic coupling between the two sites increases, and the predicted rate of electron transfer increases. Second, as the temperature of the solvent is *decreased* toward the solvent freezing point, the degree of peak coalescence and predicted reaction rate *increase.*[50] This anti-Arrhenius behavior has been explained as a transition from ergodic to nonergodic behavior as the solvent is cooled.[90] In the ergodic regime, the solvent reorganization parameter is predicted to increase with a decrease in temperature. In the nonergodic regime, the solvent reorganization parameter is predicted to decrease with a decrease in temperature. Last, the predicted rates correlate well with solvent relaxation time.[49]

The solvent relaxation time is effectively the measure of how fast a given solvent can respond to a change in charge density. This parameter has been measured comprehensively by the group of Mark Maroncelli.[89] Briefly, a coumarin 153 molecule is excited with a short laser pulse. The excitation does not change the direction of the molecular dipole but does increase the magnitude of the dipole by ca. 8 Debye. The frequency of the emission band changes as the solvent relaxes around the new charge distribution. In thermal reactions, the rate of electron transfer is limited by the ability of solvent fluctuations to reorient and adopt a transition state configuration. Basically, electron transfer cannot occur unless the solvent molecules fluctuate to the point on the nuclear coordinate where both of the electronic states are accessible. The speed with which a solvent can accommodate a change in charge distribution should, in part, determine how quickly a thermally driven charge transfer process can proceed. This type of relationship was observed for the ruthenium dimers. More highly coalesced IR spectra are generally observed in solvents with faster solvent reorganization times.[49]

Variants of the ruthenium dimers have also been studied where the symmetry between the two sites is broken.[45,47] This can be achieved by the addition of two different ancillary ligands or by substitution of the bridging ligand. The spectra of these bridge substituted compounds display similar degrees of coalescence as their unsubstituted counterparts. This

similarity indicates that full rotation of the briding ligand is not a primary cause of peak coalescence.

4.3 Two dimensional Infrared Spectroscopy Results

Full 2D-IR spectra for compounds 1*, 3* and 1^--5^- are presented in Figures 4.2-4.8. Asterisks indicate isotopic substitution of one of the two CO ligands. A single asterisk represents a compound with one $^{13}C^{16}O$ ligand and one $^{12}C^{16}O$ ligand. Two asterisks represent a compound with one $^{13}C^{18}O$ ligand and one $^{12}C^{16}O$ ligand. Isotopic labeling was used for some neutral samples to introduce a frequency shift between the two CO vibrations in the absence of mixed valence electron dynamics. The spectrograph grating used here results in a probe frequency axis range of only ca. 80 cm^{-1}. This range is not quite wide enough to observe all of the CO peaks in the 2D-IR spectra of these compounds. Scanning the spectrograph for a wider frequency range was not possible due to baseline mismatch between adjacent spectral frames. I selected the probe frequency range used here to include the v=0 → v=1 peaks for all peak pairs.

Kinetics traces for several compound-solvent combinations are listed in Figures 4.9-4.21. No significant cross peak intensity developed in any sample; all of the kinetics are for diagonal v=0 → v=1 peaks. Kinetics data were collected by taking horizont al slices of the two dimensional spectra across one pump frequency. The peaks at each delay time were integrated to yield a trace of central peak area versus time. Fits of the kinetics traces to mono- or biexponential functions were performed with Matlab programs written by previous researchers in the Harris group. Fit time constants are listed with the corresponding data figures and are also summarized in Tables 4.1-4.5. Table 4.1 contains all fit data, the other four tables sort the data to highlight the relationships between certain subsets of the samples.

Spectra of compound 1^- in acetonitrile typically exhibit only one maximum; however, in these experiments the sample had two nearly collapsed maxima. NMR spectra of this sample were taken after 2D-IR data collection to verify the identity and quality of the sample. No problems with the sample were apparent. Perhaps some small change in lab conditions, such as temperature, between the Harris lab in Berkeley and the Kubiak lab in San Diego were enough to account for this small change in coalescence. Based on previous analysis, the predicted time constant for compound 1^- in acetonitrile is 0.35 ps and the IR spectrum typically has only one maximum. The predicted time constant for compound 2^- is 0.38 ps and the IR spectrum typically has two maxima.[49] This is only a 30 fs difference in time constant. While these figures likely do not represent an actual rate of electron transfer, they do indicate that the degree of coalescence in these two systems is quantitatively very similar and only a small change is required to shift the spectrum from one maximum to two maxima.

Preliminary data on a variant of the dimers with an isocyanide ligand in the bridging position[91] were also taken. These experiments sought to more directly examine the electron dynamics by probing the cyano vibration at the bridging ligand itself. Unfortuantely, the vibrational lifetime for the neutral sample was only ca. 1.5 ps; much faster than any of the other neutral samples. Torsional motion has previously been reported to enhance IVR in nearby vibrations.[92] If the bridging ligand is torsionally active, this much faster decay rate could be explained by IVR in a similar manner. No further data were taken on this sample, and the preliminary data were not included in this work.

4.3.1 Sample Preparation

Details of the synthesis of the dimers of ruthenium trimers have been described previously.[35,36] All dimer compounds in this work were synthesized by either Starla Glover or Jane Henderson, graduate students in the Kubiak lab, and provided to me for the 2D-IR experiments as part of this collaboration.

Neutral samples were prepared by dissolving crystals of the compound in solvent on a lab bench. Preparation of the -1 mixed valence and -2 samples was more intensive due to the high air sensitivity in the reduced states. Solutions of a chemical reducing agent, cobaltocene or decamethyl cobaltocene, were titrated into solutions of the dimer compounds in a nitrogen glovebox.[50] All samples were loaded into air tight sample cells (*Specac*, 500 μm pathlength CaF_2 windows), and proper reduction was verified at the beginning and end of each experimental run with FTIR. The samples remained sufficiently reduced for the duration of the experiments.

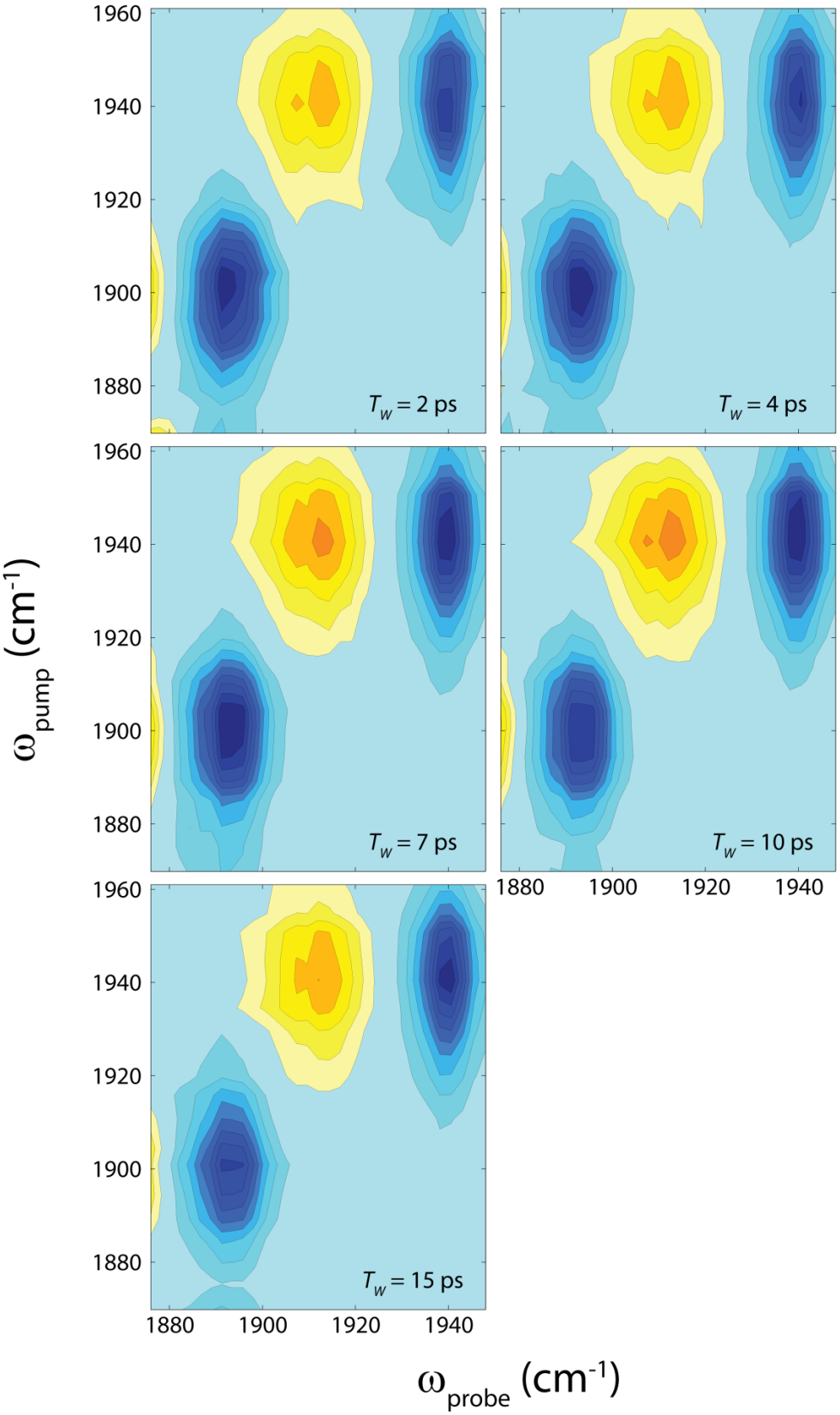

Figure 4.2: 2D-IR spectra of neutral compound 1* in acetonitrile.

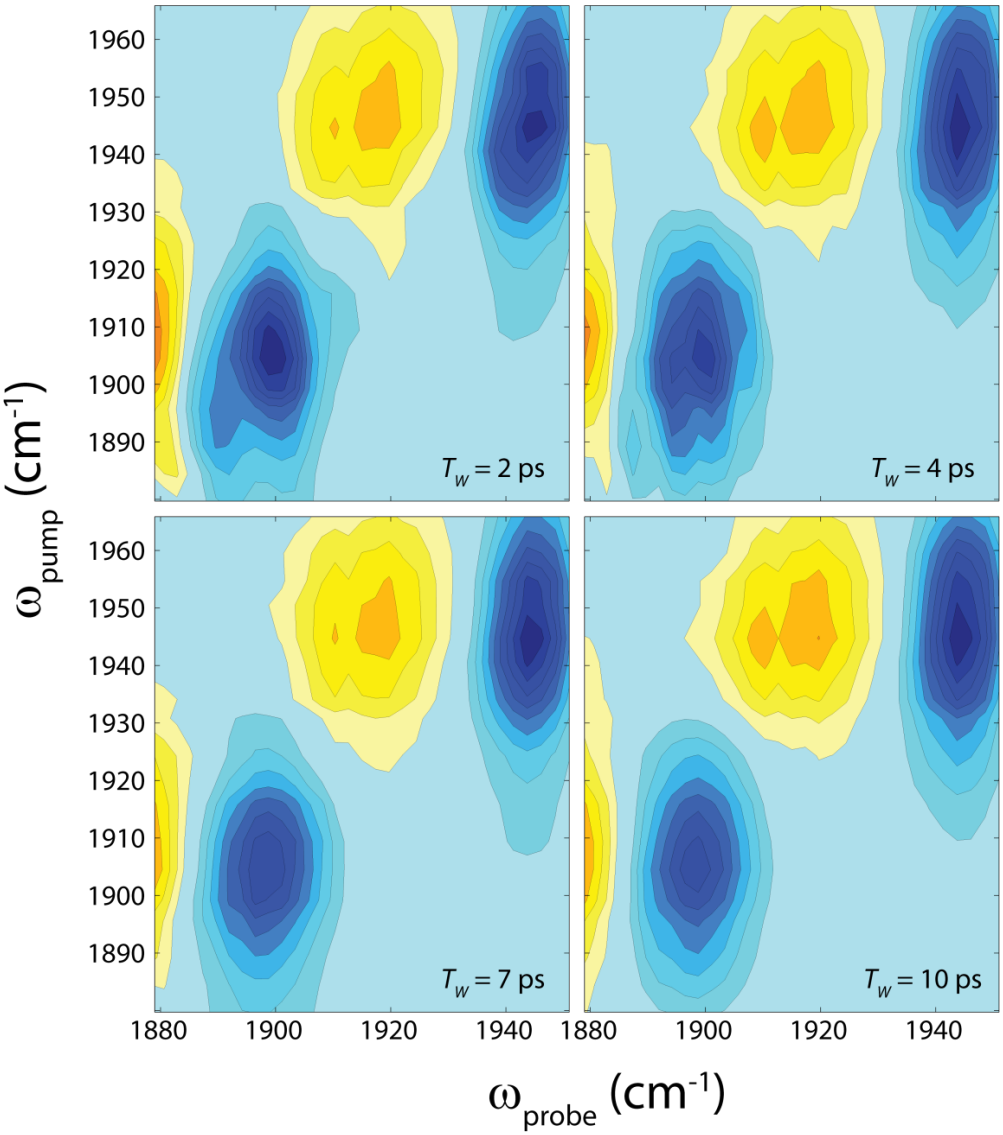

Figure 4.3: 2D-IR spectra of neutral compound 3* in dichloromethane.

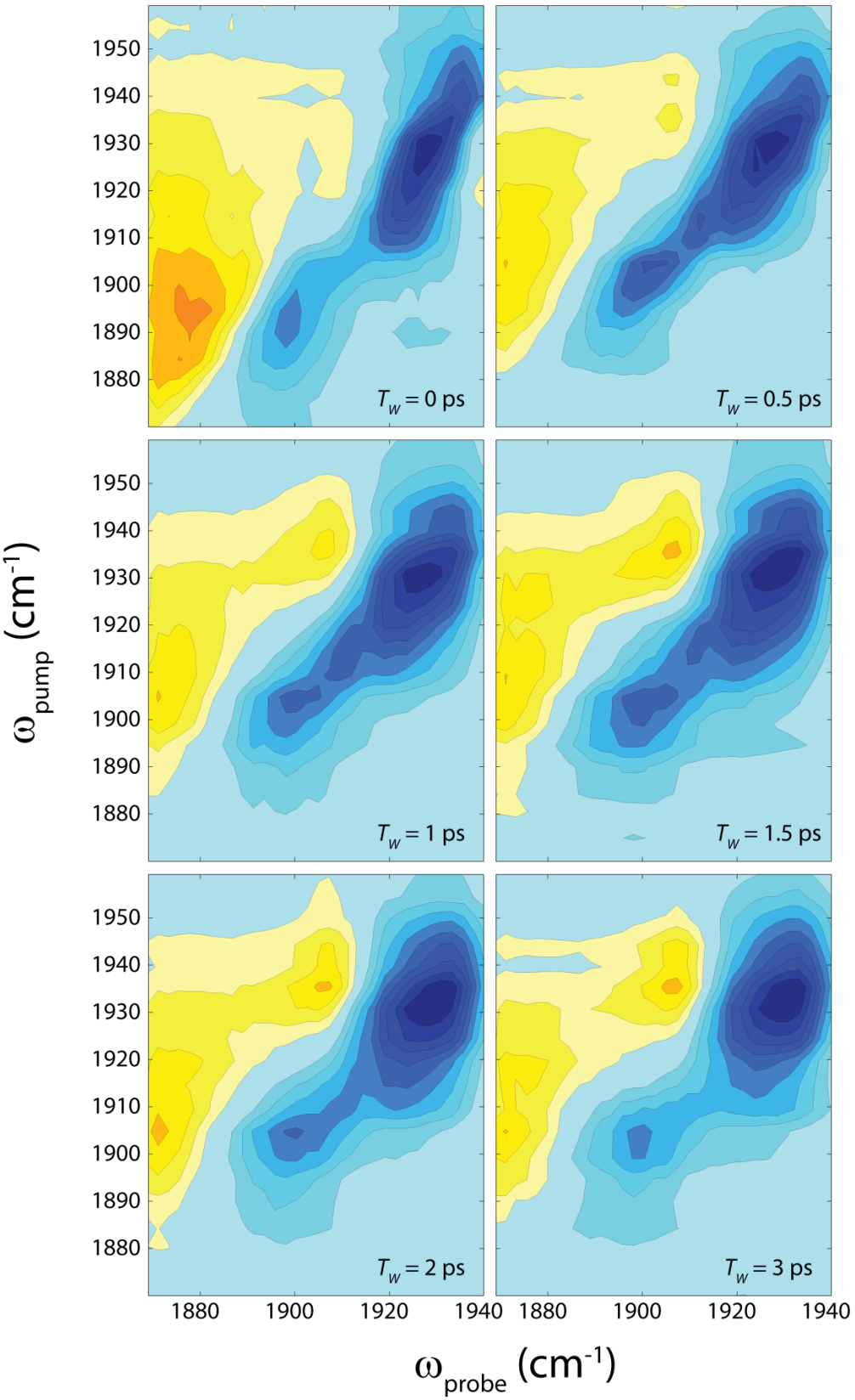

Figure 4.4a: 2D-IR spectra of -1 compound 1 in acetonitrile.

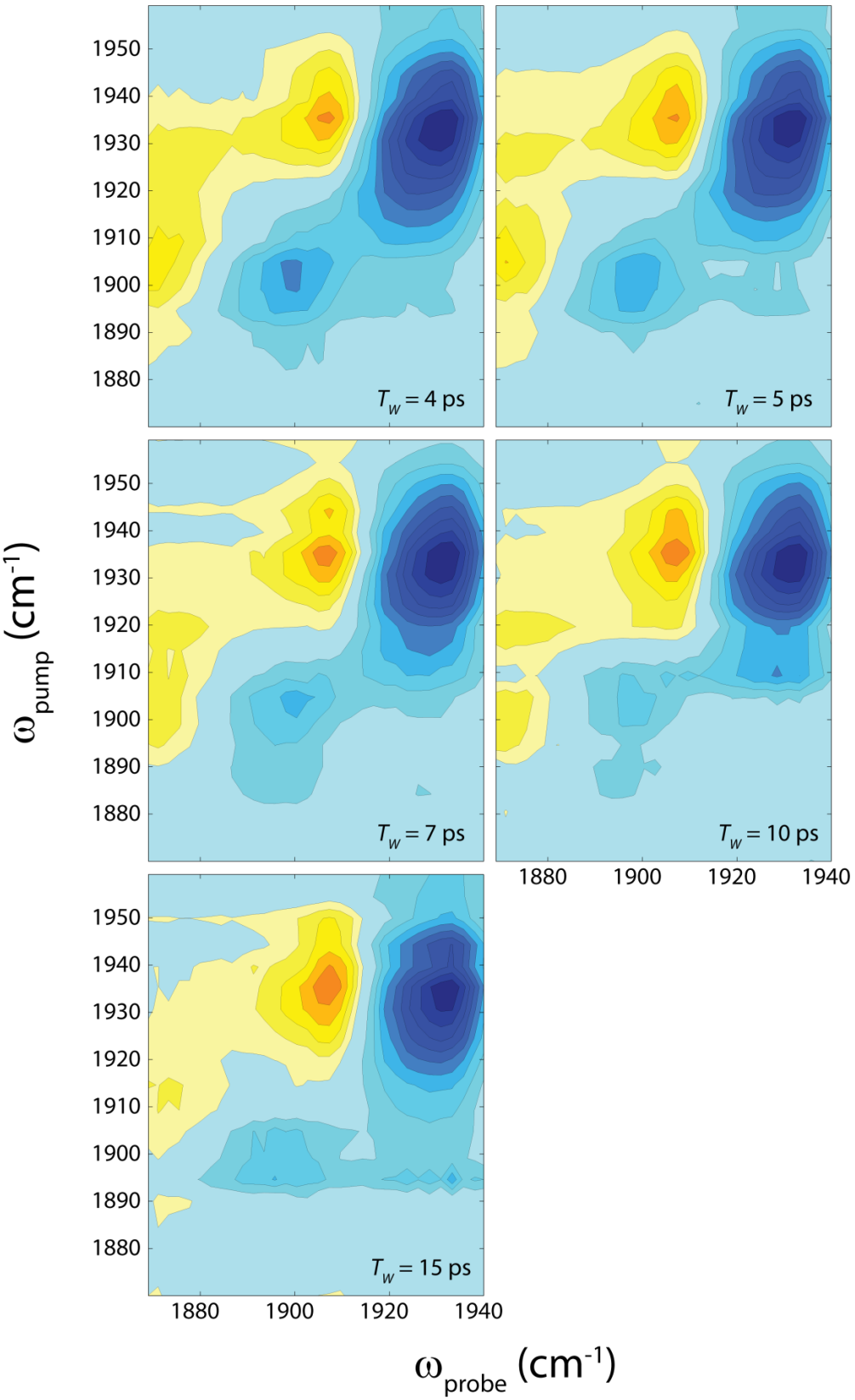

Figure 4.4b: 2D-IR spectra of -1 compound 1 in acetonitrile.

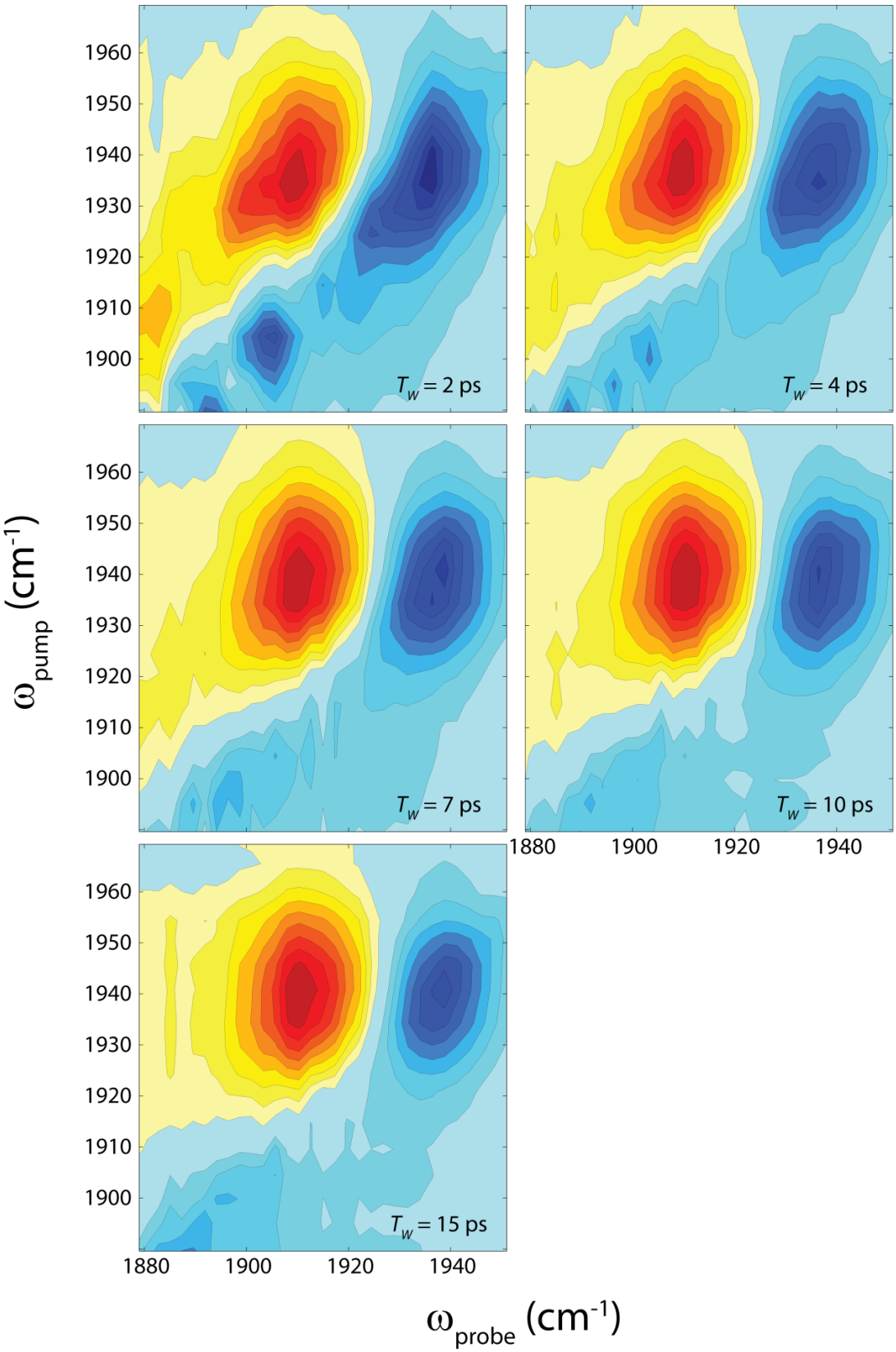

Figure 4.5: 2D-IR spectra of -1 compound 2 in dichloromethane.

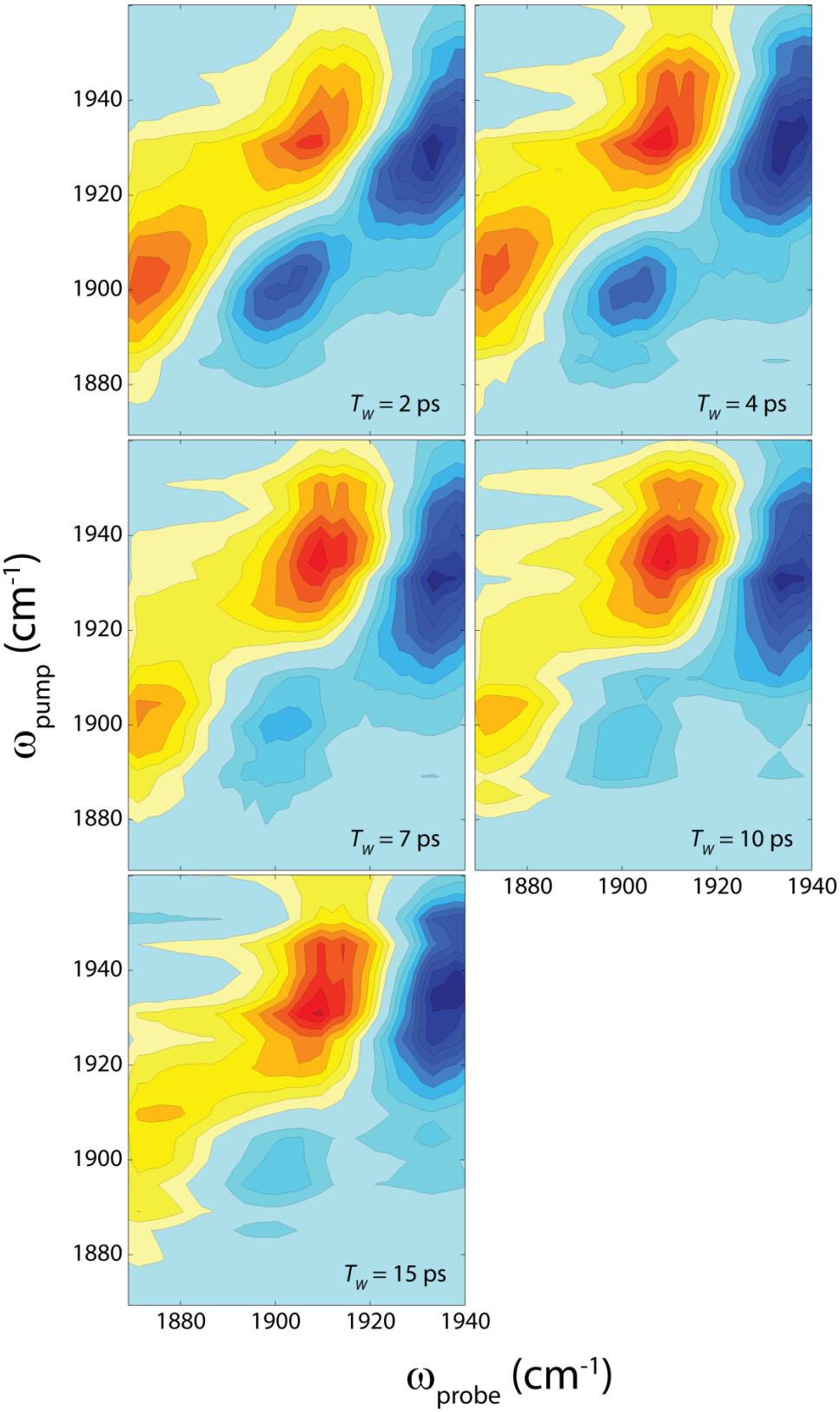

Figure 4.6: 2D-IR spectra of -1 compound 3 in dichloromethane.

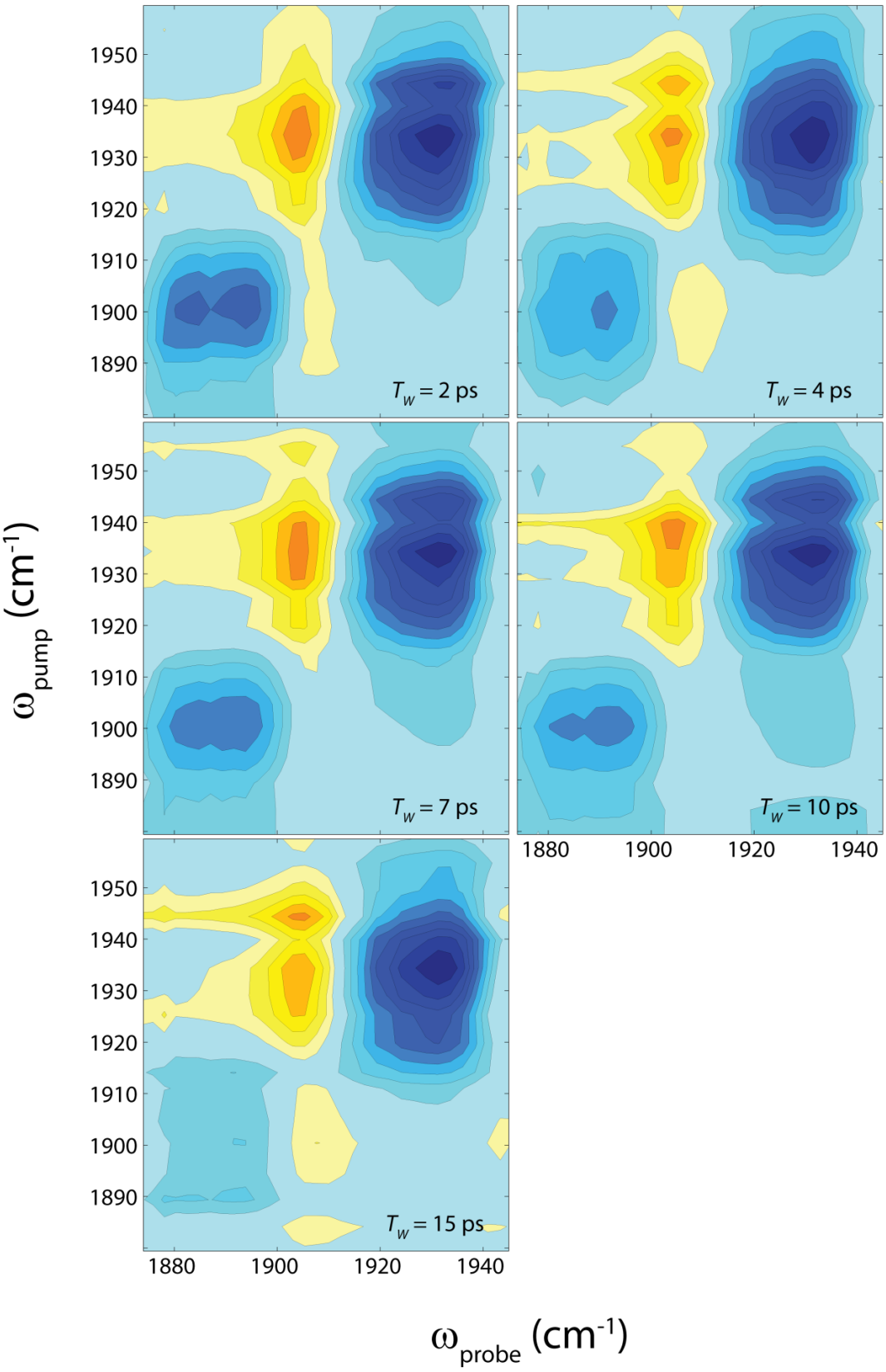

Figure 4.7: 2D-IR spectra of -1 compound 4 in acetonitrile.

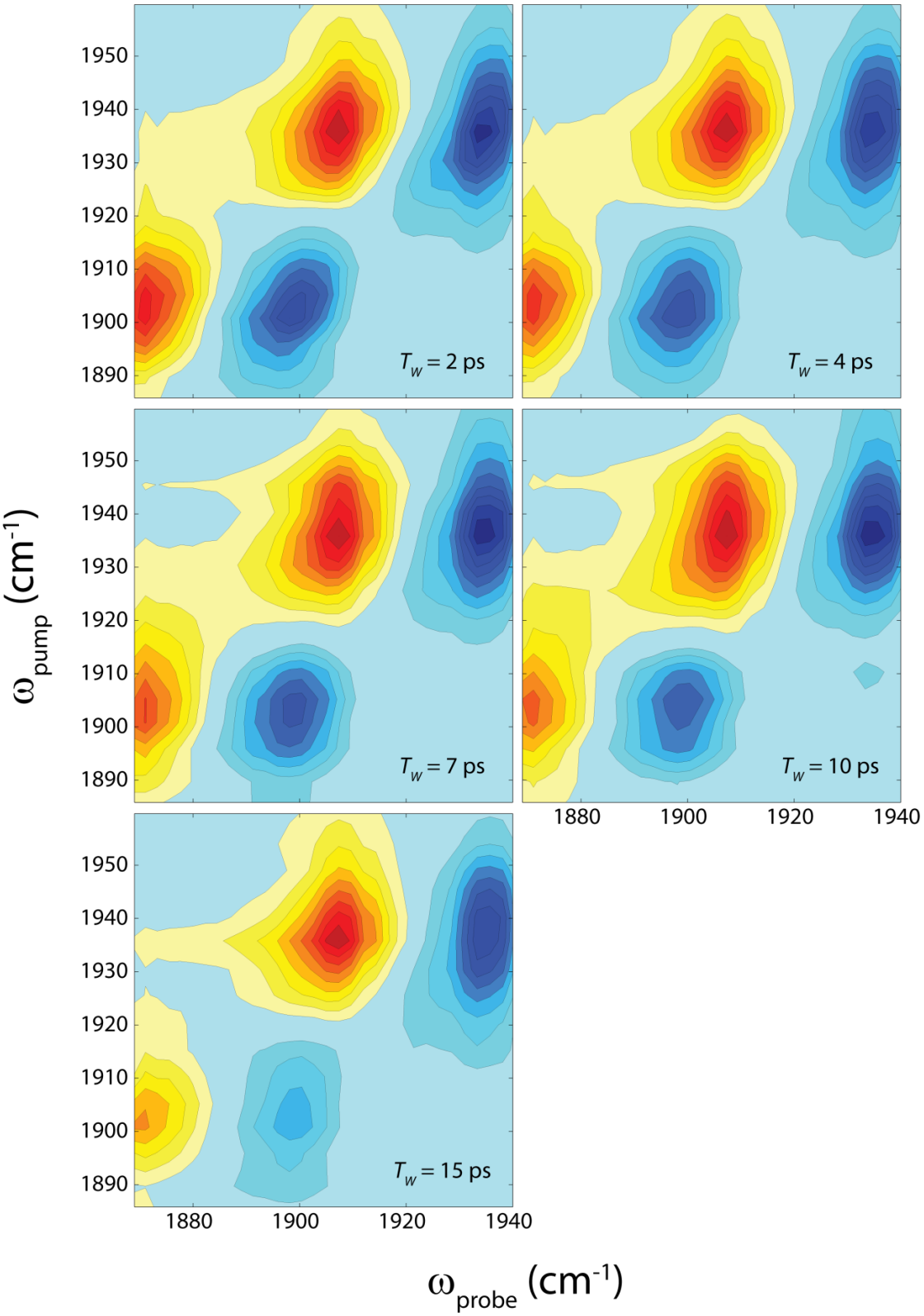

Figure 4.8: 2D-IR spectra of -1 compound 5 in acetonitrile.

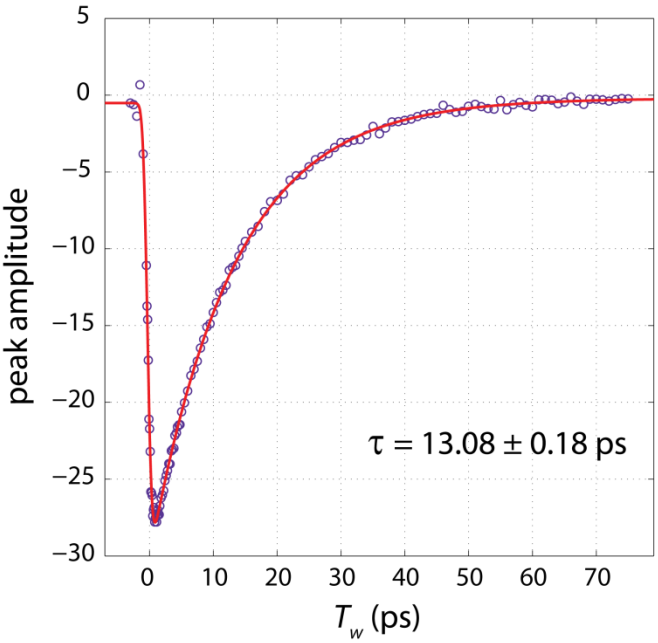

Figure 4.9a Kinetics of the low frequency diagonal peak of neutral compound 1* in acetonitrile.

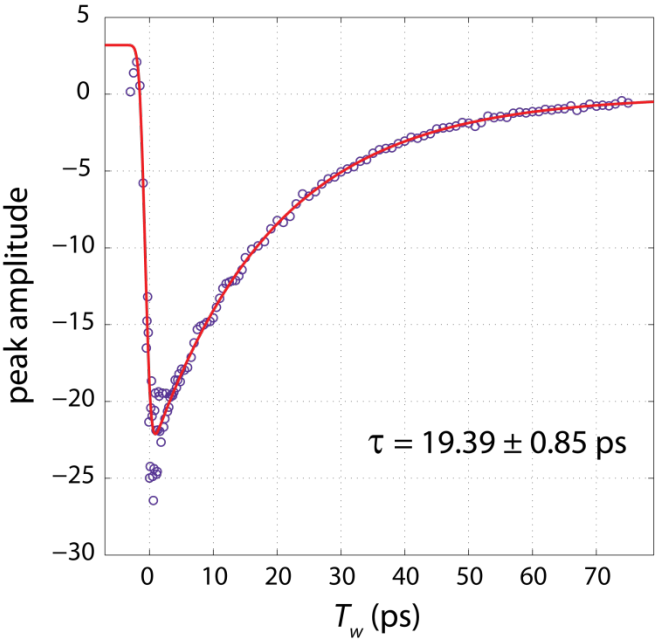

Figure 4.9b: Kinetics of the high frequency diagonal peak of neutral compound 1* in acetonitrile.

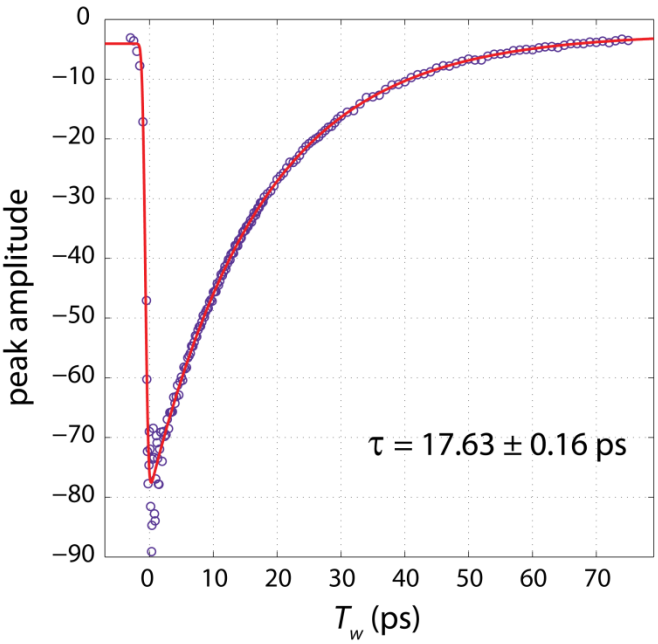

Figure 4.10: Kinetics of the high frequency diagonal peak of neutral compound 2** in acetonitrile.

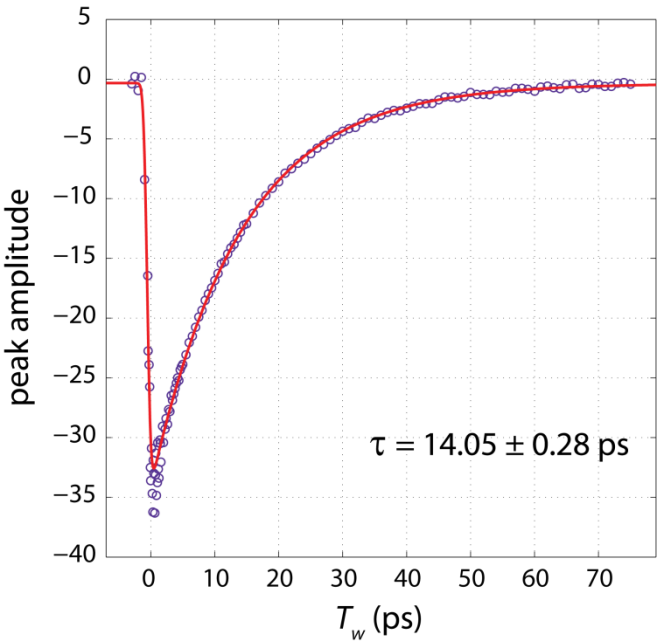

Figure 4.11: Kinetics of the low frequency diagonal peak of neutral compound 3* in dichloromethane.

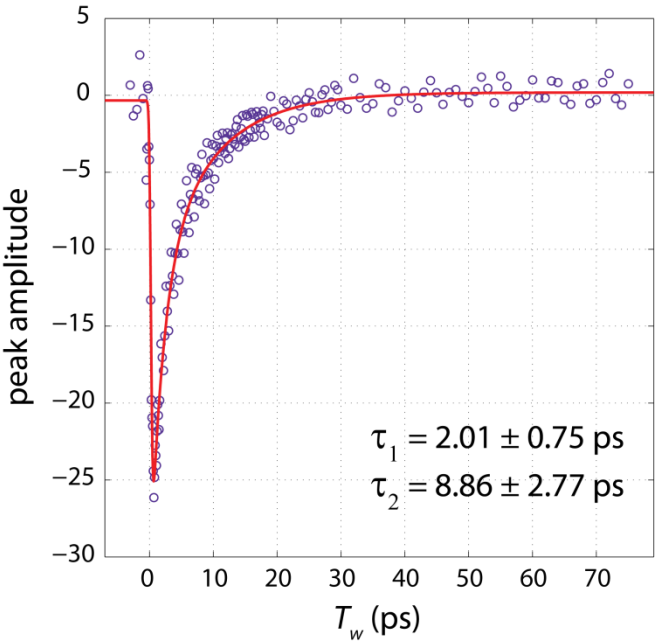

Figure 4.12: Kinetics of the low frequency diagonal peak of -1 compound 1 in acetonitrile.

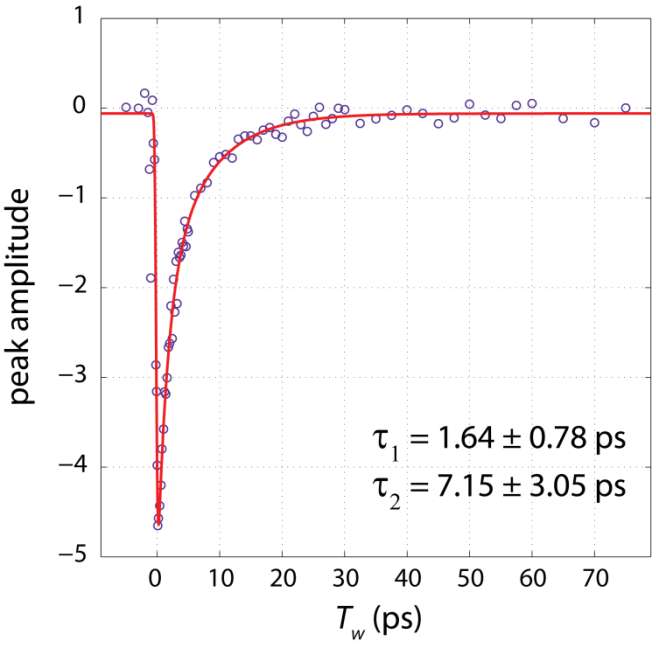

Figure 4.13a: Kinetics of the low frequency diagonal peak of -1 compound 2 in acetonitrile.

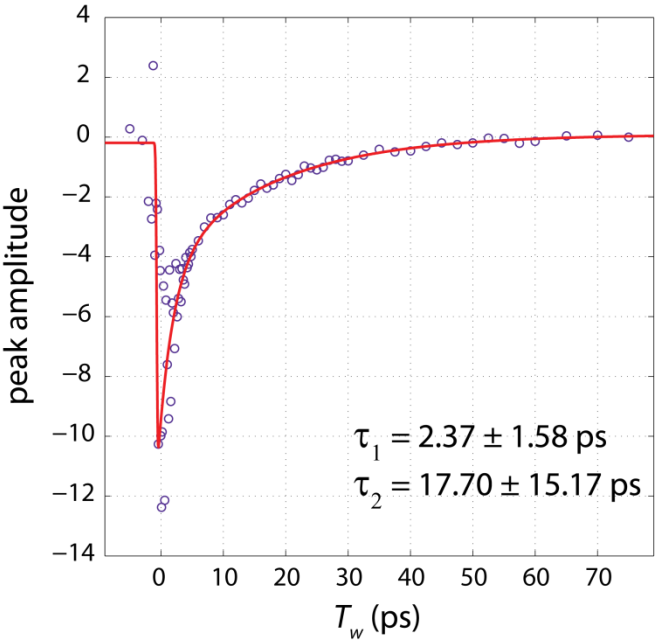

Figure 4.13b: Kinetics of the high frequency diagonal peak of -1 compound 2 in acetonitrile.

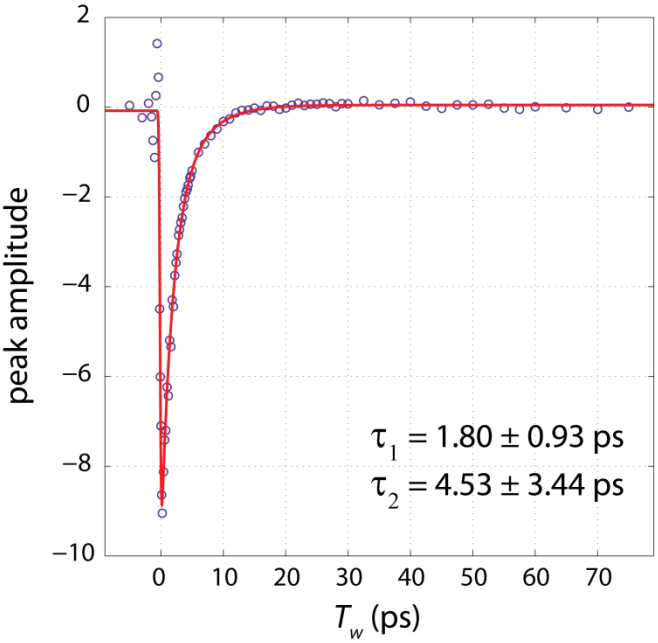

Figure 4.14a: Kinetics of the low frequency diagonal peak of -1 compound 2 in dichloromethane.

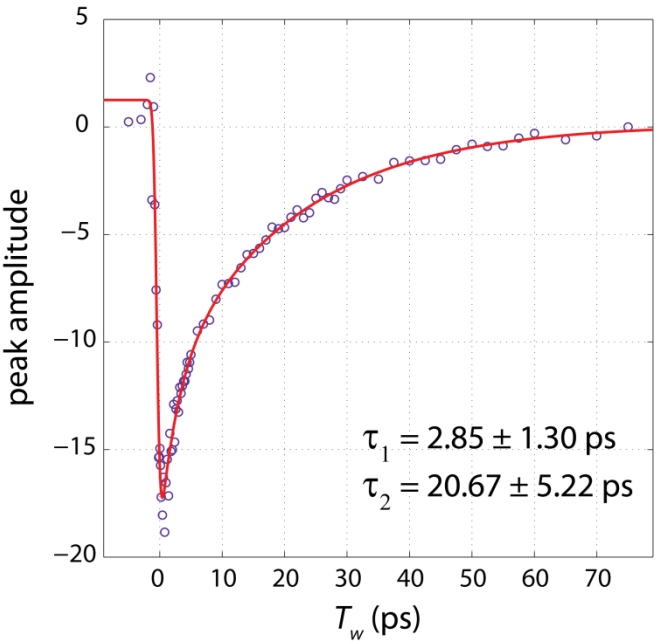

Figure 4.14b: Kinetics of the high frequency diagonal peak of -1 compound 2 in dichloromethane.

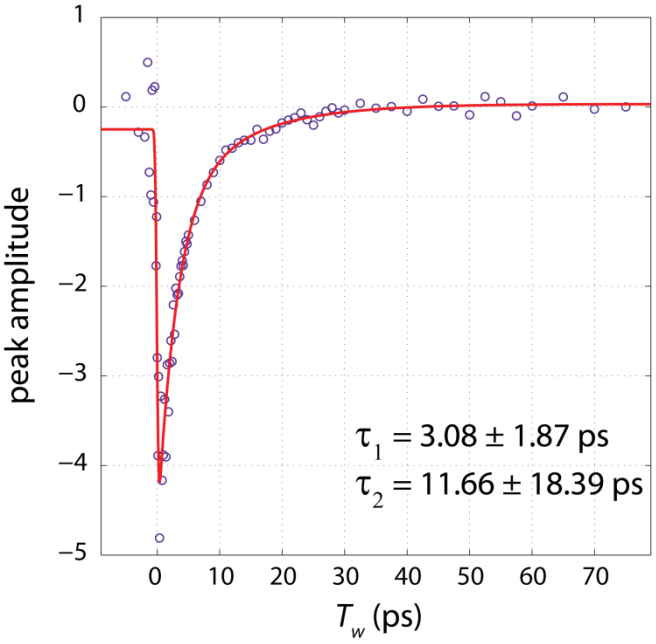

Figure 4.15a: Kinetics of the low frequency diagonal peak of -1 compound 2 in dimethyl sulfoxide.

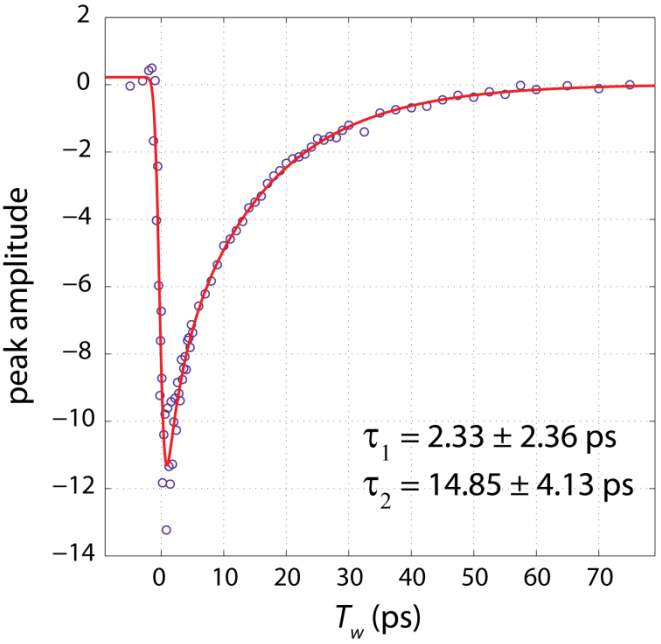

Figure 4.15b: Kinetics of the high frequency diagonal peak of -1 compound 2 in dimethyl sulfoxide.

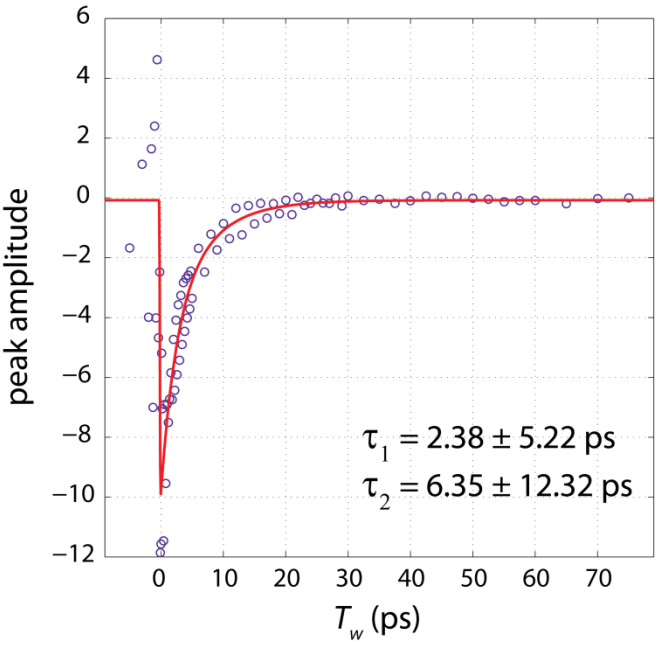

Figure 4.16a: Kinetics of the low frequency diagonal peak of -1 compound 3 in acetonitrile.

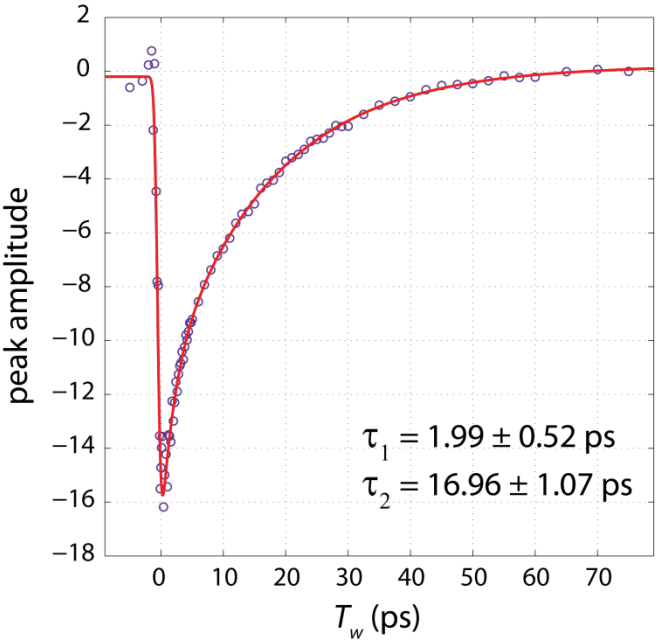

Figure 4.16b: Kinetics of the high frequency diagonal peak of -1 compound 3 in acetonitrile.

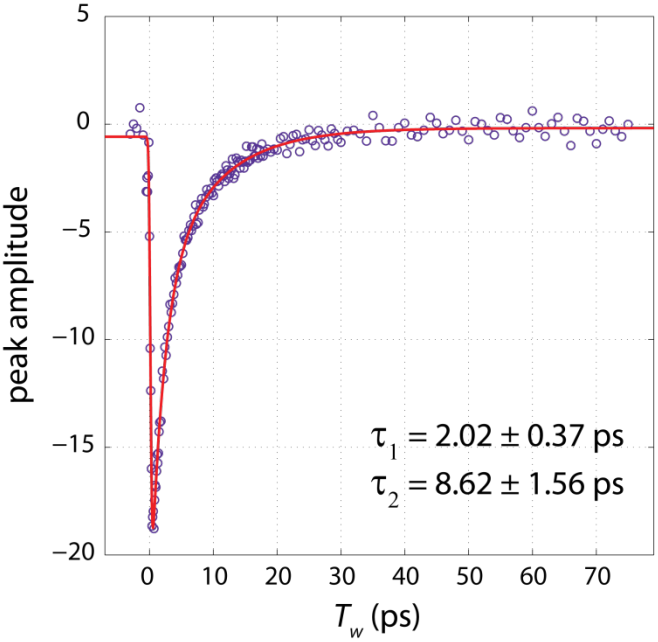

Figure 4.17a: Kinetics of the low frequency diagonal peak of -1 compound 3 in dichloromethane.

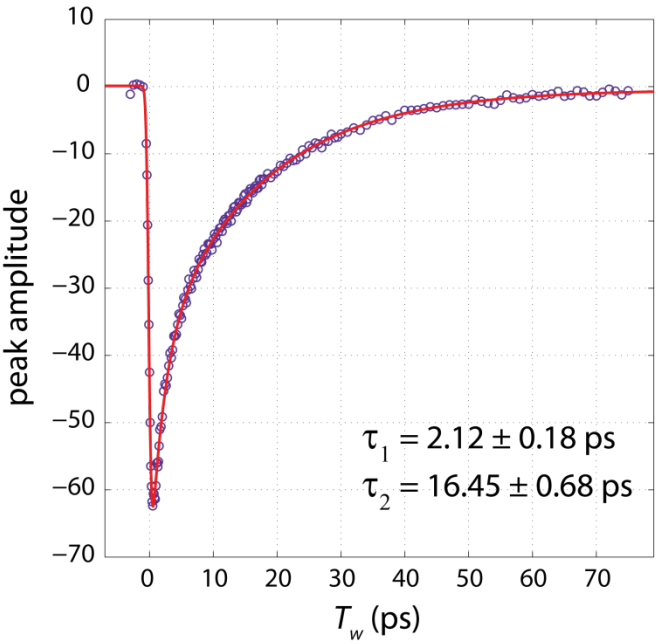

Figure 4.17b: Kinetics of the high frequency diagonal peak of -1 compound 3 in dichloromethane.

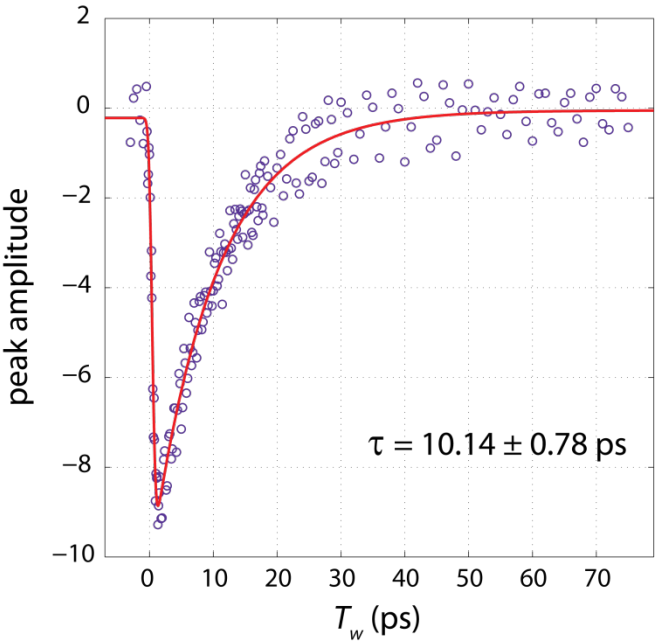

Figure 4.18: Kinetics of the low frequency diagonal peak of -1 compound 4 in acetonitrile.

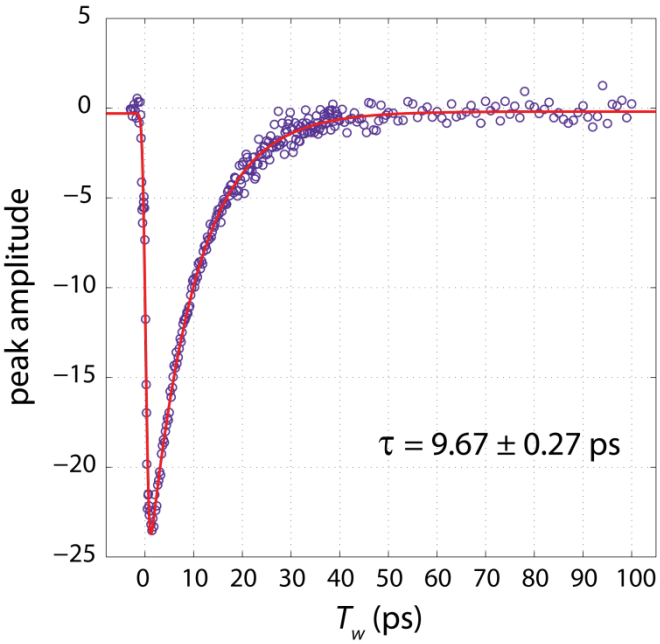

Figure 4.19: Kinetics of the low frequency diagonal peak of -1 compound 5 in acetonitrile.

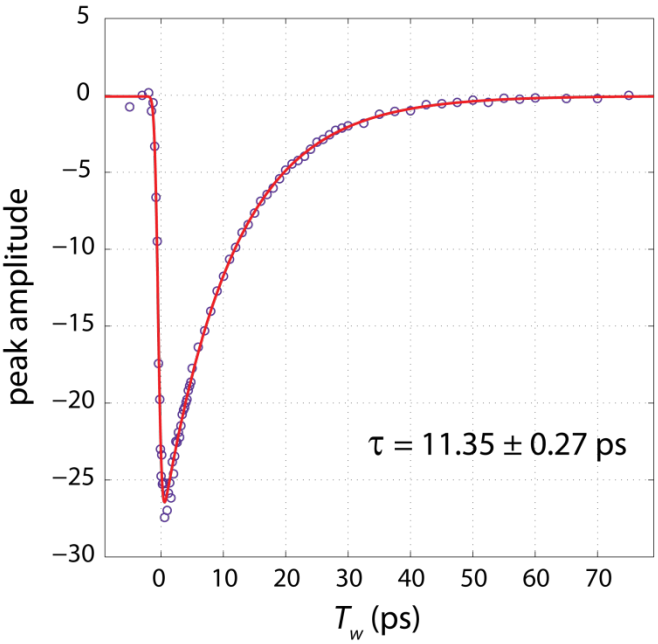

Figure 4.20: Kinetics of the diagonal peak of -2 compound 2 in acetonitrile.

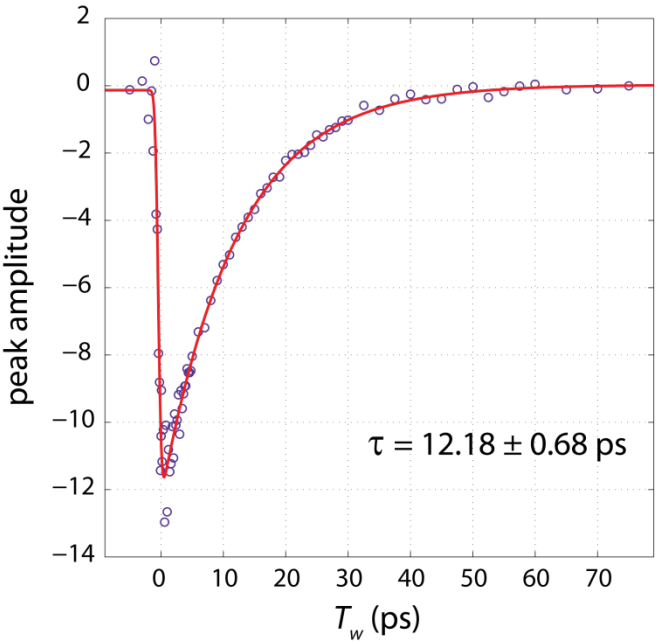

Figure 4.21: Kinetics of the diagonal peak of -2 compound 3 in acetonitrile.

compound	charge	solvent	τ_1 (ps)	τ_2 (ps)
1*	0	MeCN	-	13.08 ± 0.18
1*	0	MeCN	-	19.39 ± 0.85
2**	0	MeCN	-	17.63 ± 0.16
3*	0	DCM	-	14.05 ± 0.28
1	-1	MeCN	2.01 ± 0.75	8.86 ± 2.77
2	-1	MeCN	1.64 ± 0.78	7.15 ± 3.05
2	-1	MeCN	2.37 ± 1.58	17.70 ± 15.17
2	-1	DCM	1.80 ± 0.93	4.53 ± 3.44
2	-1	DCM	2.85 ± 1.30	20.67 ± 5.22
2	-1	DMSO	3.08 ± 1.87	11.66 ± 18.39
2	-1	DMSO	2.33 ± 2.36	14.85 ± 4.13
3	-1	MeCN	2.38 ± 5.22	6.35 ± 12.32
3	-1	MeCN	1.99 ± 0.52	16.96 ± 1.07
3	-1	DCM	2.02 ± 0.37	8.62 ± 1.56
3	-1	DCM	2.12 ± 0.18	16.45 ± 0.68
4	-1	MeCN	-	10.14 ± 0.78
5	-1	MeCN	-	9.67 ± 0.27
2	-2	MeCN	-	11.35 ± 0.27
3	-2	MeCN	-	12.18 ± 0.68

Table 4.1: Time constants for the decay of the diagonal peaks for the indicated samples. Red and blue highlighting indicate low and high frequency diagonal peaks, respectively. No highlighting indicates a non-isotopically labeled isovalent sample with only one CO peak.

compound	charge	solvent	τ_1 (ps)	τ_2 (ps)
2	-1	MeCN	1.64 ± 0.78	7.15 ± 3.05
2	-1	DCM	1.80 ± 0.93	4.53 ± 3.44
2	-1	DMSO	3.08 ± 1.87	11.66 ± 18.39
2	-1	MeCN	2.37 ± 1.58	17.70 ± 15.17
2	-1	DCM	2.85 ± 1.30	20.67 ± 5.22
2	-1	DMSO	2.33 ± 2.36	14.85 ± 4.13

Table 4.2: Time constants for the decay of the diagonal peaks for -1 compound 2 in three different solvents. Red and blue highlighting indicate low and high frequency diagonal peaks, respectively.

compound	charge	solvent	τ_1 (ps)	τ_2 (ps)
2**	0	MeCN	-	17.63 ± 0.16
2	-1	MeCN	1.64 ± 0.78	7.15 ± 3.05
2	-1	MeCN	2.37 ± 1.58	17.70 ± 15.17
2	-2	MeCN	-	11.35 ± 0.27

Table 4.3: Time constants for the decay of the diagonal peaks for compound 2 in all three oxidation states. Red and blue highlighting indicate low and high frequency diagonal peaks, respectively. No highlighting indicates a non-isotopically labeled isovalent sample with only one CO peak. Note that while compound 2** has a $^{13}C^{18}O$ isotopic label, the measured kinetics are for the $^{12}C^{16}O$ vibration.

compound	charge	solvent	τ_1 (ps)	τ_2 (ps)
1	-1	MeCN	2.01 ± 0.75	8.86 ± 2.77
2	-1	MeCN	1.64 ± 0.78	7.15 ± 3.05
3	-1	MeCN	2.38 ± 5.22	6.35 ± 12.32
2	-1	MeCN	2.37 ± 1.58	17.70 ± 15.17
3	-1	MeCN	1.99 ± 0.52	16.96 ± 1.07

Table 4.4: Time constants for the decay of the diagonal peaks for -1 samples of all three pyrazine bridged dimers. Red and blue highlighting indicate low and high frequency diagonal peaks, respectively.

compound	charge	solvent	τ_1 (ps)	τ_2 (ps)
1*	0	MeCN	-	13.08 ± 0.18
3*	0	DCM	-	14.05 ± 0.28
1	-1	MeCN	2.01 ± 0.75	8.86 ± 2.77
2	-1	MeCN	1.64 ± 0.78	7.15 ± 3.05
2	-1	DCM	1.80 ± 0.93	4.53 ± 3.44
2	-1	DMSO	3.08 ± 1.87	11.66 ± 18.39
3	-1	MeCN	2.38 ± 5.22	6.35 ± 12.32
3	-1	DCM	2.02 ± 0.37	8.62 ± 1.56
4	-1	MeCN	-	10.14 ± 0.78
5	-1	MeCN	-	9.67 ± 0.27
1*	0	MeCN	-	19.39 ± 0.85
2**	0	MeCN	-	17.63 ± 0.16
2	-1	MeCN	2.37 ± 1.58	17.70 ± 15.17
2	-1	DCM	2.85 ± 1.30	20.67 ± 5.22
2	-1	DMSO	2.33 ± 2.36	14.85 ± 4.13
3	-1	MeCN	1.99 ± 0.52	16.96 ± 1.07
3	-1	DCM	2.12 ± 0.18	16.45 ± 0.68

Table 4.5: Time constants for the decay of the diagonal peaks for the indicated samples with an emphasis on the difference between high and low frequency peaks. Red and blue highlighting indicate low and high frequency diagonal peaks, respectively. No highlighting indicates a non-isotopically labeled isovalent sample with only one CO peak.

4.4 Density Functional Theory Results

I performed ground state geometry optimizations for two different isomers of the representative compound 2 in both the neutral and -1 states. As a starting geometry, I used the previously reported crystal structure for the neutral dimer where the ancillary ligand is azabicyclooctane and the bridging ligand is pyrazine.[38] I chose compound 2 for the optimizations since it has the least number of atoms of all the dimers. I attempted geometry optimizations with different ligands, but they were not successful. Reaching convergence in these large systems is a challenge, and I think compound 2 is representative of the class of pyrazine bridged dimers.

All geometry optimizations were performed in Gaussian 09. Neutral calculations used the BP86 functional; -1 calculations used the unrestricted BP86 functional. The basis set for ruthenium atoms is LANL2DZ. All other atoms used 6-31G.

Ball and stick figures for both isomers of the two charges are shown in Figure 22. The frontier molecular orbitals, including both alpha and beta orbitals for the unrestricted calculations are shown in Figures 23-32.

Constrained DFT (CDFT) calculations[93] on the dimers were also used in an attempt to localize the electron density on one monomer in geometry optimizations of the -1 compound. None of these CDFT calculations fully converged. Increases in computational power and efficiency may make such calculations more feasible in the future.

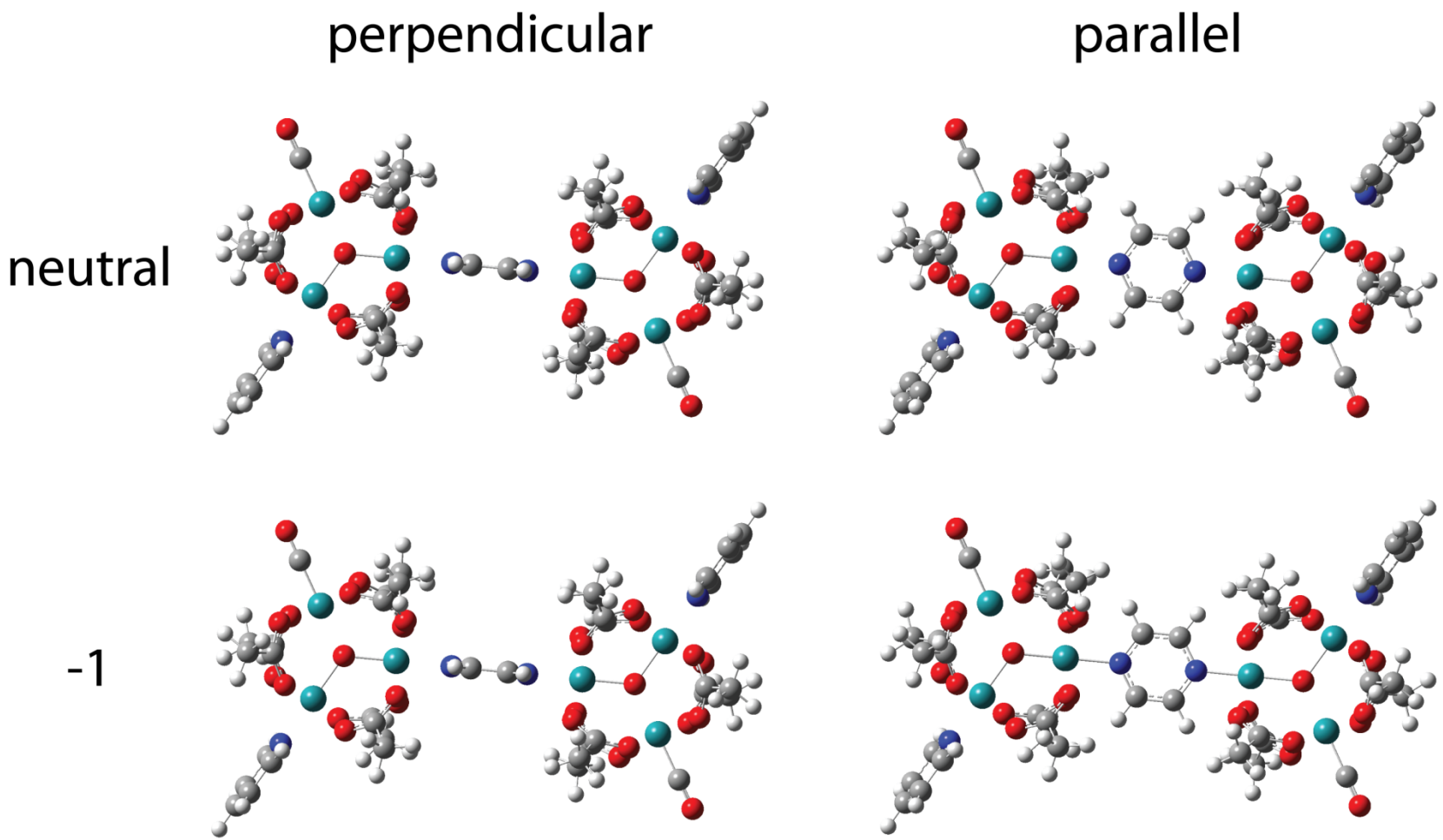

Figure 4.22: Perpendicular and parallel bridged structures of the neutral and -1 dimers.

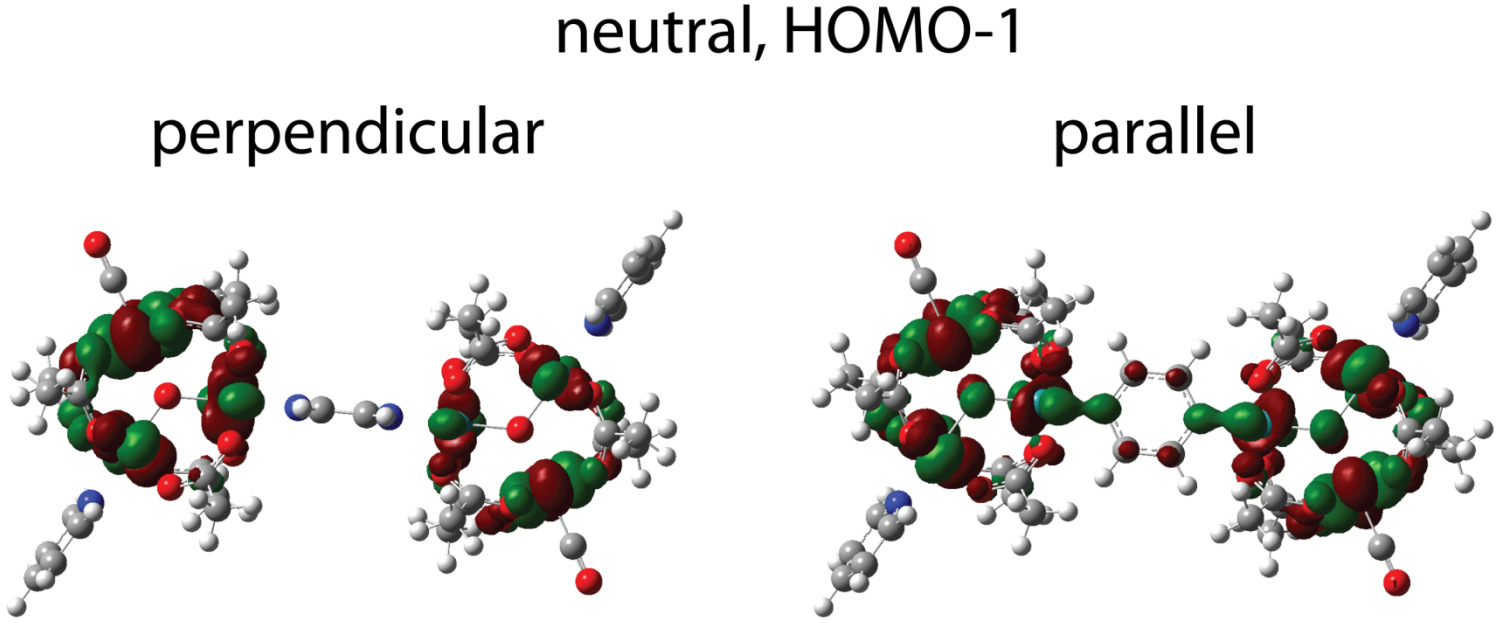

Figure 4.23: HOMO-1 orbitals of the neutral dimers.

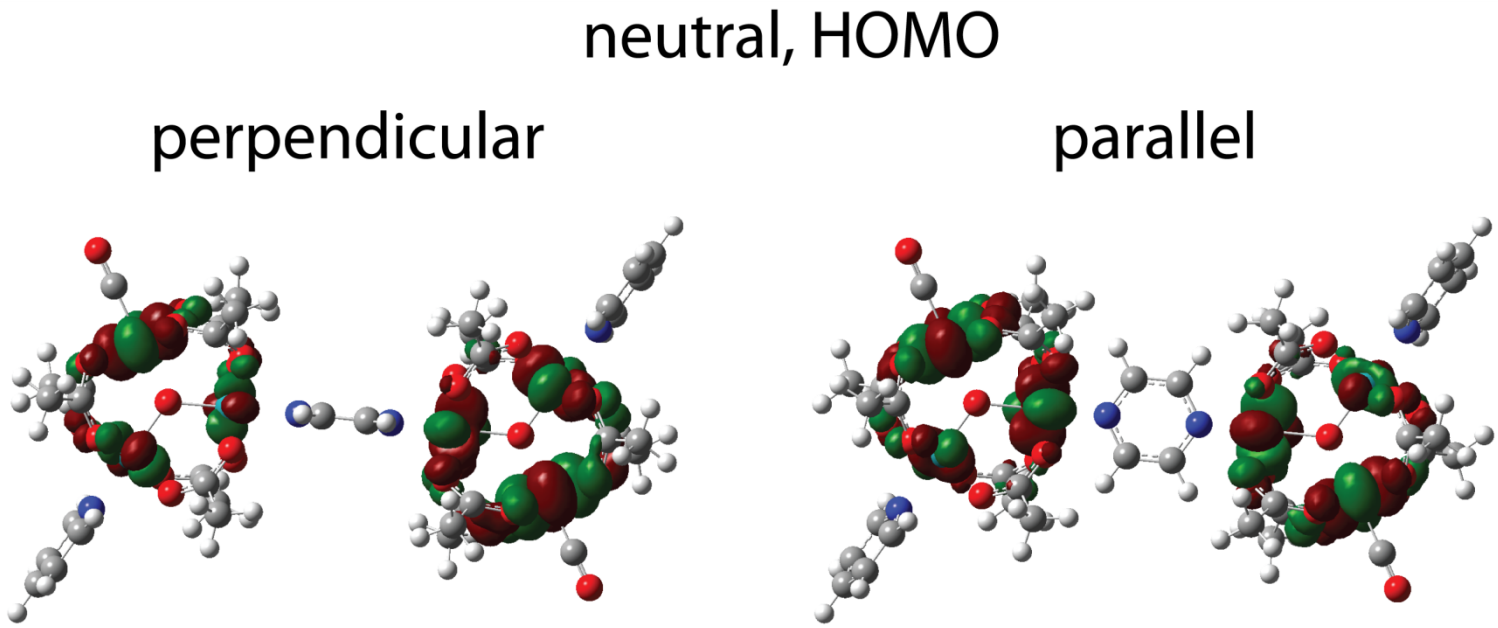

Figure 4.24: HOMO orbitals of the neutral dimers.

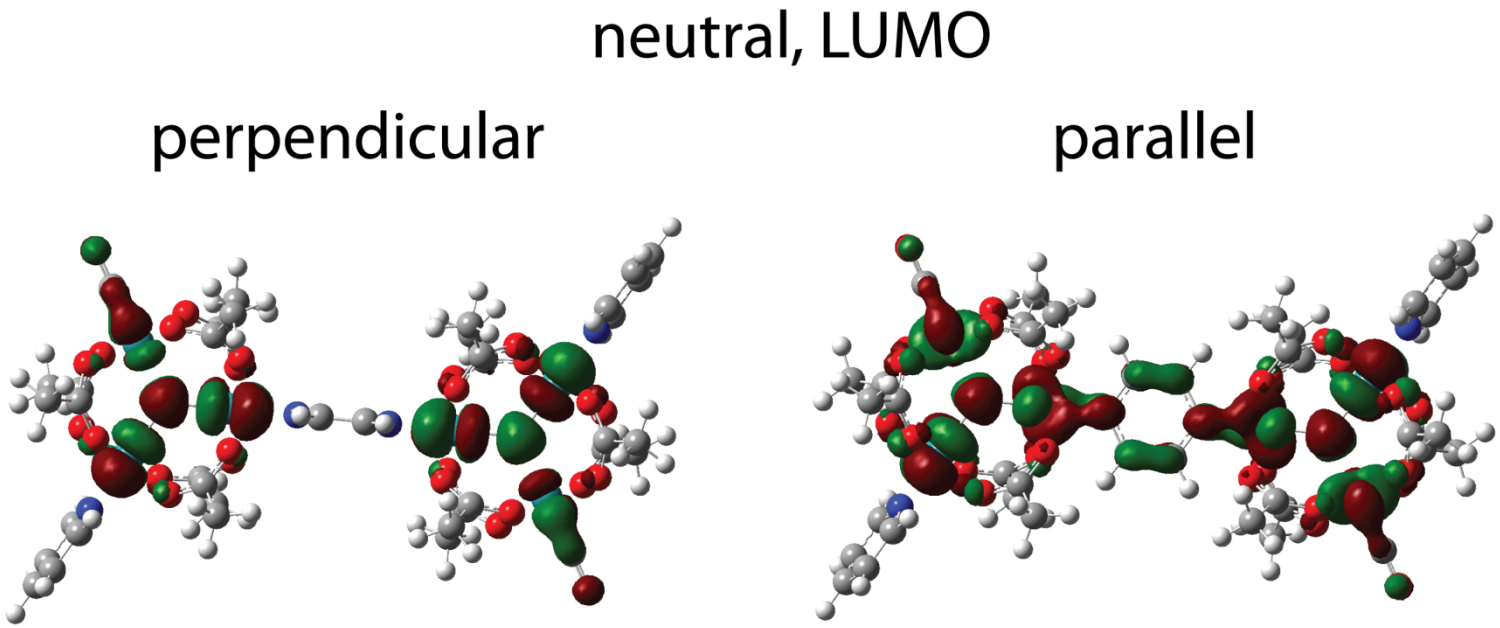

Figure 4.25: LUMO orbitals of the neutral dimers.

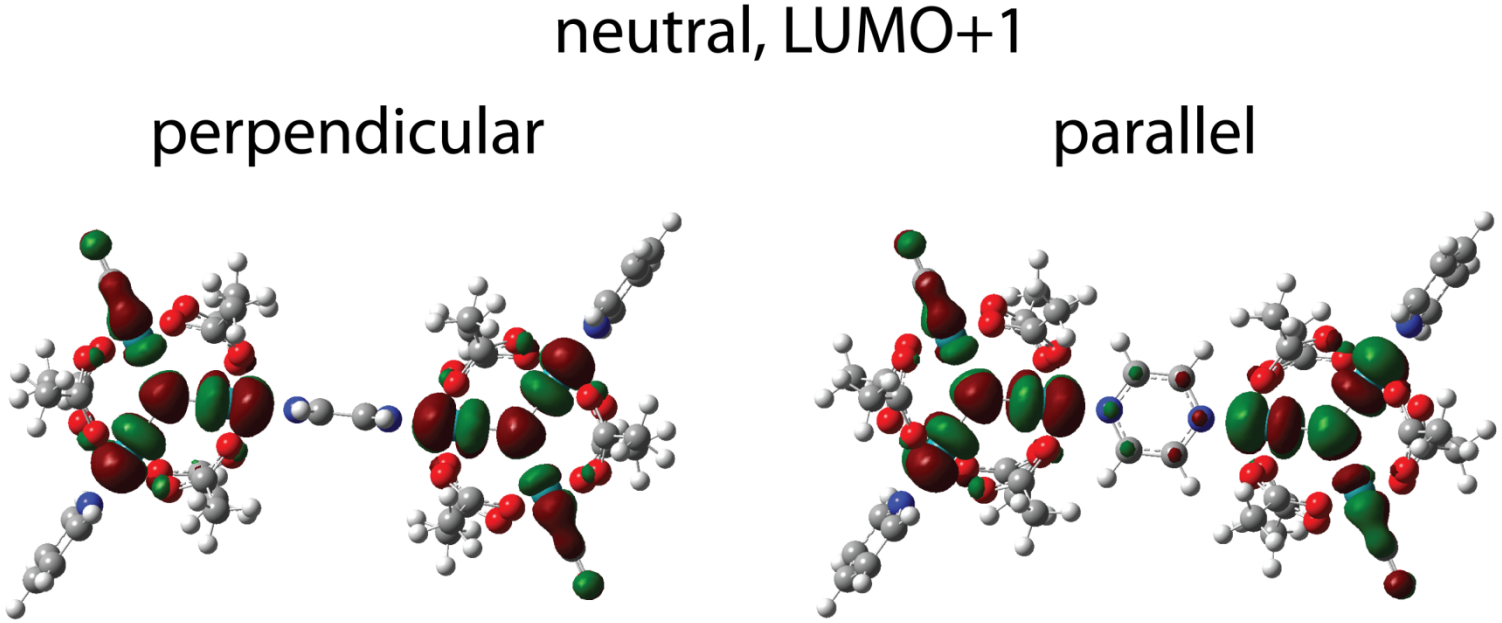

Figure 4.26: LUMO+1 orbitals of the neutral dimers.

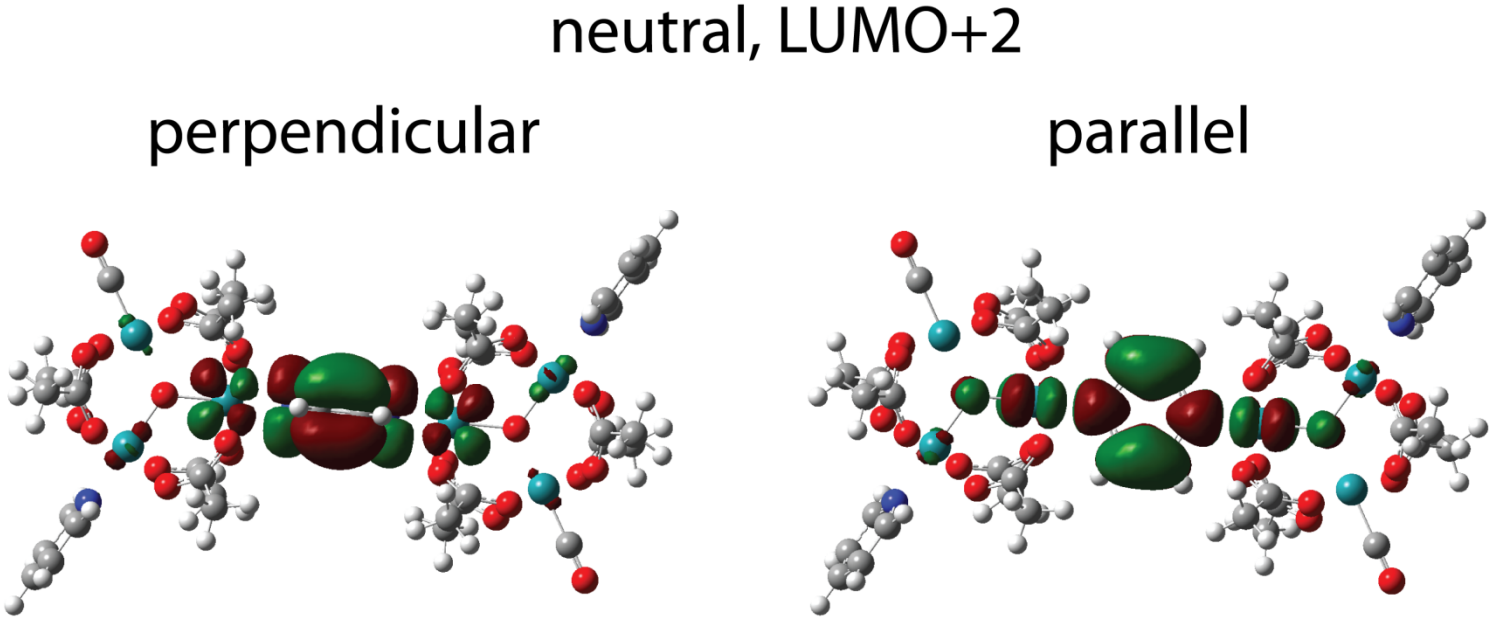

Figure 4.27: LUMO+2 orbitals of the neutral dimers.

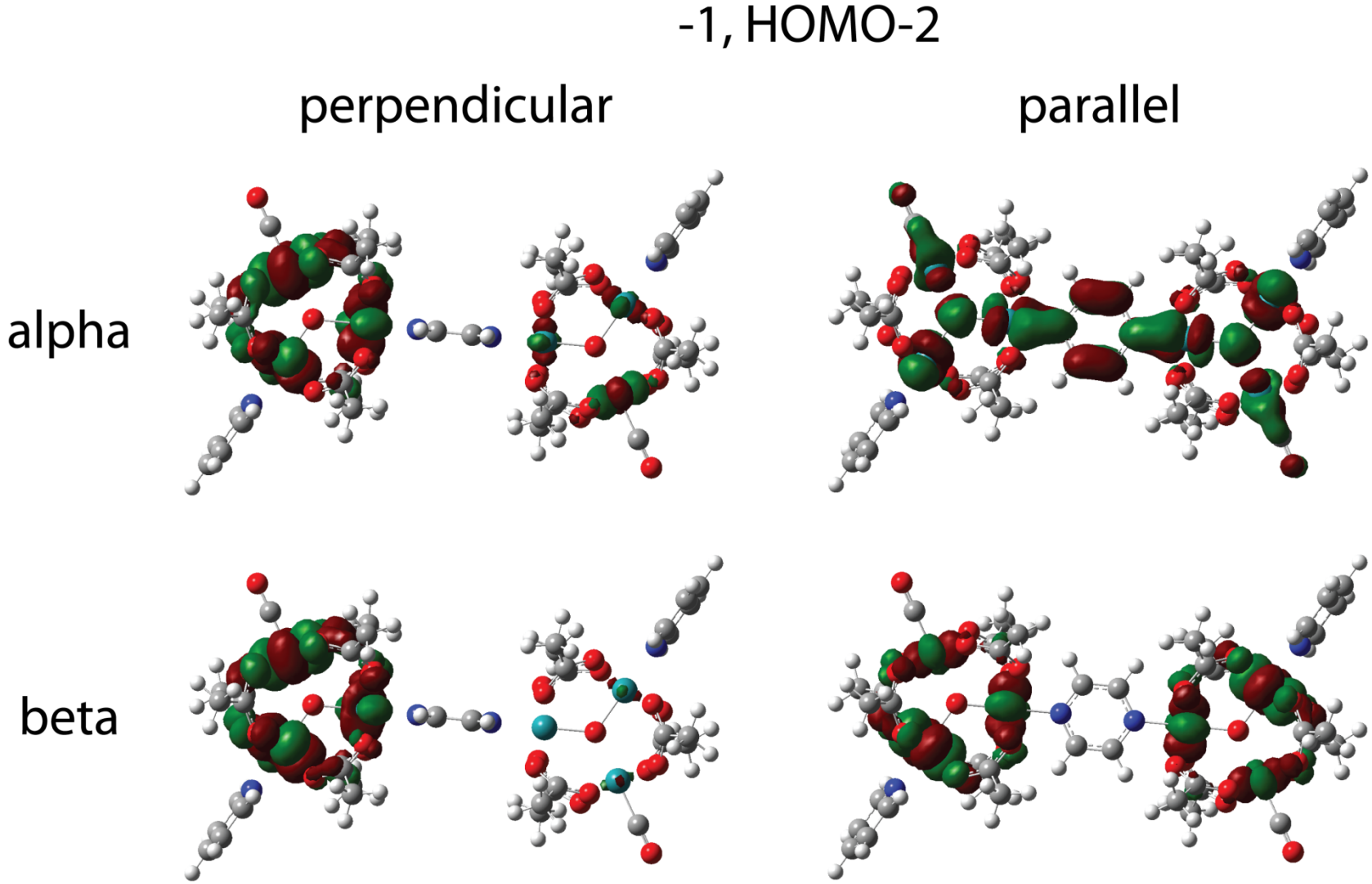

Figure 4.28: Alpha and beta molecular orbitals for the HOMO-2 state of the -1 mixed valence dimers.

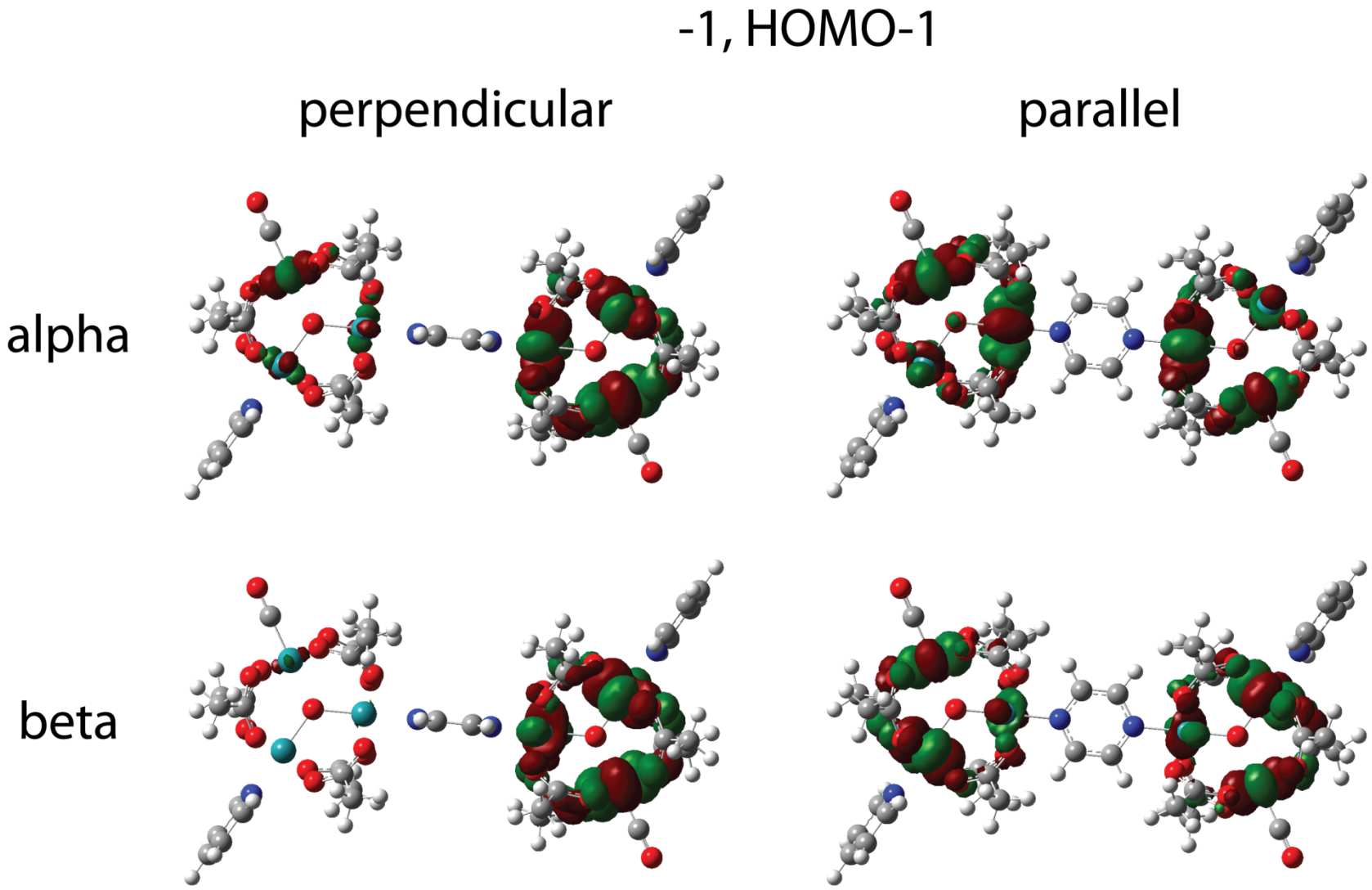

Figure 4.29: Alpha and beta molecular orbitals for the HOMO-1 state of the -1 mixed valence dimers.

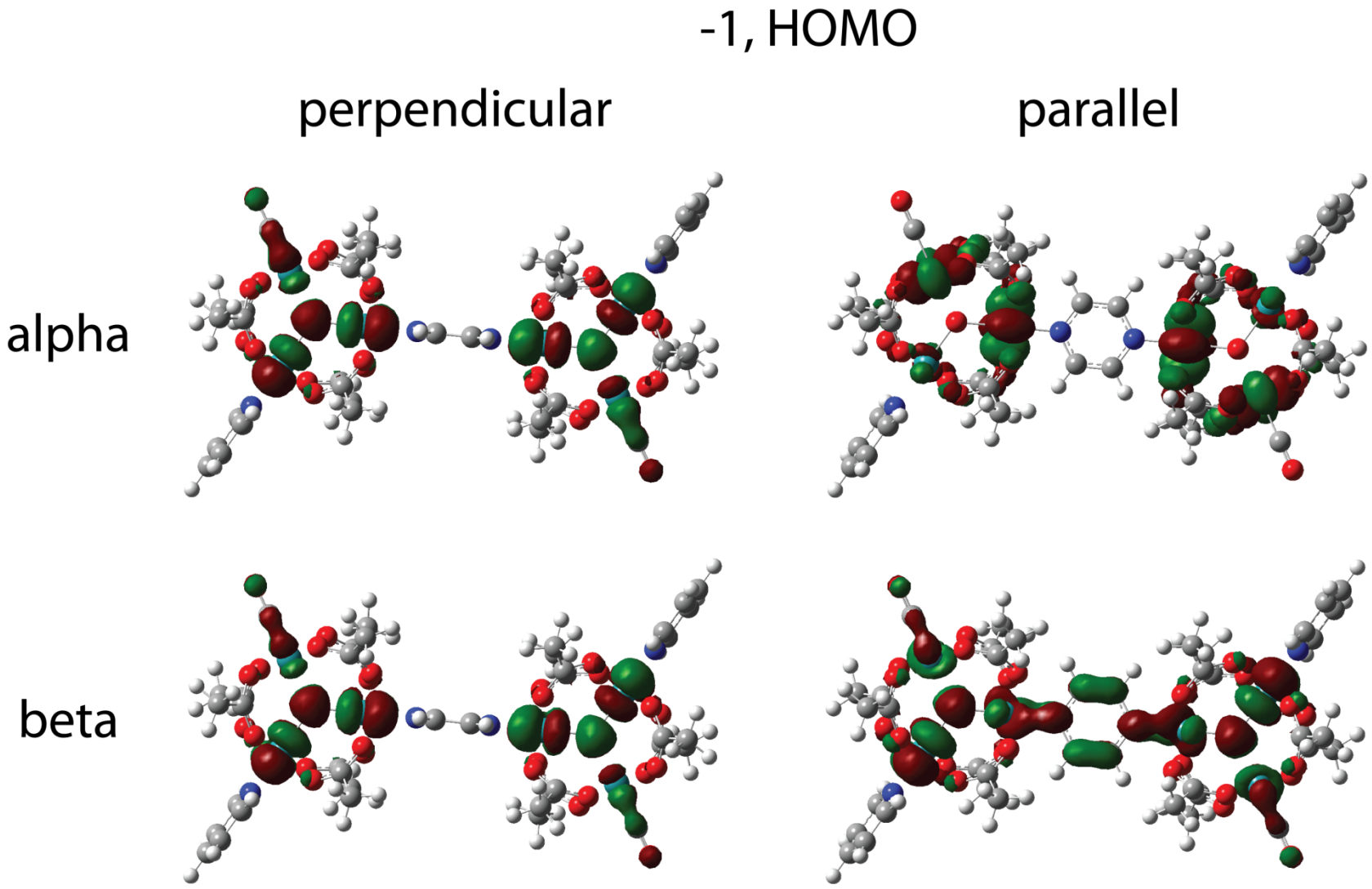

Figure 4.30: Alpha and beta molecular orbitals for the HOMO state of the -1 mixed valence dimers.

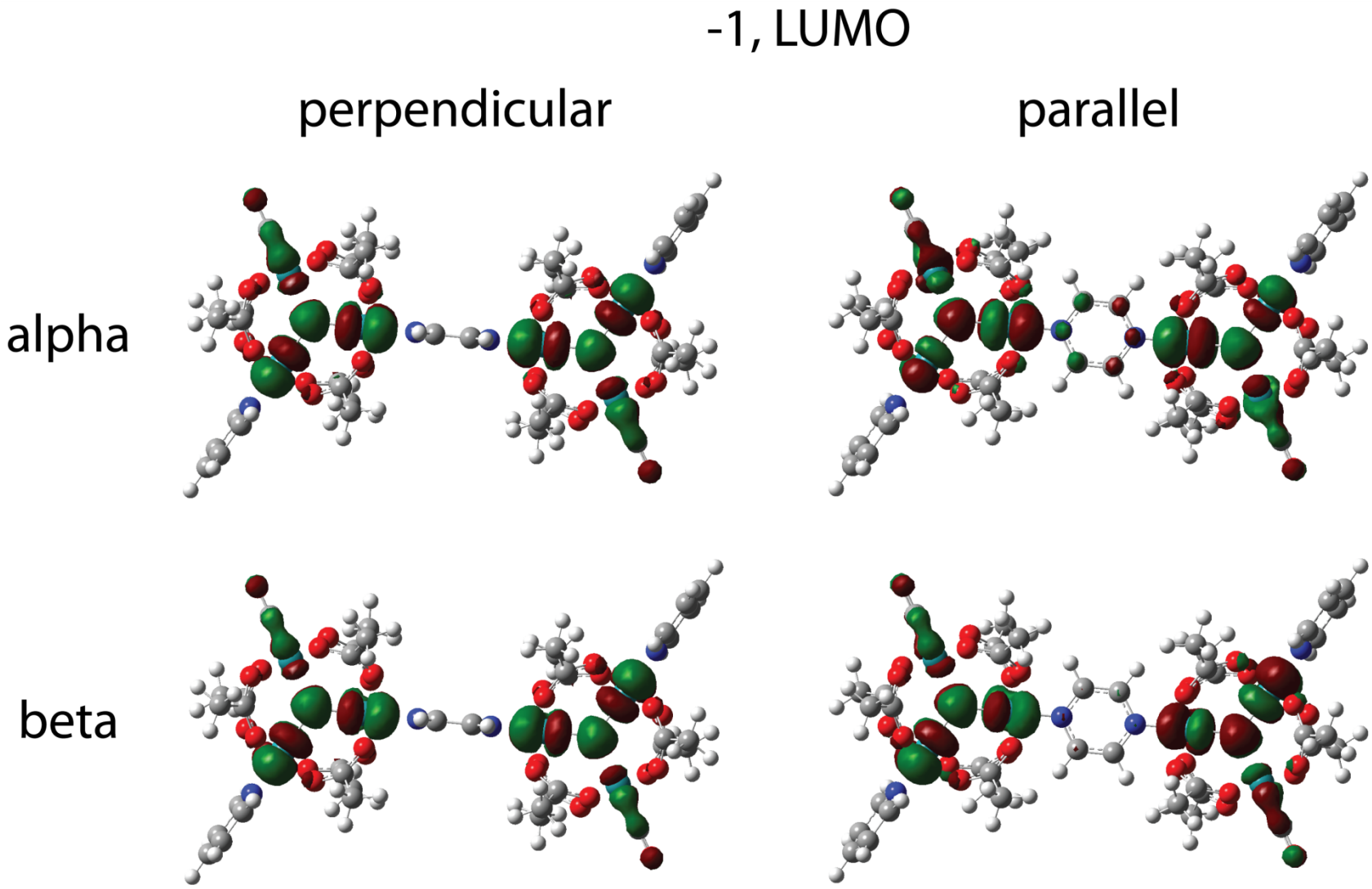

Figure 4.31: Alpha and beta molecular orbitals for the LUMO state of the -1 mixed valence dimers.

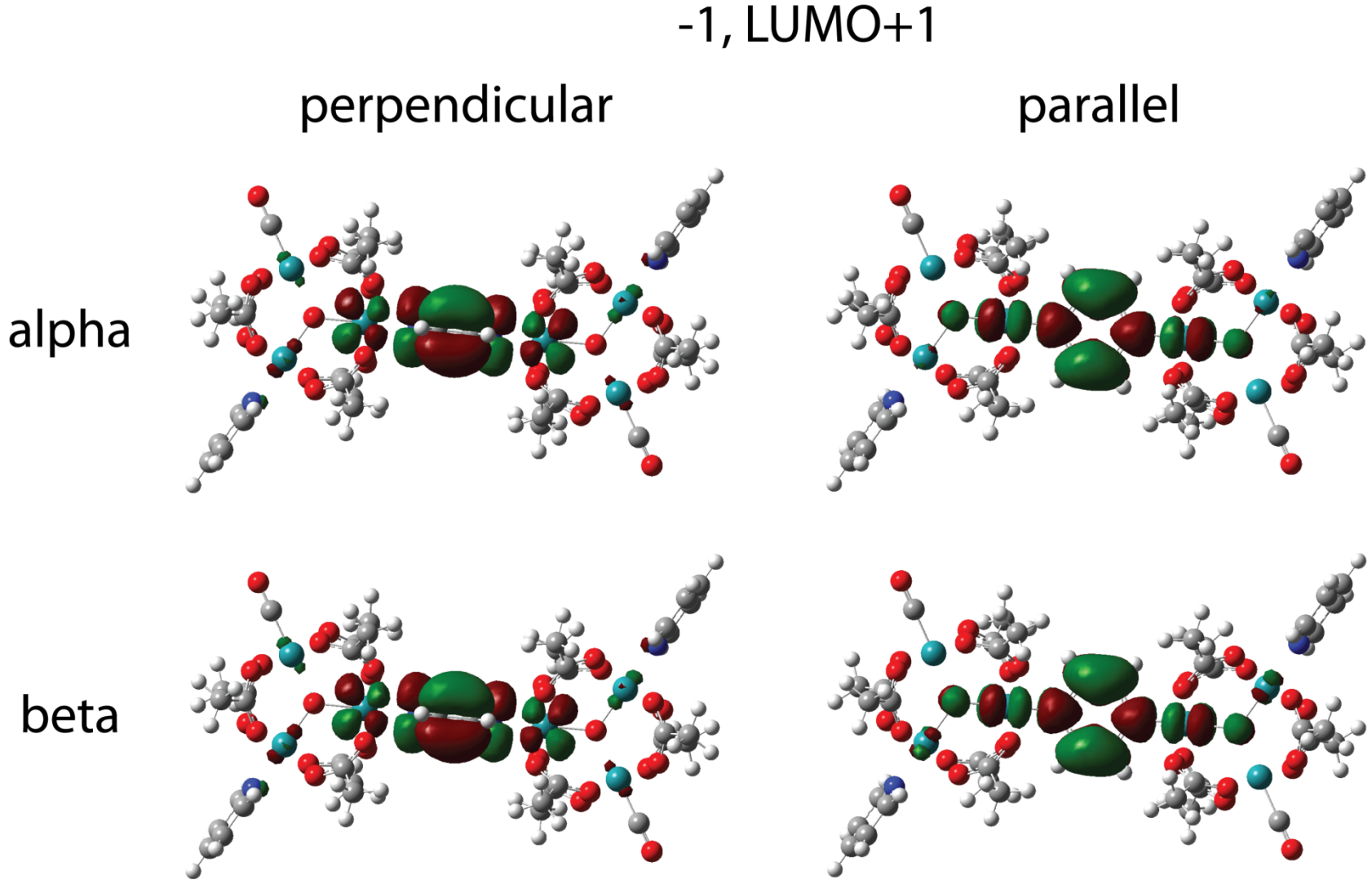

Figure 4.32: Alpha and beta molecular orbitals for the LUMO+1 state of the -1 mixed valence dimers.

4.5 Discussion

The 2D-IR experiments cover a large variety of different compound-solvent combinations and represent nearly the full range of coalescence phenomena associated with these compounds. I focused primarily on the pyrazine bridged dimers since their -1 spectra are generally the most coalesced and sensitive to system changes.

In contrast to the other bridging ligands used in this work, diazabicyclooctane (dabco) and bipyridine (bpy), the pyrazine ligand has a delocalized π system over the full extent of the ligand. The two rings of bipyridine are rotated out of plane from one another, breaking the planarity of the ligand and lowering the interaction of the π systems on the two rings. The bridging ligand length is also approximately doubled in the bpy ligand relative to the pyrazine bridge. The length of diazabicyclooctane is similar to pyrazine, but this bridge has no delocalized π system to facilitate electronic dynamics. As a result, the FTIR spectra of bpy and dabco bridged dimers show very little coalescence. A direct comparison of the -1 spectra of bpy and dabco bridged dimers with the 0 and -2 spectra may show a slight shift of the CO peak center frequencies, but this should not be confused with IR peak coalescence. While the peaks are separated by ca. 50 cm^{-1}, the tails of the peaks overlap slightly. Summing the profiles of both peaks results in a small shift in the frequency of the maximum peak intensity, and the spectrum does not go to baseline between the two peaks. In contrast, the spectra of pyrazine bridged dimers exhibit significantly more overlap than can be explained by a simple summation of the 0 and -2 peaks.

Previous analysis with the Bloch equations led to predicted exchange time constants of less than 1 ps for all of the pyrazine bridged -1 samples in this work. Attempts have been made to make similar predictions for the bpy bridged compounds at close to 10 ps. For these peak splittings, the exchange rate has to be faster than ca. 10 ps to cause any change in the IR spectrum. As mentioned above, the spectral overlap for bpy and dabco bridged dimers can be explained as a simple sum of two peaks without any dynamical contributions. From the outset, it was uncertain if we would observe exchange on the picosecond timescale for the bpy and dabco bridged compounds. For the pyrazine bridged compounds, it was clear that exchange must occur within a few picoseconds to cause such a high degree of coalescence.

Prior to considering the dynamics of the mixed valence species, it is useful to see how the two CO ligands interact with one another in the absence of exchange. The Kubiak lab synthesized isotopically labeled dimers with either a $^{13}C^{16}O/^{12}C^{16}O$ (singly labeled) or $^{13}C^{18}O/^{12}C^{16}O$ (doubly labeled) configuration. In both labeled compounds, one CO ligand has natural isotopes and the other has either one or both atoms of the ligand labeled. The heavier CO ligand will vibrate with a lower frequency due to a Hooke's law type relationship between frequency and mass. The singly labeled compounds provide a similar frequency splitting between ligands as the weakly coalesced mixed valence samples. These isotopically labeled compounds provide us with the opportunity to observe any communication between the two ligands such as intramolecular vibrational redistribution (IVR) or anharmonic coupling that could interfere with the measurement of true exchange dynamics. In these experiments, there is no ligand exchange; simply the frequency of each vibration should change if the electron density near the ligand changes. We want the vibrational excitation to stay localized in one ligand so that any changes in frequency can be correlated to changes in electron position rather than migration of vibrational energy between the two ligands. 2D-IR spectra of compounds 1* and 3* are

presented in Figures 4.2 and 4.3. No crosspeak growth is observed in either of these sets of 2D-IR spectra. This is not very surprising in light of the large distance, through space (>16Å) or through bond (11 bonds), between the two ligands. No vibrational dynamics *between* the CO ligands are expected for any of the samples.

This lack of communication is advantageous for these experiments and deserves further comment. The two ligands in these compounds are completely isolated from one another. Communication between vibrations in a chemical exchange 2D-IR experiment is usually undesirable. In the case of geometric transformation, one vibration may *become* another vibration by physically moving the atoms from one location to another.[94,95] In the case of an environmental transformation, such as a change in electron density (this work) or the coordination of a hydrogen bonding species,[96,97] the vibrational frequency simply changes as the surroundings change. These experiments require a vibrational label to be imparted to the vibration of interest. The frequency of the labeled vibration is monitored over time and any changes can be correlated with either a change in geometry or environment. If the vibrational label does not remain local, either by anharmonic coupling or redistribution to other vibrations, the frequency of the label can change in the absence of exchange. If two vibrations are highly coupled, it is difficult, if not impossible, to separate any exchange dynamics from the vibrational communication.

More specific to this experiment, the exchange and coalescence phenomenon is fundamentally a one CO ligand process. The exact same spectral coalescence phenomena would be observed even if there was only one CO ligand on the molecule. This is effectively shown in isotopically labeled mixed valence samples.[44,45,48] The spectrum is split into two pairs of coalesced peaks, one pair for the unlabeled CO and one pair for the labeled CO. There are two possible electronic configurations at each local CO vibration yielding two possible frequencies for each individual CO ligand. For 2D-IR measurements, we hope to measure the change in frequency of one CO ligand at a time. We do not want the other CO ligand to interfere with this measurement.

I have also measured the kinetics of these neutral CO vibrations (Figures 4.9-4.11). The integrated intensities of the peaks decay monoexponentially. I collected the data under magic angle conditions, so the effects of rotational diffusion are not expected to contribute to the dynamics. This monoexponential decay can be assigned to vibrational relaxation. Values for the kinetic fits are collected in Tables 4.1-4.5.

2D-IR spectra for mixed valence compounds 1^{-1}-5^{-1} are presented in Figures 4.4-4.8. The most obvious feature relative to the neutral samples is that the diagonal peak pairs tend to be much closer, particularly for the pyrazine bridged compounds. This is expected from the increased peak coalescence already observed in FTIR spectra. The peak separation for compounds 4^{-} and 5^{-}, the bpy and dabco bridged dimers, is comparable to the neutral compounds. The signal to noise in these samples also tended to be lower than the corresponding neutral samples. The -1 state for all of the 2D-IR experiments was achieved through the addition of a chemical reducing agent (either cobaltocene or decamethyl cobaltocene). The solubility and stability of the -1 compounds is somewhat less than for the neutral compounds. Further, the sample also contains the counter ion of the oxidized cobaltocene. Aside from these two features, the 2D-IR spectra for the mixed valence species are remarkably similar to the neutral compounds. In particular, there is a marked lack of cross peak growth in all samples. The lack of cross peak growth indicates that the frequency of each CO ligand is constant for the duration of

the experiment. In other words, there is no site exchange in the experimentally accessible temporal range.

The kinetics traces for the diagonal peaks of compounds 1^{-1}-5^{-1} are presented in Figures 4.12-4.19 and the associated time constants are also compiled in Tables 4.1-4.5. The average vibrational lifetime for the CO peaks in the -1 samples is ca. 12 ps. One common limitation to 2D-IR spectroscopy is that the experimentally accessible temporal window is limited by the relaxation times of the vibrations of interest. For such large molecules, fast vibrational relaxation times are not surprising due to the large number of degrees of freedom available to dissipate the vibrational label energy. Unfortunately, the small experimental window for these experiments does not allow the observation of cross peak growth. As mentioned above, exchange must be faster than ca. 10 ps to cause any change in the IR spectrum by peak coalescence. The temporal window for these experiments, therefore, *does* allow me to access the full timescale relevant to addressing the phenomenon of peak coalescence. While I was not able to directly measure the rates of site exchange in these mixed valence dimers, there is quite a lot to be learned from the *lack* of exchange.

4.5.1 Lack of Cross Peaks

As a null result, the lack of exchange in these spectra requires further justification. This situation also requires a thorough examination of different ways exchange could manifest itself these spectra. In an ideal situation, vibrational relaxation will be much longer than any of the dynamics of interest. Further, no other relaxation or energy transfer pathways will affect the intensity of the labeled vibration. For our experimental setup, we also do not expect any effects from rotational diffusion. In this hypothetical case, the only dynamics affecting the intensities of the vibrations of interest are the dynamics associated with exchange. At $T_w = 0$, only two peak pairs are present. Since no time has passed for dynamics to occur, the pump and probe frequencies are identical and the two peaks pairs lie on the diagonal. The peak ratios along the diagonal are representative of the equilibrium populations of the two vibrations. Along the probe axis for a given pump frequency, we see only one peak pair reflecting the selective labeling of only one of the two vibrations. As T_w increases, exchange results in a loss of diagonal peak intensity and a corresponding increase in cross peak intensity. Due to detailed balance, at equilibrium the forward and backward reaction rates will be identical and the two cross peak pairs will grow in at the same rate.[96] Eventually, the labeled vibration will achieve an equilibrium population in the two vibrations. After this equilibrium is reached, the spectral slice across the probe axis will be equivalent to the slice through the diagonal. In our case, the two peaks have approximately the same intensity in FTIR. Full equilibration would result in four equal intensity peak pairs.

Another hypothetical situation which is very relevant to these systems is that where exchange is faster than the time resolution of the experiment. This was a specific concern for this project since the predicted time constants for the pyrazine bridged dimers were all less than 1 ps in these solvents. Using a Fabry-Perot interferometer to shape the pump pulse for these experiments stretches the pulse duration and limits the time resolution of the double resonance technique to approximately 1 ps. What would the spectrum look like with 1 ps time resolution and 0.35 ps exchange? In this case, exchange would be occurring within the temporal envelope of the pump pulse. This would prevent our ability to selectively excite only one vibration with

the pump pulse. In effect, the 2D-IR spectrum would appear as fully equilibrated at the earliest delay times. This is clearly not the case for these systems since there is never a significant population in the cross peak regions at any delay time.

In reality, for these compounds, vibrational relaxation occurs before any significant frequency shift in the carbonyl ligands. The intensities of the diagonal peaks decrease without any corresponding increase in the cross peak intensities. Importantly, the higher frequency peak always has a slower relaxation rate than the lower frequency peak. In some of the 2D-IR spectra, weak intensity can be observed in the cross peak region. This intensity does not grow with time. Instead it is likely that these features are a product of the high overlap of the two diagonal peaks. The pump pulse has a finite spectral bandwidth at ca. 15 cm^{-1}. The 2D-IR spectra of all of the mixed valence compounds show two maxima along the diagonal, but all are overlapped at the baseline. It is not possible with this technique to excite only one of the two vibrations. There will always be a small percentage of the second peak excited at most frequencies within the first peak. I refer to this feature as double pumping, since both peaks are pumped at the same time. While this situation is not ideal, as long as the two vibrations are excited by different amounts, we can monitor the evolution of the nonequilibrium labeled intensity. The situation is slightly complicated by the fact that the higher frequency vibration persists for longer than the lower frequency vibration. The double pumped peak at the lower frequency pump position is in the least overlapped of the two cross peak areas. Since this artificial peak is really the higher frequency vibration, it has a longer lifetime than the diagonal peak at this pump frequency. All of the 2D-IR spectra here are normalized to the tallest peak in the spectrum; usually the high frequency diagonal peak. As T_w is increased, the height of the high frequency diagonal peak increases relative to the low frequency diagonal peak. The double pumped peak in the cross peak position appears to grow in, but is actually just increasing in size relative to the low frequency diagonal peak, which is decaying much more rapidly. Despite these small artifact peaks in the cross peak region, the intensity in these regions never appears equilibrated at any delay time.

From the 2D-IR spectra, we can conclude that there is no significant exchange in any sample faster than ca. 15 ps. There is no clear evidence of any degree of site-to-site electron exchange in any of the spectra. Since exchange must be faster than ca. 10 ps to cause *any* coalescence behavior in the FTIR spectrum, this implies that the dynamic IR peak coalescence must have another origin. This also indicates that the Bloch equations are not reliable for predicting the reaction rates for these systems.

4.5.2 On the Origin of Biexponential Kinetics

Upon first inspection, it seems that 2D-IR does not give much more than a null result in the lack of cross peaks. However, we can learn more by examining the time dependent peak amplitudes. I have organized the kinetics traces of the diagonal peaks from several sets of spectra in Figures 4.9-4.21 and their decay time constants in Tables 4.1-4.5. Table 4.1 contains the data for all samples. Tables 4.2-4.5 reorganize the data to draw attention to the correlations, or lack thereof, between different subsets of the data.

All of the data sets can be fit well to either mono- or biexponential decays. As mentioned above, the monoexponential decays can be interpreted as simple vibrational relaxation. No other dynamics have any strong effects on the spectra. The data sets with biexponential decay kinetics are all -1 pyrazine bridged samples. These are also the only samples that show significant peak

coalescence. The bpy and dabco bridged mixed valence compounds, as well as all isovalent compounds, exhibit simple vibrational relaxation fit well to a monoexponential decay.

One possible source for the faster decay component is IVR. The fast time component of the biexponential fits range from 1.64 ± 0.78 ps to 3.08 ± 1.87 ps. These time constants are typical of IVR. IVR is a very structurally sensitive phenomenon. While coupling to the solvent can allow IVR to redistribute energy to slightly higher energy vibrations, it is more often a downhill process. The observation and rates of IVR are largely dictated by the availability of lower frequency vibrations to accept energy from the originally excited vibration. It is not surprising to see IVR in the dynamics of organometallics, especially systems as large as these dimers. It is a little surprising to see IVR in only this subset of the dimers. For the pyrazine bridged compounds, this pathway is not generally available. The 0 and -2 pyrazine bridged compounds do not exhibit this behavior. It is also not a general behavior of the -1 dimers. The -1 bpy and dabco bridged dimers also do not exhibit this behavior. For IVR to be present in these compounds implies that the -1 pyrazine bridged compounds have a unique structural difference that opens up a second, much more efficient, pathway for energy relaxation or redistribution. Another possibility is that two isomers of the -1 pyrazine bridged dimers are present. This possibility implies that the second isomer either has a faster vibrational relaxation rate or its decay is dominated by IVR. The distinction between these two possibilities is primarily in whether or not we have measurable equilibrium populations of multiple structures in the -1 state.

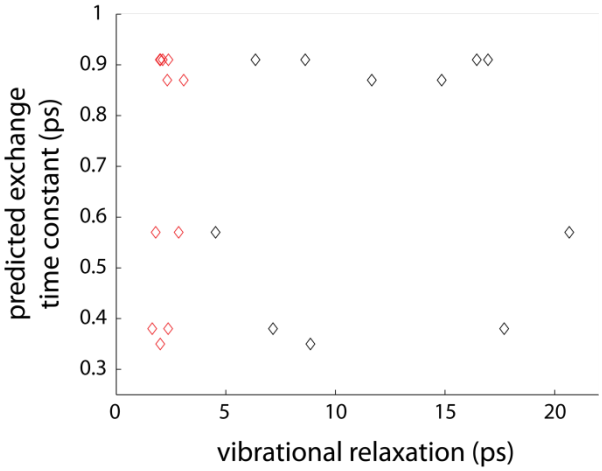

Figure 4.33: Plot of predicted time constant versus peak relaxation time. No correlation is observed between the degree of peak coalescence and the vibrational dynamics.

Another possibility worth mentioning is whether or not the biexponential decays can be correlated in some way to electron transfer. For the -1 pyrazine bridged dimers, the Bloch equations predict exchange times constants less than 1 ps. While the fast components of the biexponential decays are somewhat slower than this, experimental errors in both the FTIR fitting and the 2D-IR measurements, plus uncertainty in the quality of predictions based on peak coalescence, require us to consider this as a possibility. If any of the observed signal decay rates were correlated with electron transfer rates, it would imply that the act of electron transfer is causing simultaneous loss of the vibrational label. The labeled carbonyl ligand is expected to change vibrational frequency as the electron density changes. This should result in loss of diagonal peak amplitude and a concomitant increase in cross peak amplitude. If the vibrational

label is lost during the transfer, no signal would be observed at the new frequency and no cross peak would form. This behavior is *not* expected and previous work with 2D-IR has shown vibrational labels can persist through changes in both geometry and electron distribution. If this scenario were valid, as the electron transfer occurred and the CO frequency shifted, a loss in diagonal peak amplitude would be observed with a rate corresponding to electron transfer.

I have plotted the predicted exchange times against both the slow and fast components of the biexponential fits to the diagonal peak amplitudes from 2D-IR measurements. As can be seen in Figure 4.33, there is very clearly no correlation between the previous rate predictions and the decay rates. If the rate predictions do not represent an actual exchange process, they do at least represent a quantitative measure of the degree of coalescence. This figure can be more meaningfully interpreted as a lack of correlation between the degree of peak coalescence and rates of decay of the vibrational label. If exchange *did* cause peak coalescence, it would have to cause some corresponding decay of the diagonal peak amplitude. Even if electron transfer somehow destroyed the vibrational label and prevented the growth of a cross peak, the destruction of the vibrational label would itself result in decay of the diagonal peak amplitude. If none of the decay rates can be correlated to the degree of peak coalescence, then *electron site exchange cannot be the source of peak coalescence*.

4.5.3 Possible Sources of Peak Coalescence

The 2D-IR results strongly indicate that electron site exchange is too slow to cause IR peak coalescence. Unfortunately, these experiments were not able to give direct information on other possible origins of peak coalescence. Only spectra of the -1 pyrazine bridged dimers show significant coalescence. These same compounds all result in biexponential decays of the diagonal peaks in 2D-IR spectra. As mentioned above, the appearance of biexponential decay is likely a result of some change in structural flexibility, possibly including the presence of a second isomer.

It is a well known property of mixed valence compounds that the bridge connecting donor and acceptor sites has a huge influence on the properties of the system.[28,34,98] My DFT calculations pursued this idea by investigating the effects of bridging ligand orientation. I focused on the simplest of the dimers, compound 2. The crystal structure of a related dimer, where the ancillary ligands are azabicyclooctane and the bridge is pyrazine, indicates that in the ground state structure the two trinuclear ruthenium clusters are approximately planar with the bridge rotated ca. 90° out of the plane. All of my calculations on neutral and -1 dimers agree that this bridge orientation is the lowest energy orientation. I was also able to optimize structures with the bridge in plane with the metal sites. For compound 2^0, this second structure is 4.436 kcal/mol above the ground state structure. This structure should not have a significant population (0.05%) at room temperature according to a simple Boltzmann ratio. However, in 2^{-1}, the energy separation between the two geometries is only 1.356 kcal/mol. This corresponds to 8.9% in the second geometry at room temperature. There is currently no direct experimental evidence for a second isomer; however, based on both the 2D-IR and DFT results it seems very feasible. Future experiments on these compounds may be able to address this more conclusively.

Previous experiments on polymeric systems with conjugated π systems have addressed how intramolecular charge transport depends on the planarity of the conjugated orbital system. The highest intramolecular charge mobility was observed when the π system was planar.

Electron transfer was effectively turned off when a phenyl group in the chain was rotated 90°. Even small rotations of the phenyl group away from 90° made a significant increase in charge mobility.

This idea of a molecular switch is particularly interesting from a device standpoint. Perhaps electron transfer in the ruthenium dimers is effectively turned off in the lower energy structure. Isomerization to the parallel bridged structure may allow much more efficient electron transfer. Even if full exchange between the isomers is not occurring on the timescale of these experiments, fluctuations around the potential minimum could result in some orbital rehybridization and charge "leaking."

DFT calculations also give some support to the idea that a parallel bridge geometry allows more effective intersite communication. DFT typically over-delocalizes electron density for open shell systems, so care must be taken in interpreting the extent of charge distributions from these types of calculations. For all calculations in this work, DFT predicts a symmetric charge distribution in the HOMO with equal density on each metal site. This is obviously unrealistic for the -1 dimers where the presence of two CO peaks in the IR spectrum indicates electronic asymmetry. Figures 23-32 show the frontier orbitals for both geometries of neutral and -1 compound 2. For the -1 open shell calculations, I have included both the alpha and beta molecular orbitals. None of the occupied molecular orbitals for the perpendicular bridged geometry have significant density on the bridging ligand. In the parallel geometry, however, significant contributions from the pyrazine bridge π system contribute to multiple orbitals. Interestingly, the alpha SOMO of the HOMO-2 in the -1 parallel bridged geometry has both high density on the bridge and in the CO π^* orbital. The corresponding orbital of the neutral structure, the HOMO-1 has less orbital density on the bridge and none on the CO ligands. The unoccupied beta SOMO for the HOMO of the parallel bridged -1 structure also has significant orbital density on both the bridge and the CO ligands. A similar orbital density is shared by the counterpart LUMO of the closed shell neutral structure. It is unclear how large, if any, of a contribution this orbital should be expected to make to the actual highest occupied orbital.

These types of calculations are not very reliable for predicting the symmetry of the charge distribution in these compounds; however, the large orbital density on the briding ligand indicates that parallel geometry could facilitate much more efficient electronic communication between the metal sites. The possibility of intersite communication in the HOMO-2 and the HOMO does seem possible, and the participation of the CO ligands in both orbitals indicates that such orbital overlap could influence the CO frequency. The experimental observation of this type of dependence of electron mobility on molecular planarity in polymeric systems mentioned above lends some credence to this interpretation of the DFT results. Even if we assume that electronic communication between the two metal sites is increased in the parallel geometry, it is difficult to know for sure exactly how, or if, this will affect the relative charge densities at the metal sites. This could lead to much more efficient electron transfer between metal sites, or perhaps true charge delocalization.

Another common example of IR peak coalescence involves the turnstile rotation of iron tricarbonyl diene compounds. The origin of peak coalescence in these systems has been discussed previously in several articles.[16-21] A possible alternative to exchange was suggested by Strauss and has been discussed in detail with regards to peak coalescence in general.[14,15] Rather than full rotation of the tricarbonyl turnstile unit, Strauss suggested that significant coalescence could be also caused by a hindered torsional motion around the equilibrium angle. Intrawell fluctuations around the ground state geometry may result in very similar spectral features to full

interwell exchange between adjacent minima on the ground state potential. Whether the peak coalescence in iron tricarbonyl diene compounds is due to interwell exchange or intrawell fluctuations has not been answered definitively, although the barrier to exchange in some members of this class of molecules is generally accepted as very low.

There has not previously been a reasonable suggestion for an intrawell reaction coordinate for the ruthenium dimers. The hindered bridge rotation suggested by this work provides such a possibility. Experimental evidence in favor of this specific intrawell mechanism would be difficult to find. The apparent lack of exchange in 2D-IR spectra does make this type of intrawell mechanism, or some other fluctuation based mechanism, seem likely.

4.5.4 Argument Against Exchange Intensity

Some previous criticisms of intrawell mechanisms emphasize that frequency shifts of the peaks are not enough to recreate the coalesced lineshape. These discussions usually invoke the idea of "exchange intensity."[19,21,36] If two peaks are simply shifted toward one another, the intensity between the two peaks is less than that predicted for exchanging coalesced peaks. This is often provided as proof that the experimental coalesced lineshapes cannot be properly fit by only two nonexchanging peaks and a third peak must be introduced to fit the experimental lineshape. This is not only wrong, but extremely misleading. Peak coalescence involves not only peak shifts, but also an increase in peak width. It is true that simulating a spectrum with only peak shifts does not recreate a dynamically coalesced lineshape. The purpose of the "exchange intensity" peak is primarily to increase the peak widths to match coalesced lineshape. Another approach is to simply increase the Gaussian width of the peaks. Gaussian lineshapes correspond to inhomogeneous broadening, representing the fact that the solute has a statistical distribution of possible environments and, therefore, frequencies. If a molecule is undergoing large enough fluctuations to make a significant impact on the peak frequencies, it is not only reasonable, but expected, that some increase in inhomogeneous broadening will be apparent. The possibility of increased inhomogeneous broadening for these types of mechanisms should not be ignored. While this extra intensity is expected for, and can be a sign of, exchange induced coalescence, more information is needed to prove the presence of interwell dynamics.

With the IR simulation program, Zoerbex,[87] I have compared dynamically coalesced exchanging lineshapes with static overlapping peaks. In all cases, a reasonable match could be found with only two peaks. Figure 4.34 presents this comparison for two sets of exchanging peaks. In the left two panels, lineshapes are shown in black for two peaks separated by 50 cm^{-1} with initial Voigt profiles having FWHM values of 13 cm^{-1} for both the Lorentzian and Gaussian contributions. The exchange time constants are listed for each panel. The center two panels show the same Voigt profiles, in red, without exchange effects and shifted toward the center by 40% (30 cm^{-1} peak separation) and 11.2% (44.4 cm^{-1} peak separation). These center panels clearly do not match the exchange averaged lineshapes. The "exchange intensity" argument would simply say that the overlapped peaks do not match the exchanging peaks and that the corresponding intrawell mechanism was invalid. However, if we introduce additional inhomogeneous broadening due to a distribution of fluctuating geometries, the two nonexchanging peaks match the exchanging peaks quite well.

The argument based on "exchange intensity" has been used in several publications to refute the possibility of an intrawell mechanism.[19,21,36] A thorough discussion of possible peak

broadening mechanisms does not usually accompany the presentation. A full comparison of possible inter- and intrawell mechanisms must include details on both peak shifts and peak broadening. In the case of the mixed valence dimers, it is feasible that intrawell fluctuations in geometry could cause fluctuations in the electron density at each site and increase the statistical distribution of electron density and, therefore, CO frequency. A secondary point is related to the fact that the "exchange intensity" peaks are usually modeled as much smaller peaks at a central frequency. For the dimers, the possibility of a more highly electronically communicating second isomer with a population of ca. 9% could also introduce an actual third peak with a central frequency. If the second isomer were completely delocalized, the peak would also have contributions from both of the equivalent CO ligands, doubling the contribution of such an isomer to the overall lineshape relative to the two single CO peaks. While such a scenario is speculative, the presence of a second isomer with more active bridge participation makes this possibility worth consideration.

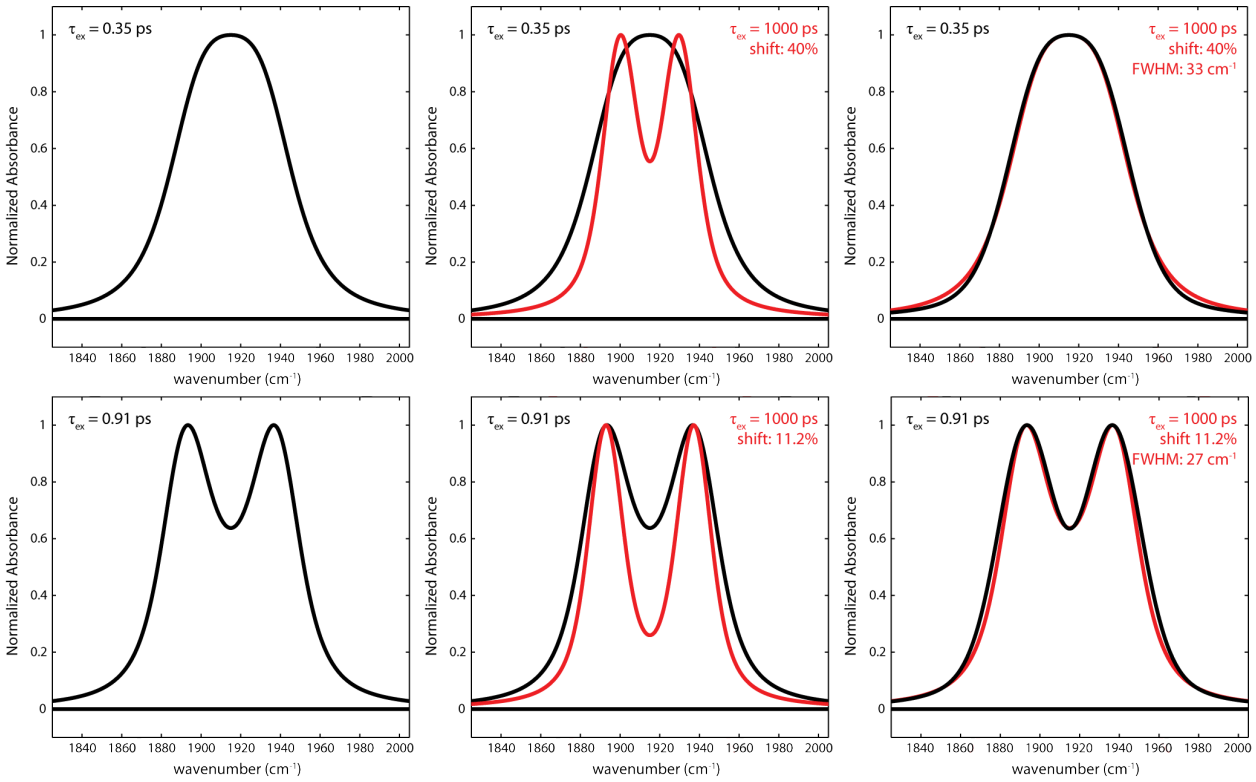

Figure 4.34: Simulated comparison of exchange averaged peaks (black) using the Bloch equations and similar lineshapes of two overlapping Voigt peaks (red) with and without additional inhomogeneous broadening.

4.6 Conclusions

The initial goal of this project was both to assess the validity of the Bloch equations in describing the electron dynamics of the mixed valence dimers, as well as to measure these dynamics directly with 2D-IR. The lack of electron transfer during the experimental window afforded by this technique and during the temporal window for coalescence dictated by the Bloch

equations allows me to readily comment on the first objective. Quantitative analysis of coalesced IR lineshapes with the Bloch equations is *not* a reliable method. There are simply too many alternate sources of frequency shifts and peak broadening to be confident in this method. In this case, no electron site exchange was observed despite predictions that the process proceeds in less than 1 ps.

The observation of tunable coalescence in the lineshapes of these compounds may still have qualitative merit. The increase in peak coalescence does genuinely seem correlated to the electronic dynamics. In particular, the correlation between solvent relaxation times and peak coalescence is worth addressing. If increases in peak coalescence are related to an increase in the magnitude of charge fluctuations, faster solvent relaxation times could help facilitate larger amplitude or faster fluctuations. Increases in the electronic coupling between metal sites could also contribute to larger fluctuations and more coalesced lineshapes. This could explain the spectral dependence on the identity of the ancillary ligands. If a second, more highly delocalized isomer is present in solution, the fluctuations could also represent a balance between the geometric stability of the lower energy isomer versus the resonance stability afforded by a delocalized electron distribution.

Although 2D-IR did not directly measure exchange in these systems, the interpretation of coalescence in the absence of exchange gives new insight into several possibilities for a revised description of the ground state electron dynamics for the dimers. It is possible that full site-to-site electron transfer is much slower than previously anticipated. Future work may allow a more direct measurement of the timescale of any electron transfer as well as offer a more definitive description of the origin of peak coalescence.

Chapter 5

Ground State Isomerization of $Ru(S_2(CCF_3)_2)(PPh_3)_2CO$

5.1 Introduction

Vibrational peak coalescence is most often associated with ultrafast geometrical rearrangements. The most well known example is the turnstile rotation of CO ligands in the class of $Fe(CO)_3(\eta^4$-diene) compounds.[16-21] A different type of mechanism has been suggested as the source of peak coalescence in a similar compound, $Ru(S_2(CCF_3)_2)(PPh_3)_2CO$.[99-103] This compound has two dominant isomers, both with a square pyramidal geometry. The CO ligand is in a different position for the two isomers and is a convenient IR probe of their relative populations. Liquid phase IR spectra of this compound are very sensitive to changes in temperature and solvent, and the relative intensities of the CO stretches can be used to determine the equilibrium constants for isomerization. More interestingly, this system shows a range of peak coalescence, indicating that the equilibrium exchange between isomers may be ultrafast. As mentioned previously 2D-IR is uniquely suited to studying ultrafast reactions at thermal equilibrium. Unfortunately, in dichloromethane the peaks are too highly coalesced to resolve the features in the 2D spectrum. Slightly better peak resolution is possible in several nitrile solvents, but the solubility is too low to collect useful 2D-IR spectra.

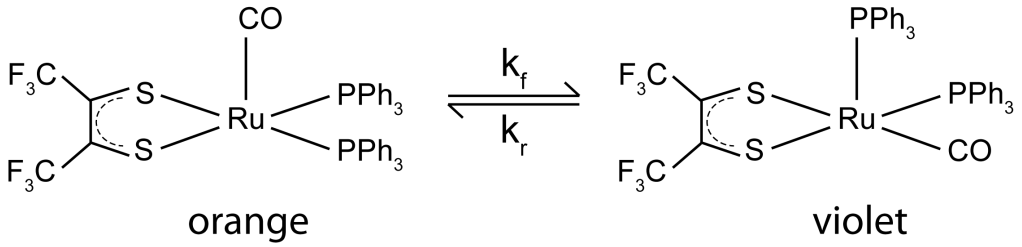

Figure 5.1. The orange and violet isomers of $Ru(S_2(CCF_3)_2)(PPh_3)_2CO$.

Previous FTIR peak analysis with the Bloch equations suggests that isomerization in dichloromethane proceeds in less than 1 ps.[104] While the 2D-IR results are inconclusive, examination of the crystal structures for the two dominant isomers and ground state DFT calculations shed some light on the isomerization mechanism. Our DFT results are consistent with an ultrafast exchange process, but they do not give direct support to such a mechanism. At present, my calculations for transition state structures of the possible mechanisms have failed to converge.

5.2 Isomerization Mechanism

The geometries of the two isomers of the ruthenium compound have been determined experimentally with x-ray crystallography and discussed in detail previously.[99-102] Tube models of the crystal structures are shown in Figure 5.4 panels A and B. The general structure of both isomers involves square pyramidal coordination to the metal center. Lewis structures of the two isomer do not show the structural details of the triphenylphosphine ligands and can be a little misleading. As drawn in Figure 5.1, it seems that the isomerization involves a turnstile rotation similar to $Fe(CO)_3(\eta^4$-diene) compounds. In reality, a pseudorotation mechanism is much more likely.[103,105] A simple turnstile rotation of the CO and two PPh_3 units requires both PPh_3 propellers to reverse their direction. This can be best seen in 3D with a visualization software package. The Cartesian coordinates for the DFT calculations are included in Appendix A.

A turnstile of the CO and PPh_3 ligands would involve two steps. The propeller direction must reverse, followed by the ligand rotation. Or, these two motions could occur in concert. To investigate this possibility further, I first performed DFT optimizations using the experimental crystal structure coordinates. I then reversed the propeller direction to obtain the intermediate geometry. I denote these second geometries as orange' and violet'. I have drawn all four isomers schematically in Figure 5.2, emphasizing the propeller direction relative to the rest of the molecule.

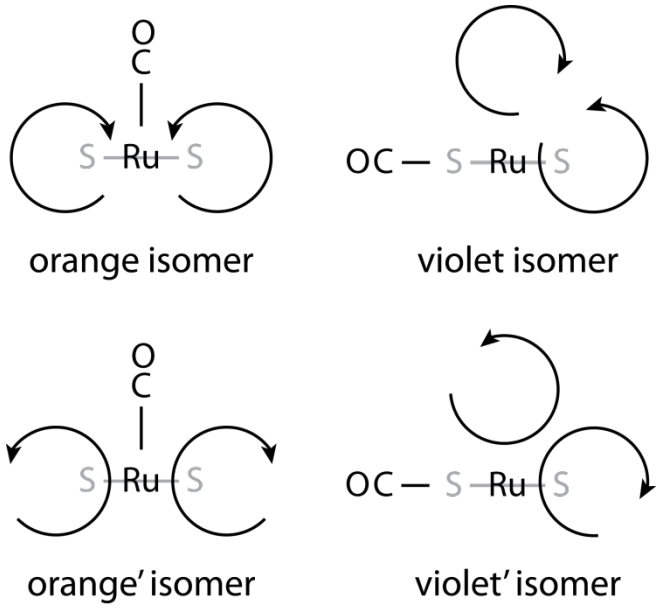

Figure 5.2 Rotation direction of PPh_3 ligand propellers for all four DFT optimized geometries with the dithiolene ligand at the back of the figure and the basal PPh_3 and CO ligands coming out of the plane of the page.

The pseudorotation mechanism from orange to violet can be envisioned as a rotation of the dithiolene ligand to give the molecule a trigonal bipyramidal structure where one dithiolene sulfur atom and one phosphine group are in the axial positions. A rotation of the CO and

dithiolene ligands, similar to a turnstile rotation, past the two PPh_3 ligands forms the square pyramidal geometry of the violet isomer. This mechanism is likely much lower in energy, although it is less immediately apparent based on the Lewis structures alone. The position of the CO ligand relative to the propeller direction is particularly important to properly visualize this mechanism. Relative to the PPh_3 ligands on the orange and violet isomers, the CO ligand must rotate >90° between the two isomers. This mechanism can be difficult to visualize, even with 3-dimensional models. Difficulties in visualizing the fluxional mechanisms of square pyramidal five-coordinated metal complexes has been addressed in multiple

5.3 Two Dimensional Infrared Spectroscopy Results

We collected 2D-IR spectra of $Ru(S_2(CCF_3)_2)(PPh_3)_2CO$ in dichloromethane solvent at room temperature (Figure 5.3). FTIR spectra of the CO vibrations in this solvent are very highly coalesced. In the 2D-IR spectra it is not possible to clearly resolve both peaks along the diagonal. For such highly coalesced 2D-IR spectra, cross peaks at the higher pump frequency may overlap with the v=1→v=2 peaks of the higher frequency vibration. The cross peak at the lower pump frequency is typically less overlapped with other features. In this case, we see some increase in the amplitude of the region in the 2D-IR spectrum corresponding to the lower pump frequency cross peak. With such little peak resolution, reliable kinetics fits are not possible. It is difficult to separate any possible increase in cross peak amplitude from spectral diffusion of the diagonal peaks. Previous analysis of the exchange time constant using the optical Bloch equations have predicted that exchange occurs in less than 1 ps.[104] Spectral diffusion usually occurs on a similar timescale.[61,106,107] The lack of peak resolution, in addition to the similarity in the timescales of these two processes, prevents even a qualitative analysis of these spectra.

Better resolution of the CO peaks for the two isomers is possible in several nitrile solvents such as acetonitrile and n-butyronitrile. Unfortunately, the compound is only very weakly soluble in these solvents and precludes the collection of 2D-IR data. Follow up experiments to this work could focus on indentifying a solvent that allows both high enough solubility and high enough peak resolution to directly measure the exchange process.

This compound was synthesized and provided to me by Starla Glover, a graduate student in the Kubiak lab. This compound is relatively stable. Sample preparation consisted of dissolving crystals of the compound in neat solvent on a lab bench or in a fume hood, depending on the solvent. All samples were loaded into air tight sample cells (*Specac*, 500 μm pathlength CaF_2 windows).

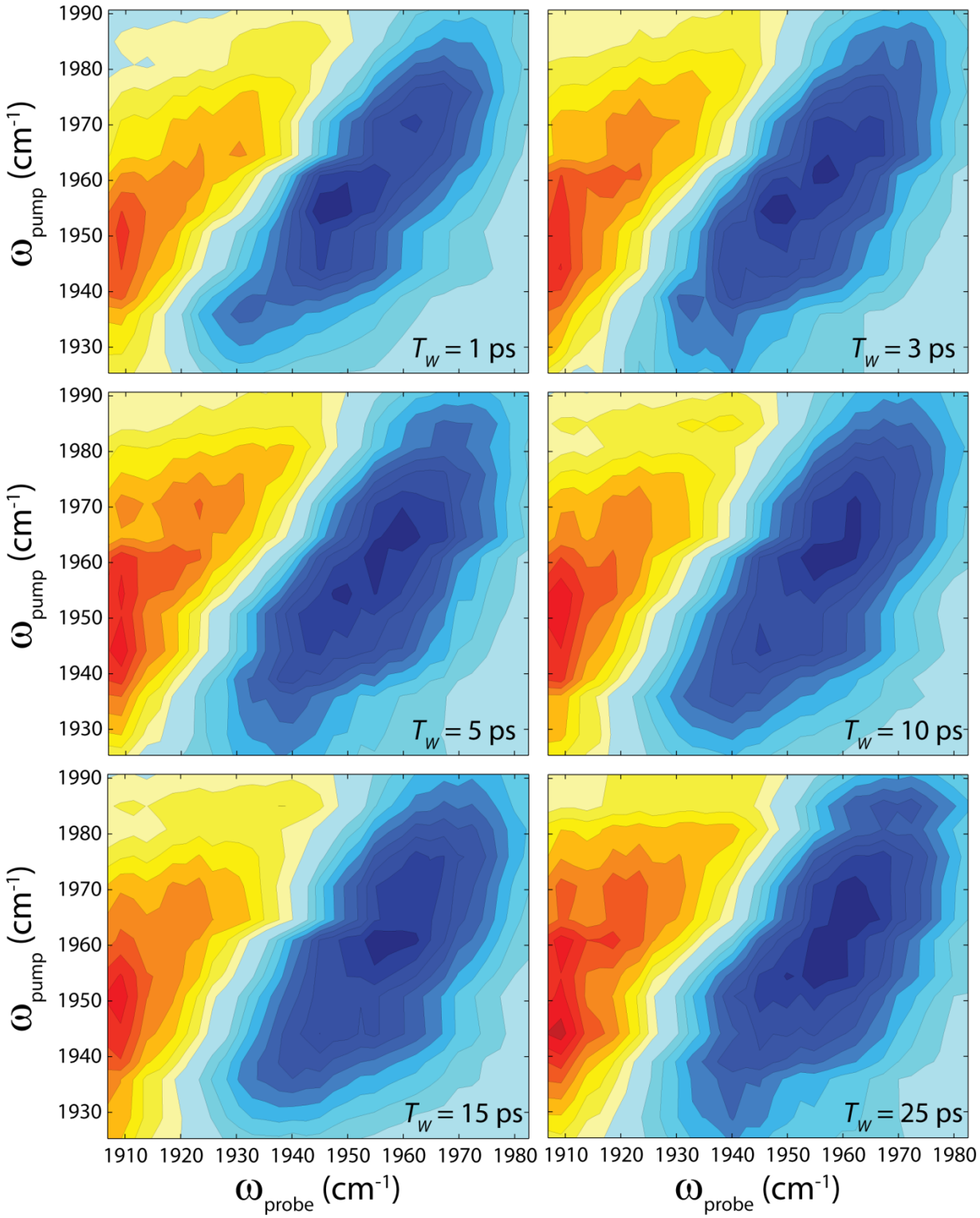

Figure 5.3 2D-IR spectra of $Ru(S_2(CCF_3)_2)(PPh_3)_2CO$ in room temperature dichloromethane.

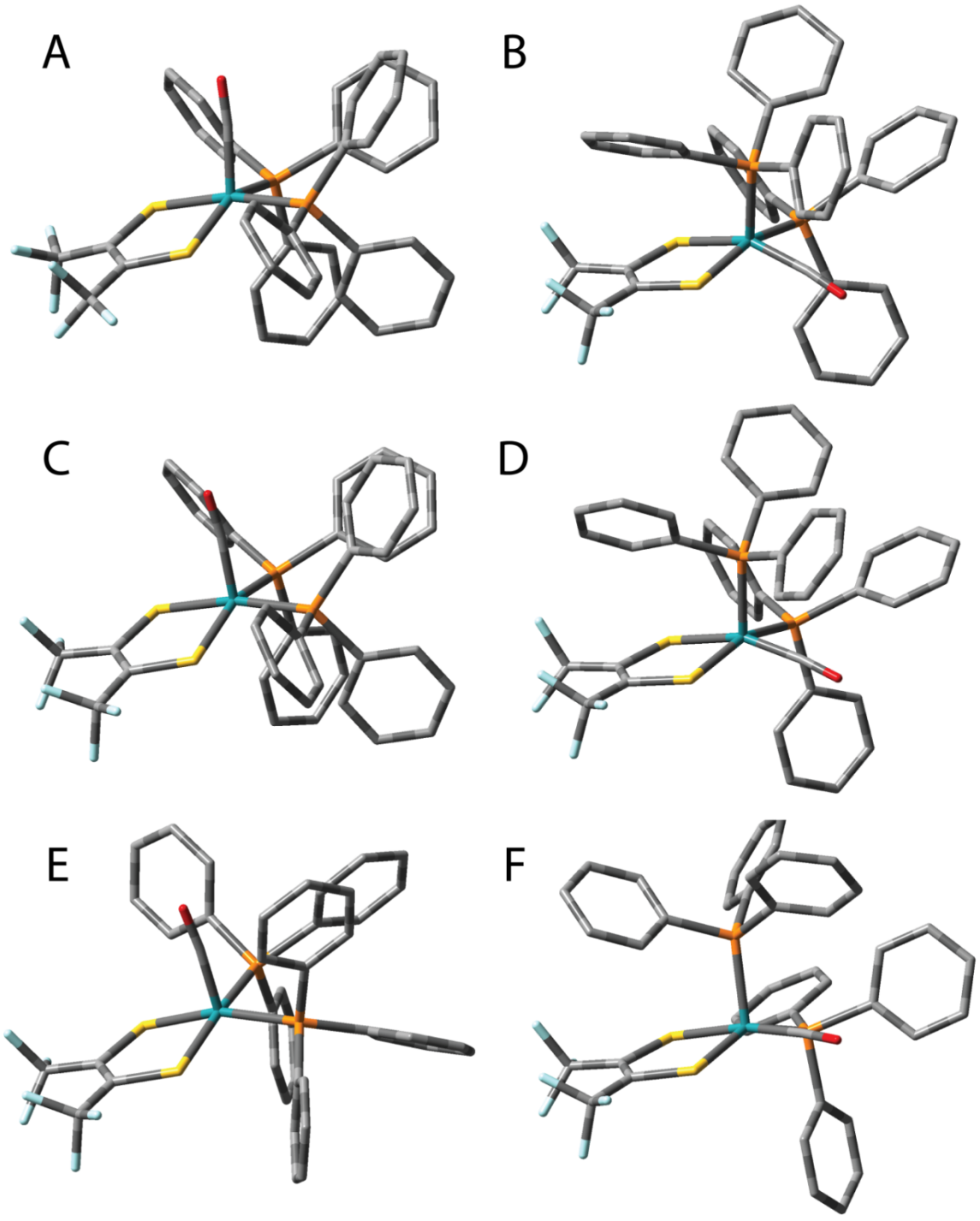

Figure 5.4 Crystal structures and DFT optimized geometries for $Ru(S_2(CCF_3)_2)(PPh_3)_2CO$; crystal structure of the orange isomer from ref. 101 (A), crystal structure of the violet isomer from ref. 102 (B), DFT optimized geometry of the orange isomer (C), DFT optimized geometry of the violet isomer (D), DFT optimized geometry of the orange' isomer (E), and DFT optimized optimized geometry of the violet' isomer (F). Hydrogen atoms are not pictured.

5.4 Density Functional Theory Results

Despite the lack of direct experimental information on the isomerization, there is much to learn from DFT calculations on the isomers of $Ru(S_2(CCF_3)_2)(PPh_3)_2CO$. I used the literature crystal structure coordinates as starting points for these calculations.[101,102] To address the possibility that the mechanism might involve reversal of the PPh_3 propeller direction, I also successfully optimized the geometries of the reversed propeller equivalents of both the orange and violet isomers, denoted as orange' and violet'. All calculations reported in this section were performed in Gaussian 09 using the BP86 functional, the LANL2DZ basis set for Ru, and the 6-31++(d,p) basis set for all other atoms. The relative energies and CO frequencies for each of the four isomers are listed in Table 5.1.

For the orange and violet isomers, the DFT optimized geometries agree qualitatively with the crystal structures. I have included figures of both the literature crystal structures and calculated structures for comparison. The Cartesian coordinates for the DFT structures are listed in Appendix A. The orange' and violet' isomers have not been observed experimentally, and their energies are significantly higher than the other two isomers. The orange and violet isomers are much closer in energy; however, based on these calculations, the orange isomer is more stable.

isomer	energy (kcal/mol)	CO frequency (cm^{-1})
orange	0	1837.02
violet	1.5119	1835.31
orange'	4.8451	1852.56
violet'	3.0698	1852.46

Table 5.1 Relative energies and CO frequencies of the 4 DFT optimized geometries.

5.5 Discussion and Conclusions

The results of this project to date have been largely inconclusive. Experimentally, 2D-IR spectroscopy has been able to offer little quantitative or qualitative information on the isomerization reaction. Theoretically, the reaction coordinate and solvent dependence have been difficult to model. Despite these shortcomings, this system is still very interesting with regards to dynamic IR spectroscopy, and it is worth further investigation to determine the origin of peak coalescence. The compound is not commercially available, and I had a very limited amount of sample to work with. A more thorough study should examine the IR spectra in larger set of solvents. Ideally, a reasonable compromise could be made between peak resolution and solubility. Given that these criteria are met, 2D-IR should be able to measure how much, if any, of the IR lineshape can be attributed to ultrafast site exchange.

DFT calculations may be able to reveal significantly more about the solvent dependence of the IR spectra in these compounds. First, the gas phase ground state energies of the two dominant isomers do not reflect the high solvent dependence of the equilibrium. It is unclear if this type of solvent dependence could be successfully modeled by continuum models such as the conductor like screening model (COSMO).[108] More expensive calculations with explicit solvent

molecules may be necessary. Calculations with techniques such as the growing string method (GSM) may also be more successful in predicting the barrier height to isomerization.[109]

Given that few examples of IR peak coalescence exist in the literature, further work on this system is worthwhile. At the present, theory seems more likely to succeed in predicting a barrier height, but a direct experimental measurement would be most satisfying. Although my results neither support nor refute the possibility that ultrafast site exchange causes coalescence in this system, I emphasize that much care must taken when analyzing spectra with the Bloch equations. As mentioned in Chapter 4, arguments based on "exchange intensity" have little merit. Many sources of inhomogeneous broadening exist to complicate interpretation of the lineshape, and an enhanced intensity between two peaks is, by itself, no proof of exchange. A definitive answer on the origin of peak coalescence and the rates of isomerization in this system will be a welcome addition to our knowledge of IR peak coalescence.

Chapter 6

Conclusions

This work has allowed me to address several fundamental questions on the chemistry and physics of ground state exchange reactions. Most notably, I have been able to evaluate the reliability of using the optical Bloch equations to make quantitative rate predictions from highly coalesced IR spectra. In general, this approach should be avoided and is not a reliable method. For a known rate, one can predict the contributions to the lineshape from exchange; however, separating the exchange contributions to a lineshape from all other contributions and making an accurate estimate of the exchange rate is not generally possible. Further, other sources of peak overlap and broadening may appear to be exchange and lead to incorrect assumptions about both the mechanisms and timescales of reactions. It can be very difficult to find direct evidence to support or refute such assumptions, and ultimately, any conclusions based on IR peak coalescence should be treated with caution. The exact mechanism and rate of electron transfer in the mixed valence ruthenium dimers is still somewhat ambiguous. The lack of exchange in 2D-IR spectra has led me to thoroughly reevaluate possible sources of IR coalescence for this system and to better understand the highly dynamic ground state of this class of molecules. Future work on these systems will be better understood in light of this new paradigm of the electronic ground state and the realization that it is not quite so simple as site-to-site ultrafast electron transfer.

This work has a nice complement in the study of the isomerization of the ruthenium dithiolene compound, $Ru(S_2(CCF_3)_2)(PPh_3)_2CO$. Despite the unreliability of the Bloch equations, it is still possible that peak coalescence in this system is due to ultrafast exchange. This makes another important point regarding dynamic IR spectroscopy. Even if it is not generally reliable, it is still feasible that the Bloch equations can successfully provide qualitative, or perhaps even quantitative, interpretations in some special cases. This inability in distinguishing true exchange coalescence from pseudo-collapse underscores the problem of reliability and is what makes use of the Bloch equations particularly risky. A convincing, but incorrect, interpretation can be based on the results of coalesced IR spectra. It is necessary to confirm the source of coalescence with other methods before fully trusting the results of a Bloch equations analysis. However, if a secondary method could confirm that the Bloch equations provided an accurate analysis, the secondary method would be superior and leave the Bloch equations approach unnecessary. Ultimately, this suggests that the Bloch equations are not generally applicable in IR spectroscopy and their use must be carefully evaluated on a case by case basis. Given the rarity of IR timescale coalescence and the lack of generality, the approach is best suited as an instructional exercise rather than a useful experimental tool.

Exact details on the mechanisms and timescales of exchange in the challenging systems presented in this work may be accessible through other techniques. Improvements in theoretical methods will certainly benefit the understanding of mixed valence compounds in general. More advanced spectroscopic techniques may also be able to experimentally address these reactions

with more definitive details on the time evolution of both the geometry and electron density. These future directions represent exciting possibilities for the better understanding of ultrafast ground state dynamics.

References

1. Sandström, J., *Dynamic NMR Spectroscopy*. Academic Press: London, 1982.
2. Gutowsky, H. S.; Holm, C. H., Rate Processes and Nuclear Magnetic Resonance Spectra. II. Hindered Internal Rotation of Amides. *Journal of Chemical Physics* **1956,** *25* (6), 1228-1234.
3. Thakur, A. J.; Das, S.; Phukan, A. K., Replay of Amide Type Resonance in 6-[(dimethylamino)methylene]1,3-dimethylaminouracil: A Dynamic NMR and Density Functional Theory Study. *Journal of Molecular Structure* **2009,** *929* (1-3), 134-140.
4. Bain, A. D., Chemical Exchange in NMR. *Progress in Nuclear Magnetic Resonance Spectroscopy* **2003,** *43* (3-4), 63-103.
5. Cahoon, J. F.; Sawyer, K. R.; Schlegel, J. P.; Harris, C. B., Determining Transition-State Geometries in Liquids Using 2D-IR. *Science* **2008,** *319* (5871).
6. Cotton, F. A.; Danti, A.; Waugh, J. S.; Fessenden, R. W., Carbon-13 Nuclear Resonance Spectrum and Low-Frequency Infrared Spectrum of Iron Pentacarbonyl. *Journal of Chemical Physics* **1958,** *29* (6).
7. Spiess, H. W.; Grosescu, R.; Haeberle.U, Molecular Motion Studied by NMR Powder Spectra. II. Experimental Results for Solid P_4 and Solid $Fe(CO)_5$. *Chemical Physics* **1974,** *6* (2).
8. Macphail, R. A.; Snyder, R. G.; Strauss, H. L., Motional Collapse of Methyl Group Vibrational Bands. *Journal of the American Chemical Society* **1980,** *102* (11).
9. Corn, R. M.; Strauss, H. L., An Infrared Study of the Dynamics of Weakly Bound Water in Crystalline Hydrates. *Journal of Chemical Physics* **1982,** *76* (10).
10. Macphail, R. A.; Snyder, R. G.; Strauss, H. L., The Motional Collapse of the Methyl C-H Stretching Vibration Bands. *Journal of Chemical Physics* **1982,** *77* (3).
11. Macphail, R. A.; Strauss, H. L., Can the Bloch Equations Describe the Vibrational Spectra of a Reacting Molecule? *Journal of Chemical Physics* **1985,** *82* (3).
12. Sension, R. J.; Strauss, H. L., The Far Infrared Spectra of IBr Charge-Transfer Complexes. *Journal of Chemical Physics* **1987,** *86* (12).
13. Wood, K. A.; Strauss, H. L., The Integrated Intensities of Chemically-Exchanging Vibrational Bands as Given by the Bloch Equations. *Berichte der Bunsengesellschaft für Physikalische Chemie* **1989,** *93* (5).
14. Wood, K. A.; Strauss, H. L., Broadening and Shifts of Vibrational Bands Due to the Effect of Thermal Chemical Reactions. *Journal of Physical Chemistry* **1990,** *94* (15), 5677-5684.
15. Strauss, H. L., Changes of the Carbonyl Stretching Spectra with Temperature. *Journal of the American Chemical Society* **1992,** *114* (3).
16. Grevels, F. W.; Jacke, J.; Klotzbucher, W. E.; Kruger, C.; Seevogel, K.; Tsay, Y. H., Dynamic Processes on the IR Time Scale: Coalescence of CO Stretching Vibrational Bands

in [(η^4-Diene)Fe$(CO)_3$] Complexes. *Angewandte Chemie International Edition in English* **1987,** *26* (9).
17. Grevels, F. W.; Jacke, J.; Seevogel, K., Dynamics of Metal Carbonyls on the Infrared Time Scale: Coalescence of CO Stretching Vibrational Bands. *Journal of Molecular Structure* **1988,** *174*.
18. Turner, J. J.; Grevels, F. W.; Howdle, S. M.; Jacke, J.; Haward, M. T.; Klotzbucher, W. E., Dynamic IR Spectroscopy: Occurrence and Predictability of Coalescence in the CO Stretching Vibrations of ^{13}CO-Enriched Tricarbonyl(η^4-norbornadiene)iron. *Journal of the American Chemical Society* **1991,** *113* (22).
19. Turner, J. J.; Gordon, C. M.; Howdle, S. M., Infrared Spectral Features Due to Very Rapid Fluxional Motion: Changes in the Infrared Carbonyl Stretching Spectra of Tricarbonyl(η^4-norbornadiene)iron with Temperature. *Journal of Physical Chemistry* **1995,** *99* (49).
20. Grevels, F. W.; Kerpen, K.; Klotzbucher, W. E.; McClung, R. E. D.; Russell, G.; Viotte, M.; Schaffner, K., The Very Low Barrier of CO Site Exchange in Tricarbonyl(η^4-1,5-cyclooctadiene)iron: Picosecond Kinetics in Solution Investigated by Line Shape Simulation of the ν(CO) IR Bands and Complementary Evidence from the Course of 13CO Incorporation in a Low-Temperature Matrix. *Journal of the American Chemical Society* **1998,** *120* (40).
21. Turner, J. J., Bandwidths. In *Handbook of Vibrational Spectroscopy*, J. Wiley: New York, 2002; Vol. 1.
22. Marcus, R. A.; Sutin, N., Electron Transfers in Chemistry and Biology. *Biochimica Et Biophysica Acta* **1985,** *811* (3), 265-322.
23. Moser, C. C.; Keske, J. M.; Warncke, K.; Farid, R. S.; Dutton, P. L., Nature of Biological Electron Transfer. *Nature* **1992,** *355* (6363), 796-802.
24. Jortner, J., Temperature Dependent Activation Energy for Electron Transfer Between Biological Molecules. *Journal of Chemical Physics* **1976,** *64* (12), 4860-4867.
25. Wasielewski, M. R., Photoinduced Electron Transfer in Supramolecular Systems for Artificial Photosynthesis. *Chemical Reviews* **1992,** *92* (3).
26. Sariciftci, N. S.; Smilowitz, L.; Heeger, A. J.; Wudl, F., Photoinduced Electron Transfer from a Conducting Polymer to Buckminsterfullerene. *Science* **1992,** *258* (5087).
27. Fraysse, S.; Coudret, C.; Launay, J. P., Molecular Wires Built from Binuclear Cyclometalated Complexes. *Journal of the American Chemical Society* **2003,** *125* (19), 5880-5888.
28. Rodriguez Gonzalez, S.; Ruiz Delgado, M. C.; Caballero, R.; De la Cruz, P.; Langa, F.; Lopez Navarrete, J. T.; Casado, J., Delocalization-to-Localization Charge Transition in Diferrocenyl-Oligothienylene-Vinylene Molecular Wires as a Function of the Size by Raman Spectroscopy. *Journal of the American Chemical Society* **2012,** *134* (12), 5675-5681.
29. Farazdel, A.; Dupuis, M.; Clementi, E.; Aviram, A., Electric Field Induced Intramolecular Electron Transfer in Spiro Pi-Electron Systems and Their Suitability as Molecular Electronic Devices. A Theoretical Study. *Journal of the American Chemical Society* **1990,** *112* (11).
30. Hush, N. S., Intervalence-Transfer Absorption. Part 2. Theoretical Considerations and Spectroscopic Data. In *Progress in Inorganic Chemistry; Volume 8*, Cotton, F. A., Ed. John Wiley & Sons, Inc.: 1967; Vol. 8.

31. Piepho, S. B.; Krausz, E. R.; Schatz, P. N., Vibronic Coupling Model for Calculation of Mixed-Valence Absorption Profiles. *Journal of the American Chemical Society* **1978,** *100* (10), 2996-3005.
32. Borshch, S. A.; Kotov, I. N.; Bersuker, I. B., Electron Delocalization in Trinuclear Mixed-Valence Clusters. *Chemical Physics Letters* **1982,** *89* (5), 381-384.
33. Matyushov, D. V.; Voth, G. A., Reorganization Parameters of Electronic Transitions in Electronically Delocalized Systems. 1. Charge Transfer Reactions. *Journal of Physical Chemistry A* **2000,** *104* (27), 6470-6484.
34. Launay, J.-P.; Coudret, C.; Hortholary, C., Three-Centers Models for Electron Transfer Through a Bridge. 1. Potential Energy Surfaces. *Journal of Physical Chemistry B* **2007,** *111* (24), 6788-6797.
35. Ito, T.; Hamaguchi, T.; Nagino, H.; Yamaguchi, T.; Washington, J.; Kubiak, C. P., Effects of Rapid Intramolecular Electron Transfer on Vibrational Spectra. *Science* **1997,** *277* (5326), 660-663.
36. Ito, T.; Hamaguchi, T.; Nagino, H.; Yamaguchi, T.; Kido, H.; Zavarine, I. S.; Richmond, T.; Washington, J.; Kubiak, C. P., Electron Transfer on the Infrared Vibrational Time Scale in the Mixed Valence State of 1,4-Pyrazine- and 4,4'-Bipyridine-Bridged Ruthenium Cluster Complexes. *Journal of the American Chemical Society* **1999,** *121* (19), 4625-4632.
37. Ito, T.; Yamaguchi, T.; Kubiak, C. P., Intramolecular Electron Transfer on the Vibrational Timescale and Rate Constants Estimated by IR Absorption Band Shape Analysis. *Macromolecular Symposia* **2000,** *156*, 269-275.
38. Yamaguchi, T.; Imai, N.; Ito, T.; Kubiak, C. P., A Strongly Coupled Mixed Valence State Between Ru_3 Clusters. Intramolecular Electron Transfer on the Infrared Vibrational Time Scale in a Pyrazine (pz) Bridged Dimer of Triruthenium Clusters, $[\{Ru_3(\mu_3\text{-}O)(\mu\text{-}CH_3CO_2)_6(CO)(abco)\}_2(\mu\text{-}pz)]$ (abco = 1-azabicyclo[2,2,2]octane). *Bulletin of the Chemical Society of Japan* **2000,** *73* (5), 1205-1212.
39. Londergan, C. H.; Salsman, J. C.; Ronco, S.; Dolkas, L. M.; Kubiak, C. P., Solvent Dynamical Control of Electron-Transfer Rates in Mixed-Valence Complexes Observed by Infrared Spectral Line Shape Coalescence. *Journal of the American Chemical Society* **2002,** *124* (22), 6236-6237.
40. Londergan, C. H.; Salsman, J. C.; Ronco, S.; Kubiak, C. P., Infrared Activity of Symmetric Bridging Ligand Modes in Pyrazine-Bridged Hexaruthenium Mixed-Valence Clusters. *Inorganic Chemistry* **2003,** *42* (4), 926-928.
41. Londergan, C. H.; Kubiak, C. P., Vibronic Participation of the Bridging Ligand in Electron Transfer and Delocalization: New Application of a Three-State Model in Pyrazine-Bridged Mixed-Valence Complexes of Trinuclear Ruthenium Clusters. *Journal of Physical Chemistry A* **2003,** *107* (44), 9301-9311.
42. Londergan, C. H.; Rocha, R. C.; Brown, M. G.; Shreve, A. P.; Kubiak, C. P., Intervalence Involvement of Bridging Ligand Vibrations in Hexaruthenium Mixed-Valence Clusters Probed by Resonance Raman Spectroscopy. *Journal of the American Chemical Society* **2003,** *125* (46), 13912-13913.
43. Londergan, C. H.; Kubiak, C. P., Electron Transfer and Dynamic Infrared-Band Coalescence: It Looks Like Dynamic NMR Spectroscopy, but a Billion Times Faster. *Chemistry - A European Journal* **2003,** *9* (24), 5962-5969.

44. Ito, T.; Imai, N.; Yamaguchi, T.; Hamaguchi, T.; Londergan, C. H.; Kubiak, C. P., Observation and Dynamics of "Charge-Transfer Isomers". *Angewandte Chemie International Edition* **2004,** *43* (11).
45. Salsman, J. C.; Kubiak, C. P., Mixed Valence Isomers. *Journal of the American Chemical Society* **2005,** *127* (8), 2382-2383.
46. Rocha, R. C.; Brown, M. G.; Londergan, C. H.; Salsman, J. C.; Kubiak, C. P.; Shreve, A. P., Intervalence-Resonant Raman Spectroscopy of Strongly Coupled Mixed-Valence Cluster Dimers of Ruthenium. *Journal of Physical Chemistry A* **2005,** *109* (40), 9006-9012.
47. Salsman, J. C.; Ronco, S.; Londergan, C. H.; Kubiak, C. P., Tuning the Electronic Communication and Rates of Intramolecular Electron Transfer of Dimers of Trinuclear Ruthenium Clusters: Bridging and Ancillary Ligand Effects. *Inorganic Chemistry* **2006,** *45* (2), 547-554.
48. Londergan, C. H.; Salsman, J. C.; Lear, B. J.; Kubiak, C. P., Observation and Dynamics of "Mixed-Valence Isomers" and a Thermodynamic Estimate of Electronic Coupling Parameters. *Chemical Physics* **2006,** *324* (1), 57-62.
49. Lear, B. J.; Glover, S. D.; Salsman, J. C.; Londergan, C. H.; Kubiak, C. P., Solvent Dynamical Control of Ultrafast Ground State Electron Transfer: Implications for Class II-III Mixed Valency. *Journal of the American Chemical Society* **2007,** *129* (42), 12772-12779.
50. Glover, S. D.; Lear, B. J.; Salsman, C.; Londergan, C. H.; Kubiak, C. P., Electron Transfer at the Class II/III Borderline of Mixed Valency: Dependence of Rates on Solvent Dynamics and Observation of a Localized-to-Delocalized Transition in Freezing Solvents. *Philosophical Transactions of the Royal Society A* **2008,** *366* (1862), 177-185.
51. Glover, S. D.; Kubiak, C. P., Persistence of the Three-State Description of Mixed Valency at the Localized-to-Delocalized Transition. *Journal of the American Chemical Society* **2011,** *133* (22), 8721-8731.
52. Canzi, G.; Kubiak, C. P., Mixed-Valence Nanoclusters: Fast Electron Transfer in Mixed-Valence Systems with a Gold Nanoparticle as the Bridge. *Small* **2011,** *7* (14), 1967-1971.
53. Canzi, G.; Kubiak, C. P., Ultrafast Electron Transfer Across a Gold Nanoparticle: A Study of Ancillary Ligand and Solvent Influences. *Journal of Physical Chemistry C* **2012,** *116* (11).
54. Morris-Cohen, A. J.; Aruda, K. O.; Rasmussen, A. M.; Canzi, G.; Seideman, T.; Kubiak, C. P.; Weiss, E. A., Controlling the Rate of Electron Transfer Between a Quantum Dot and a Tri-Ruthenium Molecular Cluster by Tuning the Chemistry of the Interface. *Physical Chemistry Chemical Physics* **2012,** *14* (40).
55. Khalil, M.; Demirdoven, N.; Tokmakoff, A., Coherent 2D IR Spectroscopy: Molecular Structure and Dynamics in Solution. *Journal of Physical Chemistry A* **2003,** *107* (27).
56. Kwak, K.; Zheng, J.; Cang, H.; Fayer, M. D., Ultrafast Two-Dimensional Infrared Vibrational Echo Chemical Exchange Experiments and Theory. *Journal of Physical Chemistry B* **2006,** *110* (40).
57. Nee, M. J.; Baiz, C. R.; Anna, J. M.; McCanne, R.; Kubarych, K. J., Multilevel Vibrational Coherence Transfer and Wavepacket Dynamics Probed with Multidimensional IR Spectroscopy. *Journal of Chemical Physics* **2008,** *129* (8).
58. Hamm, P.; Lim, M. H.; Hochstrasser, R. M., Structure of the Amide I Band of Peptides Measured by Femtosecond Nonlinear-Infrared Spectroscopy. *Journal of Physical Chemistry B* **1998,** *102* (31).

59. Cervetto, V.; Helbing, J.; Bredenbeck, J.; Hamm, P., Double-Resonance Versus Pulsed Fourier Transform Two-Dimensional Infrared Spectroscopy: An Experimental and Theoretical Comparison. *Journal of Chemical Physics* **2004,** *121* (12).
60. Shim, S. H.; Strasfeld, D. B.; Ling, Y. L.; Zanni, M. T., Automated 2D IR Spectroscopy Using a Mid-IR Pulse Shaper and Application of This Technology to the Human Islet Amyloid Polypeptide. *Proceedings of the National Academy of Sciences of the United States of America* **2007,** *104* (36), 14197-14202.
61. Kumar, S. K. K.; Tamimi, A.; Fayer, M. D., Comparisons of 2D IR Measured Spectral Diffusion in Rotating Frames Using Pulse Shaping and in the Stationary Frame Using the Standard Method. *Journal of Chemical Physics* **2012,** *137* (18), 9.
62. Crabtree, R. H., *The Organometallic Chemistry of the Transition Metals*. 4th ed.; John Wiley & Sons, Inc.: Hoboken, New Jersey, 2005.
63. Shanoski, J. E. Ph.D. Thesis. University of California, Berkeley, 2006.
64. Sawyer, K. R. Ph.D. Thesis. University of California, Berkeley, 2008.
65. Hamm, P.; Kaindl, R. A.; Stenger, J., Noise Suppression in Femtosecond Mid-Infrared Light Sources. *Optics Letters* **2000,** *25* (24).
66. Cahoon, J. F. Ph.D. Thesis. University of California, Berkeley, 2008.
67. Born, M.; Wolf, E., *Principles of Optics*. 7 ed.; Cambridge University Press: Cambridge, 1999.
68. Becke, A. D., Density-Functional Exchange-Energy Approximation with Correct Asymptotic Behavior. *Physical Review A* **1988,** *38* (6).
69. Perdew, J. P., Density-Functional Approximation for the Correlation Energy of the Inhomogeneous Electron Gas. *Physical Review B* **1986,** *33* (12).
70. Frisch, M. J.; Trucks, G. W.; Schlegel, H. B.; Scuseria, G. E.; Robb, M. A.; Cheeseman, J. R.; Scalmani, G.; Barone, V.; Mennucci, B.; Petersson, G. A.; Nakatsuji, H.; Caricato, M.; Li, X.; Hratchian, H. P.; Izmaylov, A. F.; Bloino, J.; Zheng, G.; Sonnenberg, J. L.; Hada, M.; Ehara, M.; Toyota, K.; Fukuda, R.; Hasegawa, J.; Ishida, M.; Nakajima, T.; Honda, Y.; Kitao, O.; Nakai, H.; Vreven, T.; Montgomery, J. A., Jr.; Peralta, J. E.; Ogliaro, F.; Bearpark, M.; Heyd, J. J.; Brothers, E.; Kudin, K. N.; Staroverov, V. N.; Kobayashi, R.; Normand, J.; Raghavachari, K.; Rendell, A.; Burant, J. C.; Iyengar, S. S.; Tomasi, J.; Cossi, M.; Rega, N.; Millam, J. M.; Klene, M.; Knox, J. E.; Cross, J. B.; Bakken, V.; Adamo, C.; Jaramillo, J.; Gomperts, R.; Stratmann, R. E.; Yazyev, O.; Austin, A. J.; Cammi, R.; Pomelli, C.; Ochterski, J. W.; Martin, R. L.; Morokuma, K.; Zakrzewski, V. G.; Voth, G. A.; Salvador, P.; Dannenberg, J. J.; Dapprich, S.; Daniels, A. D.; Farkas, Ö.; Foresman, J. B.; Ortiz, J. V.; Cioslowski, J.; Fox, D. J., *Gaussian 09, Revision B.1/C.1*. Gaussian, Inc.: Wallingford, CT, 2009.
71. Furche, F.; Perdew, J. P., The Performance of Semilocal and Hybrid Density Functionals in 3d Transition-Metal Chemistry. *Journal of Chemical Physics* **2006,** *124* (4).
72. Buhl, M.; Kabrede, H., Geometries of Transition-Metal Complexes from Density-Functional Theory. *Journal of Chemical Theory and Computation* **2006,** *2* (5), 1282-1290.
73. Dunning, T. H., Jr.; Hay, P. J., Plenum: New York, 1976; Vol. 3.
74. Hay, P. J.; Wadt, W. R., *Ab initio* Effective Core Potentials for Molecular Calculations. Potentials for the Transition Metal Atoms Sc to Hg. *Journal of Chemical Physics* **1985,** *82* (1), 14.

75. Wadt, W. R.; Hay, P. J., *Ab initio* Effective Core Potentials for Molecular Calculations. Potentials for Main Group Elements Na to Bi. *Journal of Chemical Physics* **1985,** *82* (1), 15.
76. Hay, P. J.; Wadt, W. R., *Ab initio* Effective Core Potentials for Molecular Calculations. Potentials for K to Au Including the Outermost Core Orbitals. *Journal of Chemical Physics* **1985,** *82* (1), 12.
77. Ditchfield, R.; Hehre, W. J.; Pople, J. A., Self-Consistent Molecular-Orbital Methods. IX. An Extended Gaussian-Type Basis for Molecular-Orbital Studies of Organic Molecules. *Journal of Chemical Physics* **1971,** *54* (2).
78. Hehre, W. J.; Ditchfield, R.; Pople, J. A., Self-Consistent Molecular Orbital Methods. XII. Further Extensions of Gaussian-Type Basis Sets for Use in Molecular Orbital Studies of Organic Molecules. *Journal of Chemical Physics* **1972,** *56* (5).
79. Hariharan, P. C.; Pople, J. A., Influence of Polarization Functions on Molecular-Orbital Hydrogenation Energies. *Theoretica Chimica Acta* **1973,** *28* (3).
80. Hariharan, P. C.; Pople, J. A., Accuracy of AH_n Equilibrium Geometries by Single Determinant Molecular Orbital Theory. *Molecular Physics* **1974,** *27* (1).
81. Gordon, M. S., The Isomers of Silacyclopropane. *Chemical Physics Letters* **1980,** *76* (1).
82. Francl, M. M.; Pietro, W. J.; Hehre, W. J.; Binkley, J. S.; Gordon, M. S.; Defrees, D. J.; Pople, J. A., Self-Consistent Molecular Orbital Methods. XXIII. A Polarization-Type Basis Set for Second-Row Elements. *Journal of Chemical Physics* **1982,** *77* (7).
83. Binning, R. C.; Curtiss, L. A., Compact Contracted Basis Sets for Third-Row Atoms: Ga-Kr. *Journal of Computational Chemistry* **1990,** *11* (10).
84. Blaudeau, J. P.; McGrath, M. P.; Curtiss, L. A.; Radom, L., Extension of Gaussian-2 (G2) Theory to Molecules Containing Third-Row Atoms K and Ca. *Journal of Chemical Physics* **1997,** *107* (13).
85. Rassolov, V. A.; Pople, J. A.; Ratner, M. A.; Windus, T. L., 6-31G* Basis Set for Atoms K through Zn. *Journal of Chemical Physics* **1998,** *109* (4).
86. Rassolov, V. A.; Ratner, M. A.; Pople, J. A.; Redfern, P. C.; Curtiss, L. A., 6-31G* Basis Set for Third-Row Atoms. *Journal of Computational Chemistry* **2001,** *22* (9).
87. Zoerb, M. C.; Harris, C. B., A Simulation Program for Dynamic IR Spectra, in press. *Journal of Chemical Education* **2012**.
88. Steinfeld, J. I.; Francisco, J. S.; Hase, W. L., *Chemical Kinetics and Dynamics*. 2 ed.; Prentice Hall: Upper Saddle River, NJ, 1998.
89. Stratt, R. M.; Maroncelli, M., Nonreactive Dynamics in Solution: The Emerging Molecular View of Solvation Dynamics and Vibrational Relaxation. *Journal of Physical Chemistry* **1996,** *100* (31).
90. Matyushov, D. V., Non-Ergodic Electron Transfer in Mixed-Valence Charge-Transfer Complexes. *Journal of Physical Chemistry Letters* **2012,** *3* (12), 1644-1648.
91. Ota, K.; Sasaki, H.; Matsui, T.; Hamaguchi, T.; Yamaguchi, T.; Ito, T.; Kido, H.; Kubiak, C. P., Syntheses and Properties of a Series of Oxo-Centered Triruthenium Complexes and Their Bridged Dimers with Isocyanide Ligands at Terminal and Bridging Positions. *Inorganic Chemistry* **1999,** *38* (18), 4070-4078.
92. Lee, N. K.; Park, S.; Yoon, M.-H.; Kim, Z. H.; Kim, S. K., Effect of Ring Torsion on Intramolecular Vibrational Redistribution Dynamics of 1,1'-binaphthyl and 2,2'-binaphthyl. *Physical Chemistry Chemical Physics* **2012,** *14* (2).

93. Wu, Q.; Van Voorhis, T., Direct Calculation of Electron Transfer Parameters Through Constrained Density Functional Theory. *Journal of Physical Chemistry A* **2006,** *110* (29).
94. Zheng, J. R.; Kwak, K.; Asbury, J.; Chen, X.; Piletic, I. R.; Fayer, M. D., Ultrafast Dynamics of Solute-Solvent Complexation Observed at Thermal Equilibrium in Real Time. *Science* **2005,** *309* (5739).
95. Zheng, J.; Kwak, K.; Xie, J.; Fayer, M. D., Ultrafast Carbon-Carbon Single-Bond Rotational Isomerization in Room-Temperature Solution. *Science* **2006,** *313* (5795).
96. Zheng, J. R.; Kwak, K.; Chen, X.; Asbury, J. B.; Fayer, M. D., Formation and Dissociation of Intra-Intermolecular Hydrogen-Bonded Solute-Solvent Complexes: Chemical Exchange Two-Dimensional Infrared Vibrational Echo Spectroscopy. *Journal of the American Chemical Society* **2006,** *128* (9).
97. Rosenfeld, D. E.; Kwak, K.; Gengeliczki, Z.; Fayer, M. D., Hydrogen Bond Migration between Molecular Sites Observed with Ultrafast 2D IR Chemical Exchange Spectroscopy. *Journal of Physical Chemistry B* **2010,** *114* (7).
98. Ratner, M. A., Bridge-Assisted Electron Transfer: Effective Electronic Coupling. *Journal of Physical Chemistry* **1990,** *94* (12), 4877-4883.
99. Miller, J.; Balch, A. L., 1,2-Dithiolene Complexes of Ruthenium and Iron. *Inorganic Chemistry* **1971,** *10* (7).
100. Bernal, I.; Clearfield, A.; Epstein, E. F.; Ricci, J. S., Jr.; Balch, A.; Miller, J. S., Isomeric Conformations in a Pentaco-ordinated Ruthenium Compound; Crystal and Molecular Structures of Orange and Violet Isomers of $(PH_3P)_2[(CF_3)_2C_2S_2]Ru(CO)$. *Journal of the Chemical Society-Chemical Communications* **1973,** (2).
101. Bernal, I.; Clearfield, A.; Ricci, J. S., Jr., Crystal Structure of the Orange Isomer of $[(C_6H_5)_3P]_2[C_2S_2(CF_3)_2]RuCO$. *Journal of Crystal and Molecular Structure* **1974,** *4*, 43-54.
102. Clearfield, A.; Epstein, E. F.; Bernal, I., The Crystal and Molecular Structure of the Violet Isomer of $(\phi_3)_2[(CF_3)_2C_2S_2]RuCO$. *Journal of Coordination Chemistry* **1977,** *6* (4).
103. Holmes, R. R., Five-Coordinated Structures. *Progress in Inorganic Chemistry* **1984,** *32*, 119-235.
104. Glover, S. D. Ph.D. Thesis. University of California, San Diego, 2011.
105. Berry, R. S., Correlation of Rates of Intramolecular Tunneling Processes, with Application to Some Group V Compounds. *Journal of Chemical Physics* **1960,** *32* (3).
106. Demirdoven, N.; Khalil, M.; Tokmakoff, A., Correlated Vibrational Dynamics Revealed by Two-Dimensional Infrared Spectroscopy. *Physical Review Letters* **2002,** *89* (23).
107. Park, S.; Ji, M.; Gaffney, K. J., Ligand Exchange Dynamics in Aqueous Solution Studied with 2DIR Spectroscopy. *Journal of Physical Chemistry B* **2010,** *114* (19).
108. Klamt, A., Conductor-Like Screening Model for Real Solvents: A New Approach to the Quantitative Calculation of Solvation Phenomena. *Journal of Physical Chemistry* **1995,** *99* (7).
109. Peters, B.; Heyden, A.; Bell, A. T.; Chakraborty, A., A Growing String Method for Determining Transition States: Comparison to the Nudged Elastic Band and String Methods. *Journal of Chemical Physics* **2004,** *120* (17).

Appendix A

Contents:

DFT Output Cartesian Coordinates

1) Ruthenium Dimer (Compound 2), perpendicular bridge, neutral 84
2) Ruthenium Dimer (Compound 2), parallel bridge, neutral 87
3) Ruthenium Dimer (Compound 2), perpendicular bridge, -1 90
4) Ruthenium Dimer (Compound 2), parallel bridge, -1 93

5) $Ru(S_2(CCF_3)_2)(PPh_3)_2CO$ orange isomer 96
6) $Ru(S_2(CCF_3)_2)(PPh_3)_2CO$ orange' isomer 98
7) $Ru(S_2(CCF_3)_2)(PPh_3)_2CO$ violet isomer 100
8) $Ru(S_2(CCF_3)_2)(PPh_3)_2CO$ violet' isomer 102

Ruthenium Dimer, perpendicular bridge, neutral:

C	8.23399000	3.19952200	-1.31430100
C	9.06104200	4.32792600	-1.39675100
C	8.92247800	4.54323400	1.01108000
C	8.09713900	3.41080700	1.03544700
N	7.75792300	2.74798100	-0.11309100
H	7.92396100	2.62577800	-2.18635800
H	9.42125500	4.65839200	-2.37438500
H	9.17288500	5.04456100	1.94952600
H	7.68999100	2.99351300	1.95535500
Ru	6.51916600	1.05284000	-0.03818800
O	5.62430500	1.78092200	-1.78178900
O	5.31892700	2.26630500	1.19532700
O	7.55151500	0.54503000	1.69247100
O	7.97984600	0.23483600	-1.30081700
Ru	3.46199800	-0.32549800	0.01807500
Ru	6.23068300	-2.36014500	0.10411700
O	5.38633300	-0.50998900	0.02560200
O	7.80467100	-1.75279500	1.38712100
O	7.34217700	-1.98106600	-1.64910800
O	5.16140100	-2.83195300	1.85881900
O	4.76738600	-3.22525000	-1.16592700
O	3.08837100	-1.86362700	1.39593300
O	3.19947600	-1.56445200	-1.63325200
O	3.46172400	0.95048300	1.67686800
O	3.39495800	1.26743500	-1.35564900
C	7.00525400	-4.07436600	0.16187000
O	7.49128900	-5.16003200	0.19341300
C	8.01381300	-0.90614700	-1.93608400
C	8.05257000	-0.62982600	1.98599700
C	3.77326500	-2.72626000	-1.83014700
C	3.90429600	-2.60345800	2.09873900
C	4.24645200	1.97604700	1.87367000
C	4.34469000	1.84230700	-2.03563100
C	9.00082100	-0.68802800	3.16786900
H	9.85550900	-1.34009100	2.92640900
H	9.35258600	0.31935300	3.43284400
H	8.47997200	-1.13124000	4.03592900
C	8.92648800	-0.97282100	-3.14627100
H	8.46673700	-0.42485600	-3.98893500
H	9.88896600	-0.48767500	-2.91591100
H	9.08914700	-2.01841900	-3.44352200
C	3.31892300	-3.25000500	3.34045100
H	3.23651000	-2.49784800	4.14637700
H	2.30542400	-3.62491300	3.12502300
H	3.96490200	-4.07085700	3.68297600
C	3.23178400	-3.56532100	-2.97149400
H	3.15013700	-4.61676400	-2.65226300
H	2.25195100	-3.18920700	-3.29889700

H	3.93793600	-3.53017800	-3.82074100
C	3.92636800	2.63559100	-3.25766900
H	4.68324600	3.39628100	-3.49911000
H	3.82366400	1.95465600	-4.12284300
H	2.94877800	3.11039100	-3.08155300
C	3.88899300	2.90280700	3.01850000
H	4.48330500	2.63344900	3.91115800
H	4.13400100	3.94245100	2.75038300
H	2.82122900	2.81411500	3.26632100
C	9.41539700	5.01569700	-0.22034000
H	10.06050200	5.89779300	-0.26213300
Ru	-3.46932500	0.34681200	0.01896400
O	-5.39526400	0.51380800	0.02780400
Ru	-6.51403900	-1.05823200	-0.05396600
Ru	-6.25606200	2.35534900	0.12765200
C	-7.04526700	4.06212800	0.20573800
O	-7.54016500	5.14332800	0.25013100
O	-3.21673200	1.60815800	-1.61676300
C	-3.80047400	2.76725700	-1.79979100
O	-4.79960000	3.24923600	-1.13044800
C	-3.26669700	3.62360600	-2.93186100
H	-3.22228800	4.67667500	-2.61132400
H	-2.27115100	3.27698800	-3.24441400
H	-3.95746400	3.56669000	-3.79270000
O	-7.55291700	-0.58036200	1.68096900
C	-8.06556100	0.58651400	1.98624700
O	-7.82685400	1.71819700	1.40016900
C	-9.01657500	0.62284900	3.16674700
H	-9.87452700	1.27323200	2.93256800
H	-9.36285800	-0.39017200	3.41710900
H	-8.50000500	1.05686800	4.04200700
O	-5.61177800	-1.75896400	-1.80520900
C	-4.33176800	-1.80509600	-2.06001200
O	-3.38728900	-1.22900500	-1.37372600
C	-3.90617900	-2.58015400	-3.29122200
H	-3.81233000	-1.88859300	-4.14896100
H	-2.92309100	-3.04584300	-3.12150800
H	-4.65484200	-3.34654700	-3.54018400
O	-3.45873400	-0.94859700	1.66248800
C	-4.23412300	-1.98333400	1.84780700
O	-5.30447200	-2.27509700	1.16683400
C	-3.86793900	-2.91908400	2.98252000
H	-2.79543700	-2.84209700	3.21367800
H	-4.44405800	-2.64668500	3.88617300
H	-4.12792800	-3.95485100	2.71420500
O	-7.98109800	-0.23786400	-1.30776000
C	-8.02455200	0.90979500	-1.93035900
O	-7.36277300	1.98740300	-1.63080000
C	-8.93723800	0.98190700	-3.14023100
H	-8.47541600	0.44178400	-3.98678100

H	-9.89786700	0.49133200	-2.91351600
H	-9.10411900	2.02901000	-3.42965300
O	-3.10992200	1.87141700	1.41546400
C	-3.93313600	2.59481100	2.12684800
O	-5.19228800	2.81427300	1.88906000
C	-3.35474400	3.23131500	3.37698600
H	-3.27276700	2.47160500	4.17586500
H	-2.34191500	3.61211300	3.16912900
H	-4.00521900	4.04619600	3.72526800
N	-7.73713300	-2.76386000	-0.14948000
C	-8.21007200	-3.20429500	-1.35605600
C	-8.06793600	-3.44534600	0.99057400
C	-9.02528900	-4.34015600	-1.45258000
H	-7.90736700	-2.61569300	-2.22075600
C	-8.88140600	-4.58594300	0.95210700
H	-7.66345100	-3.03654700	1.91546800
C	-9.37086300	-5.04718500	-0.28497400
H	-9.38325900	-4.66136100	-2.43414000
H	-9.12523300	-5.10233600	1.88410400
H	-10.00664600	-5.93543200	-0.33777700
N	-1.40303600	0.15961800	0.02083700
C	-0.69564400	0.09550100	-1.15342100
C	-0.69668000	0.08405600	1.19480600
C	0.69099700	-0.04255200	-1.15360100
H	-1.27752600	0.16557000	-2.07037300
C	0.68990900	-0.05948600	1.19457800
H	-1.28050200	0.13464800	2.11178400
N	1.39711400	-0.12304600	0.02041500
H	1.27374700	-0.10146800	-2.07077100
H	1.27289700	-0.12114200	2.11140400

Ruthenium dimer, parallel bridge, neutral:

C	8.35395800	3.15549300	-1.20401100
C	9.17934100	4.28715000	-1.25335700
C	8.80617700	4.60007900	1.11852300
C	7.98777300	3.46234900	1.10990200
N	7.76468000	2.74920400	-0.03708000
H	8.13470400	2.54285700	-2.07747700
H	9.63096900	4.58053700	-2.20455300
H	8.96201000	5.14168900	2.05510700
H	7.49314800	3.08089200	2.00209500
Ru	6.52819900	1.04476000	-0.00896000
O	5.79437900	1.66484000	-1.86179300
O	5.23249500	2.30736300	1.06212400
O	7.38075400	0.61698600	1.83679400
O	8.11176200	0.19845900	-1.08179200
Ru	3.45552700	-0.33127200	-0.17773100
Ru	6.24328500	-2.36230100	0.27122200
O	5.38816700	-0.52004600	0.02968500
O	7.64874300	-1.69622200	1.68851100
O	7.54929600	-2.04516600	-1.35503800
O	4.99637100	-2.78352300	1.90755600
O	4.93051300	-3.25124700	-1.13366800
O	2.97730800	-1.88104100	1.16413400
O	3.33424000	-1.66448000	-1.76049900
O	3.30599500	1.04414600	1.39390500
O	3.52599200	1.24567500	-1.56039500
C	7.00390500	-4.07359200	0.42933600
O	7.47215200	-5.16539800	0.50713600
C	8.22570600	-0.97379200	-1.64472800
C	7.83777700	-0.53843600	2.24764200
C	3.98965800	-2.78943400	-1.89839300
C	3.71598500	-2.56951800	1.99176800
C	4.10044800	2.04714300	1.65140900
C	4.53808900	1.76198700	-2.20195900
C	8.66118000	-0.53542700	3.52072000
H	9.58402400	-1.11841300	3.36596400
H	8.90931000	0.49288300	3.81945300
H	8.09193300	-1.02726800	4.32954700
C	9.24342800	-1.09079800	-2.76318400
H	8.79875800	-0.72304700	-3.70640200
H	10.12367300	-0.46831200	-2.53781700
H	9.54050000	-2.14060800	-2.89972000
C	3.00089500	-3.17835000	3.18287200
H	2.71972600	-2.37893500	3.89186500
H	2.07069400	-3.66798700	2.85037700
H	3.65138300	-3.90460500	3.69003800
C	3.61154700	-3.64519300	-3.09278800
H	3.56397000	-4.70467300	-2.79381400
H	2.64906000	-3.31923400	-3.51260300

H	4.39327300	-3.55465200	-3.86870700
C	4.22123900	2.51732000	-3.47625800
H	5.07275200	3.14465800	-3.77623700
H	4.00052300	1.79718300	-4.28520300
H	3.32239300	3.13798400	-3.33147600
C	3.67060200	2.99087800	2.75737000
H	4.14382600	2.68121300	3.70762500
H	4.00248800	4.01620600	2.53129100
H	2.57889100	2.95841600	2.88771800
C	9.41425500	5.02601600	-0.07791700
H	10.05604700	5.91138400	-0.09383400
Ru	-3.45869700	0.33520600	-0.17648300
O	-5.39168300	0.51940600	0.03231000
Ru	-6.52980300	-1.04609600	-0.02496100
Ru	-6.24876300	2.35792700	0.29368200
C	-7.01113600	4.06650900	0.47179400
O	-7.48057500	5.15677400	0.56288000
O	-3.33842200	1.68575600	-1.74427300
C	-3.99517900	2.81134300	-1.87044600
O	-4.93724200	3.26376700	-1.10153700
C	-3.61732400	3.68045000	-3.05525500
H	-3.57053000	4.73660900	-2.74460400
H	-2.65449200	3.35980700	-3.47834500
H	-4.39880100	3.59797500	-3.83231700
O	-7.38552700	-0.64116500	1.82405800
C	-7.84271900	0.50940900	2.24836600
O	-7.65362500	1.67382300	1.70314900
C	-8.66709300	0.49101700	3.52069700
H	-9.59210200	1.07188600	3.37075200
H	-8.91163300	-0.54105500	3.80922200
H	-8.10046800	0.97731400	4.33467100
O	-5.79336500	-1.64287900	-1.88477800
C	-4.53688500	-1.73507200	-2.22538800
O	-3.52552300	-1.22618400	-1.57668000
C	-4.21859500	-2.47430000	-3.50873100
H	-3.99464200	-1.74405600	-4.30765400
H	-3.32118700	-3.09847400	-3.37007400
H	-5.07051400	-3.09616300	-3.81875300
O	-3.30925300	-1.05696400	1.38000700
C	-4.10272200	-2.06351100	1.62648700
O	-5.23416300	-2.31882600	1.03383400
C	-3.67256400	-3.01819700	2.72287700
H	-2.58059000	-2.98857800	2.85183300
H	-4.14367800	-2.71658100	3.67676900
H	-4.00636600	-4.04084800	2.48778400
O	-8.11368300	-0.18944800	-1.08890400
C	-8.22988300	0.98930300	-1.63763600
O	-7.55507500	2.05828400	-1.33554600
C	-9.24811000	1.11831800	-2.75432300
H	-8.79845900	0.77592000	-3.70470800

H	-10.12160500	0.48171400	-2.54303400
H	-9.55638900	2.16751700	-2.86935200
O	-2.98226600	1.87082400	1.18221900
C	-3.72212600	2.54876100	2.01749300
O	-5.00273700	2.76198400	1.93520100
C	-3.00829000	3.14458300	3.21588700
H	-2.72788100	2.33745000	3.91640600
H	-2.07774200	3.63779300	2.88973500
H	-3.65932300	3.86520000	3.73035600
N	-7.76406900	-2.75172000	-0.07603300
C	-8.35025000	-3.14484100	-1.24899700
C	-7.98876400	-3.47867500	1.06191600
C	-9.17395000	-4.27694500	-1.31361500
H	-8.12991100	-2.52157800	-2.11464700
C	-8.80561800	-4.61755100	1.05521400
H	-7.49662400	-3.10709600	1.95965300
C	-9.41048700	-5.03003400	-0.14756300
H	-9.62308000	-4.55960300	-2.26923200
H	-8.96278300	-5.17046900	1.98494000
H	-10.05104400	-5.91600000	-0.17545100
N	-1.40286200	0.14003600	-0.30191200
C	-0.80765800	-1.09676100	-0.32857800
C	-0.58126300	1.23965100	-0.31117700
C	0.57845700	-1.23256900	-0.32536500
H	-1.47885700	-1.95284700	-0.35172800
C	0.80490200	1.10388500	-0.31490700
H	-1.07482100	2.20891500	-0.29431300
N	1.40007500	-0.13316500	-0.30240800
H	1.07195200	-2.20197500	-0.31954600
H	1.47616300	1.96016000	-0.32732200

Ruthenium dimer, perpendicular bridge, -1:

C	8.21805200	3.23943600	-1.30423900
C	9.02944800	4.37875100	-1.38119200
C	8.90458900	4.57053500	1.02806200
C	8.09548000	3.42714100	1.04852400
N	7.75311000	2.76520900	-0.10358900
H	7.90659900	2.66967800	-2.17848800
H	9.37725600	4.72271600	-2.35951700
H	9.15314000	5.06700800	1.97047000
H	7.69783100	2.99576700	1.96613800
Ru	6.54478100	1.07293300	-0.03588500
O	5.61885600	1.83081600	-1.75885700
O	5.35576400	2.23730200	1.25373700
O	7.61511400	0.54668200	1.67661800
O	7.96825500	0.27046900	-1.35355900
Ru	3.46388200	-0.34552400	0.01228700
Ru	6.28100200	-2.39253000	0.09685300
O	5.41302100	-0.52332800	0.02291300
O	7.81229400	-1.76803900	1.42594700
O	7.41483700	-1.98115300	-1.64144600
O	5.18404900	-2.88426800	1.83309900
O	4.84411200	-3.23540900	-1.21501100
O	3.12201500	-1.86214200	1.42101700
O	3.21511500	-1.61223000	-1.62596900
O	3.45257200	0.95494800	1.65885000
O	3.39962300	1.21749200	-1.39518100
C	7.06354700	-4.08277700	0.15699400
O	7.56717200	-5.16885100	0.19432700
C	8.03070800	-0.88325600	-1.95869400
C	8.06784100	-0.63514300	2.00218600
C	3.82872500	-2.74299700	-1.85366500
C	3.93780200	-2.62361200	2.09487400
C	4.26063000	1.94896100	1.89596000
C	4.34561700	1.83217800	-2.04165600
C	8.98669900	-0.69511800	3.21248100
H	9.83327300	-1.36928200	3.00371300
H	9.35300700	0.30970500	3.46963600
H	8.43356100	-1.11226000	4.07373300
C	8.91994800	-0.93859300	-3.19186900
H	8.41382900	-0.43536100	-4.03617500
H	9.86342700	-0.40244800	-2.99768300
H	9.12442200	-1.98339700	-3.46695900
C	3.36202400	-3.26714500	3.34685500
H	3.30963300	-2.51758100	4.15796000
H	2.33674900	-3.61934700	3.14819400
H	3.99791800	-4.10322000	3.67243500
C	3.30316500	-3.57386600	-3.01331500
H	3.22249600	-4.62955100	-2.70619200
H	2.32381800	-3.19871200	-3.34428300

H	4.01800100	-3.52602100	-3.85482100
C	3.92240500	2.61487300	-3.27334900
H	4.67526500	3.37837900	-3.52004100
H	3.82031700	1.92619400	-4.13260500
H	2.94171800	3.08556200	-3.09989300
C	3.90118400	2.85561400	3.06098500
H	4.48725500	2.56367200	3.95223400
H	4.15482900	3.89946600	2.81636200
H	2.83037700	2.76879100	3.29726400
C	9.38458800	5.06327300	-0.20177900
H	10.01695600	5.95529500	-0.24004800
Ru	-3.46349200	0.33774100	0.01286100
O	-5.41189200	0.52252100	0.02428800
Ru	-6.54961800	-1.06864900	-0.05260700
Ru	-6.27397400	2.39354600	0.11944300
C	-7.05040400	4.08582400	0.19870100
O	-7.54970900	5.17340400	0.24825500
O	-3.20926000	1.62319900	-1.60997600
C	-3.81907400	2.75843400	-1.82515800
O	-4.83365300	3.24664800	-1.18201000
C	-3.28974900	3.60079000	-2.97478700
H	-3.20912400	4.65318800	-2.65670100
H	-2.30985200	3.22815100	-3.30695600
H	-4.00225900	3.56202100	-3.81872300
O	-7.61895400	-0.55847800	1.66519300
C	-8.06863300	0.62106200	2.00317200
O	-7.80898300	1.75943500	1.43962500
C	-8.98859200	0.67047200	3.21309600
H	-9.83172700	1.35104300	3.01172100
H	-9.35978000	-0.33569000	3.45755600
H	-8.43452900	1.07434800	4.08001100
O	-5.62547300	-1.81032500	-1.78370600
C	-4.35214600	-1.81296900	-2.06616900
O	-3.40409500	-1.20923700	-1.41241300
C	-3.93155300	-2.58255600	-3.30699300
H	-3.83270900	-1.88494400	-4.15941800
H	-2.95001800	-3.05408300	-3.14113200
H	-4.68448100	-3.34406500	-3.55959800
O	-3.45736700	-0.98183100	1.64393900
C	-4.26913000	-1.97555200	1.86929400
O	-5.36543400	-2.25209500	1.22387200
C	-3.91321300	-2.89688100	3.02384000
H	-2.83962500	-2.82620000	3.25284300
H	-4.48818000	-2.60429000	3.92210400
H	-4.18272100	-3.93504000	2.77254300
O	-7.97045400	-0.24608100	-1.36128900
C	-8.02740700	0.91430800	-1.95414200
O	-7.40721600	2.00612300	-1.62448800
C	-8.91536200	0.98677500	-3.18733700
H	-8.41214500	0.48755300	-4.03578900

H	-9.86265600	0.45530000	-2.99850100
H	-9.11264500	2.03539900	-3.45311000
O	-3.11810700	1.83622500	1.43997800
C	-3.93207500	2.59200900	2.12244300
O	-5.17712100	2.86018100	1.86266600
C	-3.35560200	3.21763300	3.38315000
H	-3.30966900	2.45842900	4.18567000
H	-2.32783600	3.56615200	3.19104900
H	-3.98749900	4.05352200	3.71692600
N	-7.76516000	-2.75494700	-0.14039000
C	-8.23164600	-3.21245400	-1.34690800
C	-8.11191800	-3.42865600	1.00349000
C	-9.04945200	-4.34611300	-1.43798100
H	-7.91634600	-2.63406400	-2.21403500
C	-8.92757500	-4.56706400	0.96889200
H	-7.71247500	-3.01050900	1.92641600
C	-9.40947200	-5.04243700	-0.26702400
H	-9.39842200	-4.67648300	-2.42057500
H	-9.17964200	-5.07326200	1.90513500
H	-10.04698000	-5.93024900	-0.31631600
N	-1.40567700	0.13874800	0.01324500
C	-0.69247000	0.06890300	-1.15988400
C	-0.69324900	0.06097100	1.18621400
C	0.69320900	-0.07197800	-1.15995000
H	-1.27458600	0.13661000	-2.07702800
C	0.69200100	-0.08661600	1.18611400
H	-1.27674600	0.11470200	2.10336200
N	1.40550400	-0.15233400	0.01307000
H	1.27615500	-0.13111900	-2.07716100
H	1.27472300	-0.14876400	2.10323000

Ruthenium dimer, parallel bridge, -1:

C	8.33408000	3.18249700	-1.22128900
C	9.15388200	4.31727800	-1.27578700
C	8.83976300	4.59796700	1.10763400
C	8.02628300	3.45735000	1.10575800
N	7.77347700	2.75431300	-0.04479200
H	8.09212500	2.57934500	-2.09537800
H	9.57973900	4.62441200	-2.23533500
H	9.01533000	5.12865800	2.04780300
H	7.55320900	3.06181800	2.00357300
Ru	6.54972600	1.06310200	-0.00906600
O	5.75345200	1.75966800	-1.81729200
O	5.28537200	2.26751900	1.16369100
O	7.49213400	0.59822600	1.79269500
O	8.06031400	0.21712100	-1.19397500
Ru	3.44941400	-0.33116600	-0.14795200
Ru	6.26020100	-2.38408900	0.23553500
O	5.40081200	-0.52027900	0.02391400
O	7.68998300	-1.72509100	1.65337700
O	7.53026600	-2.04538400	-1.42411200
O	5.02984500	-2.80078200	1.89958300
O	4.92632300	-3.25482000	-1.16035300
O	2.99878400	-1.88852700	1.19414800
O	3.32635000	-1.65303200	-1.75193700
O	3.33031400	1.02781500	1.44675500
O	3.49730100	1.26080900	-1.52478900
C	7.02003300	-4.07763500	0.40988600
O	7.50445100	-5.16806300	0.51694900
C	8.16514600	-0.96039900	-1.74578100
C	7.91383200	-0.57041000	2.19846900
C	3.97229200	-2.77913300	-1.90026500
C	3.75214400	-2.58215500	2.00122500
C	4.14362800	2.00263800	1.73426200
C	4.49269500	1.82147900	-2.14703800
C	8.74502200	-0.58297300	3.47161300
H	9.59409400	-1.27593100	3.35419100
H	9.10696600	0.42887300	3.70691900
H	8.12684300	-0.95225400	4.31034300
C	9.13544900	-1.06334800	-2.91266900
H	8.67387700	-0.62496500	-3.81677600
H	10.05137300	-0.49145900	-2.69078600
H	9.38086900	-2.11677400	-3.11145200
C	3.05283400	-3.19243200	3.20495300
H	2.81706800	-2.39719400	3.93551700
H	2.09831300	-3.64692900	2.89176400
H	3.69660500	-3.94611300	3.68107600
C	3.56747100	-3.62993800	-3.09403800
H	3.52245400	-4.69092100	-2.79879200
H	2.59657800	-3.29900100	-3.49103400

H	4.33298300	-3.53695500	-3.88607600
C	4.15158500	2.59937000	-3.40581900
H	4.95139200	3.31585700	-3.64564800
H	4.03543100	1.89651800	-4.25148600
H	3.19195300	3.12423000	-3.27466800
C	3.72788200	2.92049800	2.87172000
H	4.22445000	2.59727900	3.80564500
H	4.04499700	3.95411700	2.65947300
H	2.63886000	2.87473700	3.02082300
C	9.41735800	5.04423400	-0.09771300
H	10.05466300	5.93334100	-0.11848200
Ru	-3.45206200	0.33399900	-0.14819300
O	-5.40367500	0.51937200	0.02542700
Ru	-6.55127000	-1.06432900	-0.02637200
Ru	-6.26434600	2.37999600	0.25791600
C	-7.02524300	4.07092300	0.45218500
O	-7.51046100	5.15963600	0.57227800
O	-3.32966900	1.67366400	-1.73710500
C	-3.97684300	2.80061600	-1.87346500
O	-4.93186200	3.26721000	-1.12899400
C	-3.57240000	3.66481200	-3.05772100
H	-3.52801000	4.72249800	-2.75075100
H	-2.60127000	3.33886000	-3.45823300
H	-4.33779700	3.58019000	-3.85080400
O	-7.49553500	-0.62173600	1.77980000
C	-7.91712300	0.54212300	2.19944800
O	-7.69309300	1.70329500	1.66834400
C	-8.74874000	0.53940000	3.47237400
H	-9.59815500	1.23323500	3.36273500
H	-9.11024700	-0.47531800	3.69572000
H	-8.13104800	0.89922100	4.31557700
O	-5.75355200	-1.73836100	-1.84272400
C	-4.49262500	-1.79563200	-2.17256300
O	-3.49778300	-1.24250600	-1.54270000
C	-4.15044400	-2.55762400	-3.44074200
H	-4.03004400	-1.84384600	-4.27659300
H	-3.19257400	-3.08685300	-3.31416600
H	-4.95153500	-3.26868300	-3.69209700
O	-3.33334100	-1.04222700	1.43135500
C	-4.14570100	-2.02113800	1.70752300
O	-5.28668700	-2.28114300	1.13314600
C	-3.72985100	-2.95078500	2.83532100
H	-2.64066600	-2.90751900	2.98406000
H	-4.22526300	-2.63640800	3.77287800
H	-4.04813100	-3.98190000	2.61297800
O	-8.06301100	-0.20598700	-1.20092100
C	-8.16974400	0.97803900	-1.73833400
O	-7.53563700	2.05977500	-1.40436300
C	-9.14087200	1.09412600	-2.90330300
H	-8.67393500	0.67993100	-3.81608900

H	-10.05047700	0.50779700	-2.69381600
H	-9.39747300	2.14873600	-3.08088200
O	-3.00218700	1.87667800	1.21102300
C	-3.75627300	2.56018700	2.02602700
O	-5.03412600	2.77877200	1.92662600
C	-3.05765600	3.15702500	3.23685400
H	-2.82001600	2.35332500	3.95747700
H	-2.10413200	3.61715300	2.92885800
H	-3.70262300	3.90360800	3.72244000
N	-7.77404600	-2.75572400	-0.08376200
C	-8.33204000	-3.17053200	-1.26625700
C	-8.02942300	-3.47169800	1.05818000
C	-9.15184000	-4.30450100	-1.33538100
H	-8.08796600	-2.55765100	-2.13295800
C	-8.84306500	-4.61214900	1.04540600
H	-7.55837100	-3.08628000	1.96144400
C	-9.41810000	-5.04463900	-0.16617300
H	-9.57555300	-4.60073700	-2.29928800
H	-9.02073700	-5.15343100	1.97911500
H	-10.05552000	-5.93332200	-0.19840300
N	-1.41105500	0.14084900	-0.26818900
C	-0.80687200	-1.09700900	-0.29142500
C	-0.57856500	1.23805100	-0.27657300
C	0.57611600	-1.23336900	-0.28827800
H	-1.47750600	-1.95379200	-0.31118300
C	0.80444300	1.10172800	-0.27897700
H	-1.06941800	2.20897400	-0.25912400
N	1.40860400	-0.13634500	-0.26747900
H	1.06695500	-2.20441200	-0.27980500
H	1.47506000	1.95869700	-0.28913700

Ru($S_2(CCF_3)_2$)(PPh_3)$_2$CO, orange isomer:

Ru	0.00008500	-0.00021900	0.00267200
C	-0.00413400	-0.00268100	1.82006400
O	0.12189000	-0.00485000	3.01753000
S	1.41644300	-1.90497800	-0.32100200
S	1.86317000	1.28700500	-0.69807700
C	3.05233100	-1.22791100	-0.71448400
C	3.24769500	0.11972100	-0.86289100
C	4.13499800	-2.27215900	-0.78325400
F	4.90307900	-2.33265500	0.39549400
F	5.03240400	-2.06093000	-1.84578500
F	3.61313600	-3.56429400	-0.97241400
C	4.55303700	0.76838900	-1.23438200
F	4.55375300	2.15110600	-0.98528300
F	4.85284200	0.62679400	-2.60644400
F	5.64799000	0.24487400	-0.52332000
P	-1.85657300	-1.60824700	-0.31518000
C	-3.62509100	-1.27582000	0.29807300
C	-4.42628600	-0.32113300	-0.36944200
C	-5.72790000	-0.04707000	0.08967800
C	-6.23628900	-0.71309800	1.22184200
C	-5.43803400	-1.65953600	1.89140200
C	-4.13711500	-1.94548100	1.43063800
H	-4.04155500	0.20310000	-1.24852100
H	-6.34158100	0.68972100	-0.43771200
H	-7.24814000	-0.49678500	1.57825500
H	-5.82752500	-2.18712900	2.76782600
H	-3.53003700	-2.69451200	1.94659200
C	-2.12840500	-1.96297800	-2.16594800
C	-1.03679200	-1.84183700	-3.05416800
C	-1.20053800	-2.14050700	-4.42079800
C	-2.45205800	-2.56025500	-4.90964600
C	-3.54105900	-2.68685600	-4.02588100
C	-3.38308000	-2.39142400	-2.65776700
H	-0.05771600	-1.53400800	-2.67386700
H	-0.34584500	-2.04870000	-5.09806100
H	-2.57789100	-2.79174800	-5.97196200
H	-4.51573200	-3.01890700	-4.39734900
H	-4.23493000	-2.49304100	-1.97979900
C	-1.50900000	-3.32665500	0.41925500
C	-0.93589300	-3.41918800	1.70758800
C	-0.70343800	-4.68172000	2.28644300
C	-1.02913000	-5.85479700	1.57997000
C	-1.59134400	-5.76338200	0.29258300
C	-1.83410400	-4.50379300	-0.28825100

H	-0.65200300	-2.51496900	2.25194900
H	-0.25267400	-4.74360500	3.28146200
H	-0.83600900	-6.83519900	2.02614900
H	-1.83619400	-6.67181800	-0.26657000
H	-2.26412600	-4.44210200	-1.29157100
P	-1.28987200	2.11297100	-0.09958200
C	-0.19216300	3.66547700	-0.06599800
C	-0.15041700	4.58162800	-1.13607900
C	0.67454600	5.72195300	-1.05151800
C	1.45491900	5.94831400	0.09660800
C	1.41454800	5.03017200	1.16471100
C	0.59735300	3.88897200	1.08496400
H	-0.75207100	4.41096400	-2.03293700
H	0.70652100	6.42811400	-1.88717200
H	2.09849800	6.83130700	0.15736100
H	2.02828700	5.19433900	2.05550200
H	0.58277400	3.17072800	1.91040300
C	-2.26925600	2.33252100	-1.70997000
C	-3.54532400	2.93522200	-1.75439700
C	-4.21118900	3.08104000	-2.98795900
C	-3.60681200	2.63240100	-4.17835200
C	-2.33303000	2.03278100	-4.13543900
C	-1.66611900	1.87813300	-2.90515900
H	-4.01956200	3.28477300	-0.83288000
H	-5.20094300	3.54798600	-3.01654400
H	-4.12673100	2.74750000	-5.13445600
H	-1.85941300	1.67792600	-5.05547200
H	-0.67783700	1.40676500	-2.86953500
C	-2.50169200	2.55923800	1.29292100
C	-2.90685900	3.90369400	1.46962500
C	-3.78793900	4.24362100	2.51319000
C	-4.25948800	3.24931800	3.39297900
C	-3.84756200	1.91447300	3.22616000
C	-2.97186700	1.56901200	2.17809000
H	-2.51692600	4.68446100	0.80941000
H	-4.09402300	5.28616300	2.64538800
H	-4.93632300	3.51726000	4.21032600
H	-4.20101300	1.13748700	3.91004700
H	-2.65349900	0.53217400	2.05501600

$Ru(S_2(CCF_3)_2)(PPh_3)_2CO$, orange' isomer:

Ru	0.00047600	0.00008600	-0.00116800
C	0.00278000	-0.00017500	1.81526900
O	0.11513000	-0.00049600	3.01097400
S	1.89521400	-1.38795000	-0.36701600
S	1.46498300	1.81843600	-0.46502600
C	3.31008400	-0.26012600	-0.51017500
C	3.13183900	1.09737800	-0.51467400
C	4.63834900	-0.96438100	-0.54517700
F	5.27831500	-0.98081900	0.70928100
F	5.54175500	-0.38804100	-1.45599000
F	4.51049200	-2.31225700	-0.93138500
C	4.23312700	2.11285500	-0.65151800
F	3.82056500	3.40169400	-0.27187700
F	4.69616500	2.23438100	-1.97820800
F	5.35313100	1.81280100	0.14491800
P	-1.31346000	-2.10415200	-0.00171500
C	-3.10414400	-2.06552900	0.63858200
C	-4.13823900	-2.82507300	0.05034800
C	-5.43428500	-2.80027800	0.60058300
C	-5.70629800	-2.02519100	1.74387600
C	-4.67917100	-1.26112100	2.32850600
C	-3.38401500	-1.27235400	1.77404200
H	-3.94186300	-3.42867700	-0.83956300
H	-6.23023100	-3.38879700	0.13336000
H	-6.71327400	-2.01254200	2.17225200
H	-4.87943800	-0.64748000	3.21189500
H	-2.59933300	-0.65772600	2.22479400
C	-1.39574800	-2.94244500	-1.69862800
C	-1.77928800	-4.29677100	-1.84205500
C	-1.82027800	-4.88569600	-3.12051300
C	-1.47255600	-4.13252300	-4.25936100
C	-1.07368600	-2.78998700	-4.11843700
C	-1.03191600	-2.19786600	-2.84112800
H	-2.01819900	-4.89635200	-0.95836400
H	-2.11306500	-5.93515700	-3.22417300
H	-1.49858800	-4.59542200	-5.25060700
H	-0.78141200	-2.20641400	-4.99653300
H	-0.68736500	-1.16378500	-2.72486100
C	-0.54989500	-3.46811300	1.08331900
C	-0.96073400	-3.63063400	2.42380700
C	-0.33968800	-4.59548800	3.23957200
C	0.69292800	-5.40156900	2.72462500
C	1.10361800	-5.24068500	1.38829600
C	0.48803000	-4.27688500	0.56689100

H	-1.76665700	-3.01723900	2.83505000
H	-0.66593400	-4.71393300	4.27747200
H	1.17697800	-6.14796900	3.36189300
H	1.91014300	-5.85772200	0.98092900
H	0.82184500	-4.15800400	-0.46664000
P	-1.84239400	1.70775300	-0.19861600
C	-1.33191400	3.30354400	-1.12178900
C	-0.88606400	3.17054900	-2.45584200
C	-0.56459900	4.31203700	-3.21042100
C	-0.68155300	5.59430600	-2.63807600
C	-1.12502900	5.72835200	-1.31061500
C	-1.45417500	4.58621500	-0.55132900
H	-0.77384100	2.17685900	-2.90041800
H	-0.21217300	4.19876000	-4.24015900
H	-0.42219900	6.48187700	-3.22329500
H	-1.21373700	6.72055800	-0.85700800
H	-1.79631000	4.70324500	0.48026300
C	-3.47650200	1.41487500	-1.13410600
C	-3.68601000	0.22259100	-1.85139600
C	-4.85479200	0.05078400	-2.62054800
C	-5.82071800	1.07117700	-2.67318100
C	-5.61064100	2.27160400	-1.96466000
C	-4.43987800	2.44902100	-1.20563800
H	-2.93602400	-0.56992800	-1.82111700
H	-5.00273000	-0.87958700	-3.17708900
H	-6.72858600	0.93890400	-3.26995900
H	-6.35175600	3.07564000	-2.01276900
H	-4.26764500	3.39675800	-0.68657500
C	-2.36810900	2.35988100	1.50232100
C	-1.36421400	2.91982100	2.32816800
C	-1.69031400	3.39435300	3.61202500
C	-3.01369200	3.30318400	4.08637900
C	-4.01005700	2.73396800	3.27186300
C	-3.69191100	2.26292400	1.98137700
H	-0.33053100	2.97919100	1.97153900
H	-0.90698500	3.82589800	4.24216000
H	-3.26415200	3.66873100	5.08699700
H	-5.03990200	2.65706300	3.63550800
H	-4.47200600	1.81946300	1.35731600

$Ru(S_2(CCF_3)_2)(PPh_3)_2CO$, violet isomer:

Ru	0.00011300	-0.00018500	-0.00058500
C	0.00109500	-0.00079200	1.86832300
O	0.12638400	-0.00119500	3.06192700
S	0.99736500	-2.18105800	-0.00269900
S	0.85903100	0.19927600	-2.23270000
C	1.59742800	-2.43469900	-1.68660000
C	1.57790500	-1.42174800	-2.61786700
C	2.16117600	-3.81255500	-1.93386700
F	3.56886500	-3.82594500	-1.96318600
F	1.71823300	-4.36256800	-3.15255500
F	1.79036700	-4.73101300	-0.93908700
C	2.01883700	-1.54962000	-4.04855500
F	2.32619700	-0.30717400	-4.62644400
F	1.00693200	-2.11124100	-4.87231400
F	3.16003500	-2.34762100	-4.22134100
P	-2.23673100	-0.81824800	-0.13540900
C	-3.61475500	0.37941200	-0.65393600
C	-4.29025200	0.21641900	-1.88417400
C	-5.30861500	1.11789800	-2.25277400
C	-5.66382300	2.17667800	-1.39571000
C	-4.99266600	2.33864600	-0.16789400
C	-3.96580000	1.44900500	0.20116600
H	-4.02836200	-0.61143700	-2.54810900
H	-5.82714500	0.98399300	-3.20731100
H	-6.45846800	2.87237000	-1.68262900
H	-5.25689200	3.16100600	0.50287600
H	-3.44196500	1.59083600	1.15022600
C	-2.44414600	-2.24126500	-1.37941600
C	-3.26736000	-3.34549200	-1.06374100
C	-3.43290100	-4.38448000	-1.99980100
C	-2.78194800	-4.32887400	-3.24702400
C	-1.96718700	-3.22557100	-3.56320400
C	-1.80106000	-2.18127700	-2.63322900
H	-3.77010900	-3.40237000	-0.09496300
H	-4.06541000	-5.24106300	-1.74632000
H	-2.90022900	-5.14672300	-3.96444700
H	-1.43361800	-3.17977500	-4.51585500
H	-1.15582300	-1.33341600	-2.87716000
C	-2.88950500	-1.59380900	1.46989700
C	-4.19386100	-1.34673900	1.94978300
C	-4.64151800	-1.98072800	3.12650700
C	-3.79812200	-2.86915200	3.81878100
C	-2.50280500	-3.12922800	3.32981200
C	-2.04639300	-2.49399000	2.16068800

H	-4.86178400	-0.66882100	1.41244100
H	-5.65200400	-1.77947200	3.49600100
H	-4.14800700	-3.35855700	4.73296400
H	-1.84252200	-3.82324600	3.85824400
H	-1.04230000	-2.70656700	1.78098400
P	-0.15062800	2.46675700	-0.01314800
C	1.52955000	3.11345300	0.61149600
C	2.69516100	2.36260700	0.33924700
C	3.94915900	2.81822400	0.78967100
C	4.04738700	4.02202100	1.51306700
C	2.88761000	4.77396900	1.78201600
C	1.63039700	4.32369300	1.33369400
H	2.62181300	1.42669800	-0.22343900
H	4.84530600	2.22755000	0.57679400
H	5.02204900	4.37144100	1.86772000
H	2.95724900	5.71077300	2.34400300
H	0.73378000	4.91061400	1.55177600
C	-0.35132100	3.29929600	-1.70302600
C	-1.41070300	2.88110600	-2.53965600
C	-1.59400700	3.48684300	-3.79668400
C	-0.71796700	4.50160800	-4.22842900
C	0.34187200	4.91276800	-3.39835700
C	0.52684100	4.31560900	-2.13595600
H	-2.08258400	2.08132500	-2.21513500
H	-2.41421500	3.15612900	-4.44105700
H	-0.85572300	4.96349400	-5.21102400
H	1.03141700	5.69417800	-3.73267000
H	1.35496600	4.63426400	-1.49705600
C	-1.34773100	3.45339600	1.08954900
C	-1.46772600	3.10830400	2.45631300
C	-2.32906200	3.83970500	3.29619300
C	-3.07379800	4.92044400	2.78221500
C	-2.95049800	5.26895400	1.42409800
C	-2.09073100	4.53883300	0.57797100
H	-0.89136700	2.27851200	2.87301100
H	-2.41306700	3.56534900	4.35229500
H	-3.74051300	5.48910000	3.43801000
H	-3.51895000	6.11185000	1.01800500
H	-2.00079300	4.81462000	-0.47600000

$Ru(S_2(CCF_3)_2)(PPh_3)_2CO$, violet' isomer:

Ru	-0.00233100	0.00034100	0.00282900
C	-0.00465000	-0.00030900	1.88234300
O	0.08492400	-0.00102100	3.07583700
S	1.72623400	-1.63307100	0.08621300
S	0.42646900	0.07073500	-2.37023600
C	2.17272200	-1.96988400	-1.63868400
C	1.62531600	-1.24409400	-2.67149200
C	3.22043200	-3.03909500	-1.80173700
F	4.50331600	-2.51186700	-2.04832000
F	2.93373900	-3.92717800	-2.85744300
F	3.35038200	-3.84106500	-0.65434400
C	1.90931500	-1.48590600	-4.13303500
F	1.53248100	-0.39743200	-4.93848000
F	1.21130300	-2.60010400	-4.63989000
F	3.27309600	-1.70388000	-4.39741600
P	-2.08617000	-1.12137600	-0.23386800
C	-3.55335900	-0.17779000	-0.98323700
C	-3.33613100	0.58502300	-2.15251000
C	-4.41152400	1.25719900	-2.76382900
C	-5.70380500	1.17717800	-2.20859500
C	-5.92146500	0.41585900	-1.04382900
C	-4.85097100	-0.26650900	-0.43140800
H	-2.33261300	0.64871000	-2.58382500
H	-4.23252800	1.84981400	-3.66537600
H	-6.53767300	1.70489300	-2.68197200
H	-6.92508300	0.34450500	-0.61250300
H	-5.02655400	-0.86642100	0.46568000
C	-1.96354400	-2.63934200	-1.37104600
C	-0.93674500	-3.58309800	-1.15027500
C	-0.84910900	-4.73131000	-1.95932700
C	-1.78103500	-4.94129200	-2.99380700
C	-2.80700700	-4.00328700	-3.21121500
C	-2.90447700	-2.85445700	-2.40168700
H	-0.19841700	-3.41372000	-0.36122200
H	-0.03995100	-5.44772100	-1.79085000
H	-1.70165100	-5.82646800	-3.63212200
H	-3.53382600	-4.15824400	-4.01472400
H	-3.70612500	-2.13379800	-2.57929200
C	-2.80799500	-1.84288200	1.36590900
C	-3.02102800	-0.98916300	2.47156500
C	-3.56837500	-1.50112300	3.66229500
C	-3.90131600	-2.86632000	3.75968300
C	-3.69152000	-3.71708800	2.65868500
C	-3.14953900	-3.20956700	1.46111600

H	-2.75828200	0.07032500	2.41049200
H	-3.72322000	-0.83284300	4.51464400
H	-4.31748200	-3.26476800	4.69014100
H	-3.94605100	-4.77930200	2.72686600
H	-2.99069500	-3.87687000	0.61055300
P	-0.67780800	2.37165100	0.05020600
C	0.92697400	3.36277000	0.32671000
C	0.93003600	4.76968200	0.19046400
C	2.11917400	5.49327300	0.39737800
C	3.30946900	4.81826300	0.73502300
C	3.30829400	3.41728900	0.86720700
C	2.11871100	2.68944900	0.66466600
H	0.01131000	5.29667800	-0.08490900
H	2.11663700	6.58242700	0.28828500
H	4.23439800	5.38283100	0.88880700
H	4.22998900	2.88536500	1.12161300
H	2.12237400	1.59692100	0.75513300
C	-1.42089200	3.36427800	-1.40043000
C	-2.53904800	4.21186600	-1.24728700
C	-3.01395800	4.96059300	-2.34325500
C	-2.37732300	4.87069400	-3.59495800
C	-1.25426200	4.03368500	-3.74694800
C	-0.77302700	3.28640200	-2.65567500
H	-3.03909500	4.29906200	-0.27964500
H	-3.87963700	5.61762200	-2.21130600
H	-2.74761400	5.45385900	-4.44399700
H	-0.74565500	3.96188900	-4.71317800
H	0.10345000	2.64602000	-2.78545600
C	-1.74707100	2.88107600	1.53270900
C	-1.17580900	3.51679400	2.65631400
C	-1.97644100	3.83639000	3.77090100
C	-3.35048400	3.53271000	3.76977700
C	-3.92348300	2.89476100	2.65207700
C	-3.12566100	2.55990300	1.54045000
H	-0.11064900	3.76191000	2.66468900
H	-1.52158000	4.32399000	4.63864700
H	-3.97074200	3.78783000	4.63459000
H	-4.99072100	2.65194200	2.64277600
H	-3.57840200	2.05277600	0.68291700

Appendix B

Contents:

Zoerbex Program Matlab Source Code
- Version 5 with GUI 105
- Version 5 for Command Line 139

Zoerbex Version 5 with GUI:

```
function varargout = Zoerbex_v5_source(varargin)
%
%Zoerbex was written by M.C. Zoerb in Spring 2011 at the UC Berkeley
%College of Chemistry in the research group of C.B. Harris.
%
%This program is based on the math from Grevels et al. J. Am. Chem. Soc.
%(1998), 120, 10423-10433.
%This program takes inputs of peak parameters and exchange time
%constant (or barrier height and temperature) and simulates the vibrational
%lineshape due to exchange between two sites.
%
%Acceptable input spectra formats are space or tab delimited text files
%with or without headers. Zoerbex automatically normalizes spectra to 1.
%
%Some code for the fft section and GUI controls were adapted from examples
%on www.blinkdagger.com
%


% Last Modified by GUIDE v2.5 15-Nov-2012 18:43:49

% Begin initialization code - DO NOT EDIT
gui_Singleton = 1;
gui_State = struct('gui_Name',       mfilename, ...
                   'gui_Singleton',  gui_Singleton, ...
                   'gui_OpeningFcn', @Zoerbex_v5_source_OpeningFcn, ...
                   'gui_OutputFcn',  @Zoerbex_v5_source_OutputFcn, ...
                   'gui_LayoutFcn',  @Zoerbex_v5_source_LayoutFcn, ...
                   'gui_Callback',   []);
if nargin && ischar(varargin{1})
    gui_State.gui_Callback = str2func(varargin{1});
end

if nargout
    [varargout{1:nargout}] = gui_mainfcn(gui_State, varargin{:});
else
    gui_mainfcn(gui_State, varargin{:});
% End initialization code - DO NOT EDIT
end

% --- Executes just before Zoerbex_v5_source is made visible.
function Zoerbex_v5_source_OpeningFcn(hObject, ~, handles, varargin)

handles.output = hObject;

set(handles.time_or_energy_buttongroup,'SelectionChangeFcn',@time_or_energy_b
uttongroup_SelectionChangeFcn);
handles.time_or_energy_buttongroup = 0;
guidata(hObject, handles);
```

```
% --- Zoerbex Startup Parameters:
function varargout = Zoerbex_v5_source_OutputFcn(~, ~, handles)
varargout{1} = handles.output;

%------------Begin Zoerbex

xla=1500;
xlb=3500;
xbase_init=xla:xlb;
baseline_init=zeros(1,length(xbase_init));
plot(xbase_init,baseline_init,'color','k','LineWidth',1.5)
xlim([1800 2000]);
ylim([-0.1 1.1]);
xlabel('wavenumber (cm^-^1)');
ylabel('Normalized Absorbance');



% ------------------------------------------------------
% --- Input Text Boxes ---
% ------------------------------------------------------

% --- Exchange Time Constant Text Box
function edit1_Callback(hObject, ~, handles)
input1 = str2double(get(hObject,'String'));
if (isempty(input1))
     set(hObject,'String','5')
end
guidata(hObject, handles);
function edit1_CreateFcn(hObject, ~, ~)
if ispc && isequal(get(hObject,'BackgroundColor'),
get(0,'defaultUicontrolBackgroundColor'))
    set(hObject,'BackgroundColor','white');
end

% --- Peak 1 Center Frequency Text Box
function edit2_Callback(hObject, ~, handles)
input2 = str2double(get(hObject,'String'));
if (isempty(input2))
     set(hObject,'String','1890')
end
guidata(hObject, handles);
function edit2_CreateFcn(hObject, ~, ~)
if ispc && isequal(get(hObject,'BackgroundColor'),
get(0,'defaultUicontrolBackgroundColor'))
    set(hObject,'BackgroundColor','white');
end

% --- Peak 2 Center Frequency Text Box
function edit3_Callback(hObject, ~, handles)
input3 = str2double(get(hObject,'String'));
if (isempty(input3))
     set(hObject,'String','1940')
end
```

```
guidata(hObject, handles);
function edit3_CreateFcn(hObject, ~, ~)
if ispc && isequal(get(hObject,'BackgroundColor'),
get(0,'defaultUicontrolBackgroundColor'))
    set(hObject,'BackgroundColor','white');
end

% --- Peak 1 Lorentzian Text Box
function edit4_Callback(hObject, ~, handles)
input4 = str2double(get(hObject,'String'));
if (isempty(input4))
     set(hObject,'String','10')
end
guidata(hObject, handles);
function edit4_CreateFcn(hObject, ~, ~)
if ispc && isequal(get(hObject,'BackgroundColor'),
get(0,'defaultUicontrolBackgroundColor'))
    set(hObject,'BackgroundColor','white');
end

% --- Peak 2 Lorentzian Width Text Box
function edit5_Callback(hObject, ~, handles)
input5 = str2double(get(hObject,'String'));
if (isempty(input5))
     set(hObject,'String','10')
end
guidata(hObject, handles);
function edit5_CreateFcn(hObject, ~, ~)
if ispc && isequal(get(hObject,'BackgroundColor'),
get(0,'defaultUicontrolBackgroundColor'))
    set(hObject,'BackgroundColor','white');
end

% --- Peak 1 Gaussian Width Text Box
function edit6_Callback(hObject, ~, handles)
input6 = str2double(get(hObject,'String'));
if (isempty(input6))
     set(hObject,'String','10')
end
guidata(hObject, handles);
function edit6_CreateFcn(hObject, ~, ~)
if ispc && isequal(get(hObject,'BackgroundColor'),
get(0,'defaultUicontrolBackgroundColor'))
    set(hObject,'BackgroundColor','white');
end

% --- Peak 2 Gaussian Width Text Box
function edit7_Callback(hObject, ~, handles)
input7 = str2double(get(hObject,'String'));
if (isempty(input7))
     set(hObject,'String','10')
end
guidata(hObject, handles);
function edit7_CreateFcn(hObject, ~, ~)
```

```
if ispc && isequal(get(hObject,'BackgroundColor'),
get(0,'defaultUicontrolBackgroundColor'))
    set(hObject,'BackgroundColor','white');
end

% --- Peak 1 Population Text Box
function edit8_Callback(hObject, ~, handles)
input8 = str2double(get(hObject,'String'));
if (isempty(input8))
     set(hObject,'String','1')
end
guidata(hObject, handles);
function edit8_CreateFcn(hObject, ~, ~)
if ispc && isequal(get(hObject,'BackgroundColor'),
get(0,'defaultUicontrolBackgroundColor'))
    set(hObject,'BackgroundColor','white');
end

% --- Peak 2 Population Text Box
function edit9_Callback(hObject, ~, handles)
input9 = str2double(get(hObject,'String'));
if (isempty(input9))
     set(hObject,'String','1')
end
guidata(hObject, handles);
function edit9_CreateFcn(hObject, ~, ~)
if ispc && isequal(get(hObject,'BackgroundColor'),
get(0,'defaultUicontrolBackgroundColor'))
    set(hObject,'BackgroundColor','white');
end

% --- Barrier Height Text Box
function edit13_Callback(hObject, ~, ~)
input13 = str2double(get(hObject,'String'));
if (isempty(input13))
     set(hObject,'String','2')
end
function edit13_CreateFcn(hObject, ~, ~)
if ispc && isequal(get(hObject,'BackgroundColor'),
get(0,'defaultUicontrolBackgroundColor'))
    set(hObject,'BackgroundColor','white');
end

% --- Temperature Text Box
function edit14_Callback(hObject, ~, ~)
input14 = str2double(get(hObject,'String'));
if (isempty(input14))
     set(hObject,'String','298')
end
function edit14_CreateFcn(hObject, ~, ~)
if ispc && isequal(get(hObject,'BackgroundColor'),
get(0,'defaultUicontrolBackgroundColor'))
    set(hObject,'BackgroundColor','white');
end
```

```
% ------------------------------------------------
% --- Input End Text Boxes ---
% ------------------------------------------------



% --- Simulates Spectrum --- Zoerbex ---
function pushbutton1_Callback(hObject, ~, handles)

% Extracts the values from the input text boxes
tau = str2double(get(handles.edit1,'String'));
w1 = str2double(get(handles.edit2,'String'));
w2 = str2double(get(handles.edit3,'String'));
L1 = str2double(get(handles.edit4,'String'));
L2 = str2double(get(handles.edit5,'String'));
G1 = str2double(get(handles.edit6,'String'));
G2 = str2double(get(handles.edit7,'String'));
p1 = str2double(get(handles.edit8,'String'));
p2 = str2double(get(handles.edit9,'String'));
BH = str2double(get(handles.edit13,'String'));
temp = str2double(get(handles.edit14,'String'));
t_or_e = handles.time_or_energy_buttongroup;

% Convert parameters from wavenumbers to Hertz
w1_Hz = w1*100*3*10^8 ;
w2_Hz = w2*100*3*10^8 ;
L1_Hz = L1*100*3*10^8*pi ; % pi is the empirical correction factor for
Lorentzian FWHM
L2_Hz = L2*100*3*10^8*pi ;
G1_Hz = G1*100*3*10^8*(8/3) ; % (8/3) is the empirical correction factor for
Gaussian FWHM
G2_Hz = G2*100*3*10^8*(8/3) ;

% Convert time constant to rate
if t_or_e == 0
    kex = 1/(tau*10^-12);
end
if t_or_e == 1
    kex = (1.3806503*10^-23)*temp/(6.626068*10^-34)*exp((-BH*6.94770014*10^-
21)/((1.3806503*10^-23)*temp));
end
% 1 kcal/mol = 6.94770014*10^-21 J



% Exchange matrix
K = kex*[-1 1; 1 -1];

% Center frequencies and Lorentzian linewidths
A = [ (-1i*2*pi*w1_Hz + L1_Hz - K(1,1)) -K(1,2) ;
     -K(2,1) (-1i*2*pi*w2_Hz + L2_Hz - K(2,2)) ];
[S,Lam] = eig(A,'nobalance') ;

% Gaussian linewidths
G = [G1_Hz^(2) 0 ; 0 G2_Hz^(2)];
```

```
Sinv = inv(S) ;
Gprime = S\G*S ;

% Generate correlation functions
% Preallocation
q = 10001;
Gcorr_11 = zeros(1,q);
Gcorr_22 = zeros(1,q);

for k = 1:q
    Fs = 10^14;
    %t = (1/Fs)*(k-1) ;
    Gcorr_11(k) = exp(-Lam(1,1)*((1/Fs)*(k-1)) - (Gprime(1,1)*((1/Fs)*(k-
1)).^2)./2 );
    Gcorr_22(k) = exp(-Lam(2,2)*((1/Fs)*(k-1)) - (Gprime(2,2)*((1/Fs)*(k-
1)).^2)./2 );
end

%--- Beginning of fft section
N = (q*100);
if mod(N,2)==0
    k=-N/2:N/2-1; % N even
else
    k=-(N-1)/2:(N-1)/2; % N odd
end
T=N/Fs;
freq=k/T;

Iw_1a=fftshift(fft(Gcorr_11,N)/Fs);

Iw_2a=fftshift(fft(Gcorr_22,N)/Fs);
%--- end of fft section

% Multiplicative terms for populations
one = [1 ; 1];
p = [p1*2*(w1+w2)/2/(1.05*10^-34);
     p2*2*(w1+w2)/2/(1.05*10^-34)] ;
pdagger = ctranspose(p) ;
pdS = pdagger*S ;
Sinvone = S\one;

% Defining each of the complete lineshape components and summing them for
% the total lineshape
Iw_11_1 = pdS(1,1)*Iw_1a*Sinvone(1,1) ;
Iw_22_1 = pdS(1,1)*Iw_2a*Sinvone(1,1) ;
Iw_11_2 = pdS(1,2)*Iw_1a*Sinvone(2,1) ;
Iw_22_2 = pdS(1,2)*Iw_2a*Sinvone(2,1) ;
Iw_11 = Iw_11_1 + Iw_11_2;
Iw_22 = Iw_22_1 + Iw_22_2;
scale = [p(1)*S(1,1)*Sinv(1,1) + p(1)*S(1,1)*Sinv(1,2) +
p(2)*S(2,1)*Sinv(1,1) + p(2)*S(2,1)*Sinv(1,2) ;
    p(1)*S(1,2)*Sinv(2,1) + p(1)*S(1,2)*Sinv(2,2) + p(2)*S(2,2)*Sinv(2,1) +
p(2)*S(2,2)*Sinv(2,2)];
Iw_1 = Iw_11*scale(1);
```

```
Iw_2 = Iw_22*scale(2);
Iw = real(Iw_1 + Iw_2);

% Correcting the fft shift to actual values
[~,zed_index]=min(abs(freq));
freq_Hz1 = freq(zed_index:length(freq));
freq_Hz2 = freq(1:zed_index-1);
freq_Hz2_rev = freq_Hz2(end:-1:1);
freq_Hz2_ind = abs(freq_Hz2_rev) + freq(length(freq));
freq_Hz = [freq_Hz1 freq_Hz2_ind];
Iw_hshift1 = Iw(zed_index:length(freq));
Iw_hshift2 = Iw(1:zed_index-1);
Iw_hshift = [Iw_hshift1 Iw_hshift2];
freq_wave = freq_Hz./(3*10^10);

% Setting the baseline to zero and normalizing the spectrum to 1
Iw_vshift = Iw_hshift - min(Iw_hshift);
Iw_norm = Iw_vshift ./ max(Iw_vshift);

% Defining the Baseline
xlim1=w1-65;
xlim2=w2+65;
xlim1a=w1-100;
xlim2a=w2+100;
xbase=xlim1a:xlim2a;
baseline=zeros(1,length(xbase));

% Plot Parameters
hold on;
order2 = plot(handles.axes1,freq_wave,Iw_norm,'color','k','LineWidth',1.5);
uistack(order2,'bottom');
plot(handles.axes1,xbase,baseline,'color','k','LineWidth',1.5)
xlim([xlim1 xlim2]);
ylim([-0.1 1.1]);
xlabel('wavenumber (cm^-^1)');
ylabel('Normalized Absorbance');
hold off;

handles.xlim1a = xlim1a;
handles.xlim2a = xlim2a;
handles.freq_wave = freq_wave;
handles.Iw_norm = Iw_norm;

guidata(hObject, handles);

% --- Defines Plot Window
function axes1_CreateFcn(hObject, ~, handles)
guidata(hObject, handles);



% ------------------------------------------------------
% --- Push Buttons ---
% ------------------------------------------------------
```

```
% --- Clear Button
function pushbutton2_Callback(hObject, ~, handles)

cla(handles.axes1);
xla=1500;
xlb=3500;
xbase_init=xla:xlb;
baseline_init=zeros(1,length(xbase_init));
plot(xbase_init,baseline_init,'color','k','LineWidth',1.5)
xlim([1800 2000]);
ylim([-0.1 1.1]);
xlabel('wavenumber (cm^-^1)');
ylabel('Normalized Absorbance');

guidata(hObject, handles);

% --- Load Data Button
function pushbutton4_Callback(hObject, ~, handles)

[filename,pathname] = uigetfile('*.*','All Files (*.*)');
file=[pathname filename];

% if user cancels save command, nothing happens
if isequal(filename,0) || isequal(pathname,0)
    return
end

fid = fopen(file);
if fid==-1
  error('File not found or permission denied');
end

no_lines = 0;
max_line = 0;

ncols = 0;

data = [];

line = fgetl(fid);
if ~isstr(line)
  disp('Warning: file contains no header and no data')
end;

[data, ncols, errmsg, nxtindex] = sscanf(line, '%f');

while isempty(data)||(nxtindex==1)
  no_lines = no_lines+1;
  max_line = max([max_line, length(line)]);
  eval(['line', num2str(no_lines), '=line;']);
  line = fgetl(fid);
  if ~isstr(line)
```

```
    disp('Warning: file contains no data')
    break
    end;
  [data, ncols, errmsg, nxtindex] = sscanf(line, '%f');
  end

data = [data; fscanf(fid, '%f')];
fclose(fid);

header = setstr(' '*ones(no_lines, max_line));

for i = 1:no_lines
  varname = ['line' num2str(i)];
    if eval(['length(' varname ')~=0'])
       eval(['header(i, 1:length(' varname ')) = ' varname ';']);
    end
end

eval('data = reshape(data, ncols, length(data)/ncols)'';', '');

xl1 = min(data(:,1));
xl2 = max(data(:,1));
basex = (xl1-100):(xl2+100);
basey = zeros(1,length(basex));
datax = data(:,1);
datay = data(:,2);
datay_norm = datay/max(datay);

handles.xl1 = xl1;
handles.xl2 = xl2;
handles.basex = basex;
handles.basey = basey;
handles.datax = datax;
handles.datay_norm = datay_norm;

guidata(hObject, handles);

% --- Plot Data Button
function pushbutton5_Callback(hObject, ~, handles)

xl1_test = isfield(handles,'xl1');
if xl1_test == 0
    xl1 = 1800;
else
    xl1 = handles.xl1;
end

xl2_test = isfield(handles,'xl2');
if xl2_test == 0
    xl2 = 2000;
else
    xl2 = handles.xl2;
end
```

```
basex_test = isfield(handles,'basex');
if basex_test == 0
    basex = 0;
else
    basex = handles.basex;
end

basey_test = isfield(handles,'basey');
if basey_test == 0
    basey = 0;
else
    basey = handles.basey;
end

datax_test = isfield(handles,'datax');
if datax_test == 0
    datax = 0;
else
    datax = handles.datax;
end

datay_norm_test = isfield(handles,'datay_norm');
if datay_norm_test == 0
    datay_norm = 0;
else
    datay_norm = handles.datay_norm;
end

hold on;
order1 = plot(handles.axes1,datax,datay_norm,'color','r','LineWidth',0.5);
uistack(order1,'top');
plot(handles.axes1,basex,basey,'color','k','LineWidth',1.5)
xlim([xl1 xl2]);
ylim([-0.1 1.1]);
xlabel('wavenumber (cm^-^1)');
ylabel('Normalized Absorbance');
hold off;

guidata(hObject, handles);

% --- Save Figure Button
function pushbutton6_Callback(hObject, ~, handles)

axesObject = gca;

[filename, pathname] = uiputfile({ '*.jpg','jpeg (*.jpg)';...
        '*.bmp','Bitmap (*.bmp)'; '*.eps', 'Encapsulated PostScript
(*.eps)';...
        '*.fig','Figure (*.fig)'}, 'Save spectrum as','default');

% if user cancels save command, nothing happens
if isequal(filename,0) || isequal(pathname,0)
    return
```

```
end
% create a new figure
newFig = figure;

% get the units and position of the axes object
axes_units = get(axesObject,'Units');
axes_pos = get(axesObject,'Position');

% copies axesObject onto new figure
axesObject2 = copyobj(axesObject,newFig);

% realign the axes object on the new figure
set(axesObject2,'Units',axes_units);
set(axesObject2,'Position',[15 5 axes_pos(3) axes_pos(4)]);

% if a legendObject was passed to this function . . .
if (exist('legendObject'))
    % get the units and position of the legend object
    legend_units = get(legendObject,'Units');
    legend_pos = get(legendObject,'Position');

    % copies the legend onto the the new figure
    legendObject2 = copyobj(legendObject,newFig);

    % realign the legend object on the new figure
    set(legendObject2,'Units',legend_units);
    set(legendObject2,'Position',[15-axes_pos(1)+legend_pos(1) 5-
axes_pos(2)+legend_pos(2) legend_pos(3) legend_pos(4)] );
end

% adjusts the new figure accordingly
set(newFig,'Units',axes_units);
set(newFig,'Position',[15 5 axes_pos(3)+30 axes_pos(4)+10]);

% saves the plot
saveas(newFig,fullfile(pathname, filename))

% closes the figure
close(newFig)
guidata(hObject, handles);

% --- Save Data Button
function pushbutton7_Callback(hObject, ~, handles)

xlim1a_test = isfield(handles,'xlim1a');
if xlim1a_test == 0
    xlim1a = 1800;
else
    xlim1a = handles.xlim1a;
end

xlim2a_test = isfield(handles,'xlim2a');
if xlim2a_test == 0
```

```
    xlim2a = 2000;
else
    xlim2a = handles.xlim2a;
end

freq_wave_test = isfield(handles,'freq_wave');
if freq_wave_test == 0
    freq_wave = 0;
else
    freq_wave = handles.freq_wave;
end

Iw_norm_test = isfield(handles,'Iw_norm');
if Iw_norm_test == 0
    Iw_norm = 0;
else
    Iw_norm = handles.Iw_norm;
end

[~,fw1_index]=min(abs(freq_wave-xlim1a));
[~,fw2_index]=min(abs(freq_wave-xlim2a));

freq_wave_short = freq_wave(fw1_index:fw2_index);
Iw_norm_short = Iw_norm(fw1_index:fw2_index);

data_file = [freq_wave_short' Iw_norm_short'];

[filename, pathname] = uiputfile({ '*.txt','text (*.txt)'},'Save data
as','default');

% if user cancels save command, nothing happens
if isequal(filename,0) || isequal(pathname,0)
    return
end

% saves the file
save(fullfile(pathname, filename), 'data_file', '-ascii');

guidata(hObject, handles);

% --- Exit Button
function pushbutton3_Callback(~, ~, ~)
close all;

% ------------------------------------------------------
% --- End Push Buttons ---
% ------------------------------------------------------



% --- Radio Buttons (needs to be at end of script)
function time_or_energy_buttongroup_SelectionChangeFcn(hObject, eventdata)
```

```
% retrieve GUI data, i.e. the handles structure
handles = guidata(hObject);

switch get(eventdata.NewValue,'Tag')   % Get Tag of selected object
    case 'Time_Constant_radiobutton'
      % execute this code when Time_Constant_radiobutton is selected
      handles.time_or_energy_buttongroup = 0;

    case 'Energy_radiobutton'
      % execute this code when Energy_radiobutton is selected
      handles.time_or_energy_buttongroup = 1;

end

% updates the handles structure
guidata(hObject, handles);


% --- Creates and returns a handle to the GUI figure.
function h1 = Zoerbex_v5_source_LayoutFcn(policy)
% policy - create a new figure or use a singleton. 'new' or 'reuse'.

persistent hsingleton;
if strcmpi(policy, 'reuse') & ishandle(hsingleton)
    h1 = hsingleton;
    return;
end
load Zoerbex_v5_source.mat


appdata = [];
appdata.GUIDEOptions = mat{1};
appdata.lastValidTag = 'figure1';
appdata.GUIDELayoutEditor = [];
appdata.initTags = struct(...
    'handle', [], ...
    'tag', 'figure1');

h1 = figure(...
'Units','characters',...
'Color',[0.729411764705882 0.831372549019608 0.956862745098039],...
'Colormap',[0 0 0.5625;0 0 0.625;0 0 0.6875;0 0 0.75;0 0 0.8125;0 0 0.875;0 0
0.9375;0 0 1;0 0.0625 1;0 0.125 1;0 0.1875 1;0 0.25 1;0 0.3125 1;0 0.375 1;0
0.4375 1;0 0.5 1;0 0.5625 1;0 0.625 1;0 0.6875 1;0 0.75 1;0 0.8125 1;0 0.875
1;0 0.9375 1;0 1 1;0.0625 1 1;0.125 1 0.9375;0.1875 1 0.875;0.25 1
0.8125;0.3125 1 0.75;0.375 1 0.6875;0.4375 1 0.625;0.5 1 0.5625;0.5625 1
0.5;0.625 1 0.4375;0.6875 1 0.375;0.75 1 0.3125;0.8125 1 0.25;0.875 1
0.1875;0.9375 1 0.125;1 1 0.0625;1 1 0;1 0.9375 0;1 0.875 0;1 0.8125 0;1 0.75
0;1 0.6875 0;1 0.625 0;1 0.5625 0;1 0.5 0;1 0.4375 0;1 0.375 0;1 0.3125 0;1
0.25 0;1 0.1875 0;1 0.125 0;1 0.0625 0;1 0 0;0.9375 0 0;0.875 0 0;0.8125 0
0;0.75 0 0;0.6875 0 0;0.625 0 0;0.5625 0 0],...
'IntegerHandle','off',...
'InvertHardcopy',get(0,'defaultfigureInvertHardcopy'),...
'MenuBar','none',...
```

```
'Name','Zoerbex_v5',...
'NumberTitle','off',...
'PaperPosition',get(0,'defaultfigurePaperPosition'),...
'Position',[103.8 20.4615384615385 167.6 41.0769230769231],...
'Resize','off',...
'HandleVisibility','callback',...
'Tag','figure1',...
'UserData',[],...
'Visible','on',...
'CreateFcn', {@local_CreateFcn, blanks(0), appdata} );

appdata = [];
appdata.lastValidTag = 'pushbutton1';

h2 = uicontrol(...
'Parent',h1,...
'Units','characters',...
'Callback',@(hObject,eventdata)Zoerbex_v5_source('pushbutton1_Callback',hObje
ct,eventdata,guidata(hObject)),...
'CData',[],...
'FontSize',10,...
'Position',[106.2 1.19230769230771 15 7],...
'String','Calculate',...
'Tag','pushbutton1',...
'UserData',[],...
'CreateFcn', {@local_CreateFcn, blanks(0), appdata} );

appdata = [];
appdata.lastValidTag = 'uitoolbar2';

h3 = uitoolbar(...
'Parent',h1,...
'Tag','uitoolbar2',...
'CreateFcn', {@local_CreateFcn, blanks(0), appdata} );

appdata = [];
appdata.toolid = 'Exploration.ZoomIn';
appdata.CallbackInUse = struct(...
    'ClickedCallback', '%default');
appdata.lastValidTag = 'uitoggletool1';

h4 = uitoggletool(...
'Parent',h3,...
'ClickedCallback','%default',...
'CData',mat{2},...
'TooltipString','Zoom In',...
'Tag','uitoggletool1',...
'CreateFcn', {@local_CreateFcn, blanks(0), appdata} );

appdata = [];
appdata.toolid = 'Exploration.ZoomOut';
appdata.CallbackInUse = struct(...
    'ClickedCallback', '%default');
appdata.lastValidTag = 'uitoggletool3';
```

```
h5 = uitoggletool(...
'Parent',h3,...
'ClickedCallback','%default',...
'CData',mat{3},...
'TooltipString','Zoom Out',...
'Tag','uitoggletool3',...
'CreateFcn', {@local_CreateFcn, blanks(0), appdata} );

appdata = [];
appdata.toolid = 'Exploration.Pan';
appdata.CallbackInUse = struct(...
    'ClickedCallback', '%default');
appdata.lastValidTag = 'uitoggletool4';

h6 = uitoggletool(...
'Parent',h3,...
'ClickedCallback','%default',...
'CData',mat{4},...
'TooltipString','Pan',...
'Tag','uitoggletool4',...
'CreateFcn', {@local_CreateFcn, blanks(0), appdata} );

appdata = [];
appdata.lastValidTag = 'pushbutton6';

h7 = uicontrol(...
'Parent',h1,...
'Units','characters',...
'Callback',@(hObject,eventdata)Zoerbex_v5_source('pushbutton6_Callback',hObje
ct,eventdata,guidata(hObject)),...
'CData',[],...
'FontSize',10,...
'Position',[122.2 6.15384615384617 20 2],...
'String','Save Figure',...
'Tag','pushbutton6',...
'UserData',[],...
'CreateFcn', {@local_CreateFcn, blanks(0), appdata} );

appdata = [];
appdata.lastValidTag = 'pushbutton4';

h8 = uicontrol(...
'Parent',h1,...
'Units','characters',...
'Callback',@(hObject,eventdata)Zoerbex_v5_source('pushbutton4_Callback',hObje
ct,eventdata,guidata(hObject)),...
'CData',[],...
'FontSize',10,...
'Position',[143.200000000001 6.15384615384617 20 2],...
'String','Load Data',...
'Tag','pushbutton4',...
'UserData',[],...
'CreateFcn', {@local_CreateFcn, blanks(0), appdata} );
```

```
appdata = [];
appdata.lastValidTag = 'pushbutton7';

h9 = uicontrol(...
'Parent',h1,...
'Units','characters',...
'Callback',@(hObject,eventdata)Zoerbex_v5_source('pushbutton7_Callback',hObje
ct,eventdata,guidata(hObject)),...
'CData',[],...
'FontSize',10,...
'Position',[122.2 3.6923076923077 20 2],...
'String','Save Data',...
'Tag','pushbutton7',...
'UserData',[],...
'CreateFcn', {@local_CreateFcn, blanks(0), appdata} );

appdata = [];
appdata.lastValidTag = 'pushbutton5';

h10 = uicontrol(...
'Parent',h1,...
'Units','characters',...
'Callback',@(hObject,eventdata)Zoerbex_v5_source('pushbutton5_Callback',hObje
ct,eventdata,guidata(hObject)),...
'CData',[],...
'FontSize',10,...
'Position',[143.200000000001 3.6923076923077 20 2],...
'String','Plot Data',...
'Tag','pushbutton5',...
'UserData',[],...
'CreateFcn', {@local_CreateFcn, blanks(0), appdata} );

appdata = [];
appdata.lastValidTag = 'pushbutton2';

h11 = uicontrol(...
'Parent',h1,...
'Units','characters',...
'Callback',@(hObject,eventdata)Zoerbex_v5_source('pushbutton2_Callback',hObje
ct,eventdata,guidata(hObject)),...
'CData',[],...
'FontSize',10,...
'Position',[122.2 1.19230769230771 20 2],...
'String','Clear',...
'Tag','pushbutton2',...
'UserData',[],...
'CreateFcn', {@local_CreateFcn, blanks(0), appdata} );

appdata = [];
appdata.lastValidTag = 'axes1';

h12 = axes(...
'Parent',h1,...
```

```
'Units','characters',...
'Position',[11.2 4.76923076923077 90 33],...
'CameraPosition',[1900 0.5 9.16025403784439],...
'CameraPositionMode',get(0,'defaultaxesCameraPositionMode'),...
'Color',get(0,'defaultaxesColor'),...
'ColorOrder',get(0,'defaultaxesColorOrder'),...
'LooseInset',[25.298 4.85692307692308 18.487 3.31153846153846],...
'XColor',get(0,'defaultaxesXColor'),...
'XLim',[1800 2000],...
'XLimMode','manual',...
'YColor',get(0,'defaultaxesYColor'),...
'YLim',[-0.1 1.1],...
'YLimMode','manual',...
'YTick',[0 0.2 0.4 0.6 0.8 1],...
'YTickMode','manual',...
'ZColor',get(0,'defaultaxesZColor'),...
'CreateFcn', {@local_CreateFcn,
@(hObject,eventdata)Zoerbex_v5_source('axes1_CreateFcn',hObject,eventdata,gui
data(hObject)), appdata} ,...
'Tag','axes1',...
'UserData',[]);

h13 = get(h12,'title');

set(h13,...
'Parent',h12,...
'Units','data',...
'FontUnits','points',...
'BackgroundColor','none',...
'Color',[0 0 0],...
'DisplayName',blanks(0),...
'EdgeColor','none',...
'EraseMode','normal',...
'DVIMode','auto',...
'FontAngle','normal',...
'FontName','Helvetica',...
'FontSize',10,...
'FontWeight','normal',...
'HorizontalAlignment','center',...
'LineStyle','-',...
'LineWidth',0.5,...
'Margin',2,...
'Position',[1899.77777777778 1.12097902097902 1.00005459937205],...
'Rotation',0,...
'String',blanks(0),...
'Interpreter','tex',...
'VerticalAlignment','bottom',...
'ButtonDownFcn',[],...
'CreateFcn', {@local_CreateFcn, [], ''} ,...
'DeleteFcn',[],...
'BusyAction','queue',...
'HandleVisibility','off',...
'HelpTopicKey',blanks(0),...
'HitTest','on',...
'Interruptible','on',...
```

```
'SelectionHighlight','on',...
'Serializable','on',...
'Tag',blanks(0),...
'UserData',[],...
'Visible','on',...
'XLimInclude','on',...
'YLimInclude','on',...
'ZLimInclude','on',...
'CLimInclude','on',...
'ALimInclude','on',...
'IncludeRenderer','on',...
'Clipping','off');

h14 = get(h12,'xlabel');

set(h14,...
'Parent',h12,...
'Units','data',...
'FontUnits','points',...
'BackgroundColor','none',...
'Color',[0 0 0],...
'DisplayName',blanks(0),...
'EdgeColor','none',...
'EraseMode','normal',...
'DVIMode','auto',...
'FontAngle','normal',...
'FontName','Helvetica',...
'FontSize',10,...
'FontWeight','normal',...
'HorizontalAlignment','center',...
'LineStyle','-',...
'LineWidth',0.5,...
'Margin',2,...
'Position',[1899.77777777778 -0.165734265734266 1.00005459937205],...
'Rotation',0,...
'String',blanks(0),...
'Interpreter','tex',...
'VerticalAlignment','cap',...
'ButtonDownFcn',[],...
'CreateFcn', {@local_CreateFcn, [], ''} ,...
'DeleteFcn',[],...
'BusyAction','queue',...
'HandleVisibility','off',...
'HelpTopicKey',blanks(0),...
'HitTest','on',...
'Interruptible','on',...
'SelectionHighlight','on',...
'Serializable','on',...
'Tag',blanks(0),...
'UserData',[],...
'Visible','on',...
'XLimInclude','on',...
'YLimInclude','on',...
'ZLimInclude','on',...
'CLimInclude','on',...
```

```
'ALimInclude','on',...
'IncludeRenderer','on',...
'Clipping','off');

h15 = get(h12,'ylabel');

set(h15,...
'Parent',h12,...
'Units','data',...
'FontUnits','points',...
'BackgroundColor','none',...
'Color',[0 0 0],...
'DisplayName',blanks(0),...
'EdgeColor','none',...
'EraseMode','normal',...
'DVIMode','auto',...
'FontAngle','normal',...
'FontName','Helvetica',...
'FontSize',10,...
'FontWeight','normal',...
'HorizontalAlignment','center',...
'LineStyle','-',...
'LineWidth',0.5,...
'Margin',2,...
'Position',[1787.33333333333 0.497202797202797 1.00005459937205],...
'Rotation',90,...
'String',blanks(0),...
'Interpreter','tex',...
'VerticalAlignment','bottom',...
'ButtonDownFcn',[],...
'CreateFcn', {@local_CreateFcn, [], ''} ,...
'DeleteFcn',[],...
'BusyAction','queue',...
'HandleVisibility','off',...
'HelpTopicKey',blanks(0),...
'HitTest','on',...
'Interruptible','on',...
'SelectionHighlight','on',...
'Serializable','on',...
'Tag',blanks(0),...
'UserData',[],...
'Visible','on',...
'XLimInclude','on',...
'YLimInclude','on',...
'ZLimInclude','on',...
'CLimInclude','on',...
'ALimInclude','on',...
'IncludeRenderer','on',...
'Clipping','off');

h16 = get(h12,'zlabel');

set(h16,...
'Parent',h12,...
'Units','data',...
```

```
'FontUnits','points',...
'BackgroundColor','none',...
'Color',[0 0 0],...
'DisplayName',blanks(0),...
'EdgeColor','none',...
'EraseMode','normal',...
'DVIMode','auto',...
'FontAngle','normal',...
'FontName','Helvetica',...
'FontSize',10,...
'FontWeight','normal',...
'HorizontalAlignment','right',...
'LineStyle','-',...
'LineWidth',0.5,...
'Margin',2,...
'Position',[1774.88888888889 1.21608391608392 1.00005459937205],...
'Rotation',0,...
'String',blanks(0),...
'Interpreter','tex',...
'VerticalAlignment','middle',...
'ButtonDownFcn',[],...
'CreateFcn', {@local_CreateFcn, [], ''} ,...
'DeleteFcn',[],...
'BusyAction','queue',...
'HandleVisibility','off',...
'HelpTopicKey',blanks(0),...
'HitTest','on',...
'Interruptible','on',...
'SelectionHighlight','on',...
'Serializable','on',...
'Tag',blanks(0),...
'UserData',[],...
'Visible','off',...
'XLimInclude','on',...
'YLimInclude','on',...
'ZLimInclude','on',...
'CLimInclude','on',...
'ALimInclude','on',...
'IncludeRenderer','on',...
'Clipping','off');

appdata = [];
appdata.lastValidTag = 'pushbutton3';

h17 = uicontrol(...
'Parent',h1,...
'Units','characters',...
'Callback',@(hObject,eventdata)Zoerbex_v5_source('pushbutton3_Callback',hObje
ct,eventdata,guidata(hObject)),...
'CData',[],...
'FontSize',10,...
'Position',[143.200000000001 1.19230769230771 20 2],...
'String','Exit',...
'Tag','pushbutton3',...
'UserData',[],...
```

```
'CreateFcn', {@local_CreateFcn, blanks(0), appdata} );

appdata = [];
appdata.lastValidTag = 'text11';

h18 = uicontrol(...
'Parent',h1,...
'Units','characters',...
'BackgroundColor',[0.729411764705882 0.831372549019608 0.956862745098039],...
'CData',[],...
'FontName','MS Serif',...
'FontSize',17,...
'Position',[18.6 38.0769230769231 75 2.69230769230769],...
'String','Zoerbex Infrared Spectrum Simulation',...
'Style','text',...
'Tag','text11',...
'UserData',[],...
'CreateFcn', {@local_CreateFcn, blanks(0), appdata} );

appdata = [];
appdata.lastValidTag = 'time_or_energy_buttongroup';

h19 = uibuttongroup(...
'Parent',h1,...
'Units','characters',...
'Title','Peak Parameters:',...
'Tag','time_or_energy_buttongroup',...
'UserData',[],...
'Clipping','on',...
'BackgroundColor',[0.729411764705882 0.831372549019608 0.956862745098039],...
'Position',[106.2 8.84615384615385 57.2 29.4615384615385],...
'SelectedObject',[],...
'SelectionChangeFcn',[],...
'OldSelectedObject',[],...
'CreateFcn', {@local_CreateFcn, blanks(0), appdata} );

appdata = [];
appdata.lastValidTag = 'Time_Constant_radiobutton';

h20 = uicontrol(...
'Parent',h19,...
'Units','characters',...
'BackgroundColor',[0.729411764705882 0.831372549019608 0.956862745098039],...
'Callback',mat{5},...
'CData',[],...
'Position',[2 26 17.4 1.92307692307692],...
'String','Time Constant',...
'Style','radiobutton',...
'Value',1,...
'Tag','Time_Constant_radiobutton',...
'UserData',[],...
'CreateFcn', {@local_CreateFcn, blanks(0), appdata} );

appdata = [];
```

```
appdata.lastValidTag = 'Energy_radiobutton';

h21 = uicontrol(...
'Parent',h19,...
'Units','characters',...
'BackgroundColor',[0.729411764705882 0.831372549019608 0.956862745098039],...
'Callback',mat{6},...
'Position',[2 21 17.8 1.92307692307692],...
'String','Energy',...
'Style','radiobutton',...
'Tag','Energy_radiobutton',...
'CreateFcn', {@local_CreateFcn, blanks(0), appdata} );

appdata = [];
appdata.lastValidTag = 'edit1';

h22 = uicontrol(...
'Parent',h19,...
'Units','characters',...
'BackgroundColor',[1 1 1],...
'Callback',@(hObject,eventdata)Zoerbex_v5_source('edit1_Callback',hObject,eve
ntdata,guidata(hObject)),...
'Position',[4 23.5 10 2],...
'String','10000',...
'Style','edit',...
'CreateFcn', {@local_CreateFcn,
@(hObject,eventdata)Zoerbex_v5_source('edit1_CreateFcn',hObject,eventdata,gui
data(hObject)), appdata} ,...
'Tag','edit1');

appdata = [];
appdata.lastValidTag = 'text1';

h23 = uicontrol(...
'Parent',h19,...
'Units','characters',...
'BackgroundColor',[0.729411764705882 0.831372549019608 0.956862745098039],...
'CData',[],...
'Position',[15 23.3 29 1.76923076923077],...
'String','Exchange Time Constant (ps)',...
'Style','text',...
'Tag','text1',...
'UserData',[],...
'CreateFcn', {@local_CreateFcn, blanks(0), appdata} );

appdata = [];
appdata.lastValidTag = 'edit13';

h24 = uicontrol(...
'Parent',h19,...
'Units','characters',...
'BackgroundColor',[1 1 1],...
'Callback',@(hObject,eventdata)Zoerbex_v5_source('edit13_Callback',hObject,ev
entdata,guidata(hObject)),...
```

```
'Position',[3.8 18.5 10 2],...
'String','5',...
'Style','edit',...
'CreateFcn', {@local_CreateFcn,
@(hObject,eventdata)Zoerbex_v5_source('edit13_CreateFcn',hObject,eventdata,gu
idata(hObject)), appdata} ,...
'Tag','edit13');

appdata = [];
appdata.lastValidTag = 'edit14';

h25 = uicontrol(...
'Parent',h19,...
'Units','characters',...
'BackgroundColor',[1 1 1],...
'Callback',@(hObject,eventdata)Zoerbex_v5_source('edit14_Callback',hObject,ev
entdata,guidata(hObject)),...
'Position',[3.8 15.5 10 2],...
'String','298',...
'Style','edit',...
'CreateFcn', {@local_CreateFcn,
@(hObject,eventdata)Zoerbex_v5_source('edit14_CreateFcn',hObject,eventdata,gu
idata(hObject)), appdata} ,...
'Tag','edit14');

appdata = [];
appdata.lastValidTag = 'text15';

h26 = uicontrol(...
'Parent',h19,...
'Units','characters',...
'BackgroundColor',[0.729411764705882 0.831372549019608 0.956862745098039],...
'CData',[],...
'Position',[15 18.3 23 1.76923076923077],...
'String','Barrier Height (kcal/mol)',...
'Style','text',...
'Tag','text15',...
'UserData',[],...
'CreateFcn', {@local_CreateFcn, blanks(0), appdata} );

appdata = [];
appdata.lastValidTag = 'text16';

h27 = uicontrol(...
'Parent',h19,...
'Units','characters',...
'BackgroundColor',[0.729411764705882 0.831372549019608 0.956862745098039],...
'CData',[],...
'Position',[15 15.3 16 1.76923076923077],...
'String','Temperature (K)',...
'Style','text',...
'Tag','text16',...
'UserData',[],...
'CreateFcn', {@local_CreateFcn, blanks(0), appdata} );
```

```
appdata = [];
appdata.lastValidTag = 'edit2';

h28 = uicontrol(...
'Parent',h19,...
'Units','characters',...
'BackgroundColor',[1 1 1],...
'Callback',@(hObject,eventdata)Zoerbex_v5_source('edit2_Callback',hObject,eve
ntdata,guidata(hObject)),...
'CData',[],...
'Position',[3.8 9.84615384615385 10 2],...
'String','1900',...
'Style','edit',...
'CreateFcn', {@local_CreateFcn,
@(hObject,eventdata)Zoerbex_v5_source('edit2_CreateFcn',hObject,eventdata,gui
data(hObject)), appdata} ,...
'Tag','edit2',...
'UserData',[]);

appdata = [];
appdata.lastValidTag = 'edit3';

h29 = uicontrol(...
'Parent',h19,...
'Units','characters',...
'BackgroundColor',[1 1 1],...
'Callback',@(hObject,eventdata)Zoerbex_v5_source('edit3_Callback',hObject,eve
ntdata,guidata(hObject)),...
'Position',[19.8 9.84615384615385 10 2],...
'String','1950',...
'Style','edit',...
'CreateFcn', {@local_CreateFcn,
@(hObject,eventdata)Zoerbex_v5_source('edit3_CreateFcn',hObject,eventdata,gui
data(hObject)), appdata} ,...
'Tag','edit3');

appdata = [];
appdata.lastValidTag = 'edit4';

h30 = uicontrol(...
'Parent',h19,...
'Units','characters',...
'BackgroundColor',[1 1 1],...
'Callback',@(hObject,eventdata)Zoerbex_v5_source('edit4_Callback',hObject,eve
ntdata,guidata(hObject)),...
'Position',[3.8 6.84615384615385 10 2],...
'String','10',...
'Style','edit',...
'CreateFcn', {@local_CreateFcn,
@(hObject,eventdata)Zoerbex_v5_source('edit4_CreateFcn',hObject,eventdata,gui
data(hObject)), appdata} ,...
'Tag','edit4');
```

```
appdata = [];
appdata.lastValidTag = 'edit5';

h31 = uicontrol(...
'Parent',h19,...
'Units','characters',...
'BackgroundColor',[1 1 1],...
'Callback',@(hObject,eventdata)Zoerbex_v5_source('edit5_Callback',hObject,eve
ntdata,guidata(hObject)),...
'Position',[19.8 6.84615384615385 10 2],...
'String','10',...
'Style','edit',...
'CreateFcn', {@local_CreateFcn,
@(hObject,eventdata)Zoerbex_v5_source('edit5_CreateFcn',hObject,eventdata,gui
data(hObject)), appdata} ,...
'Tag','edit5');

appdata = [];
appdata.lastValidTag = 'edit6';

h32 = uicontrol(...
'Parent',h19,...
'Units','characters',...
'BackgroundColor',[1 1 1],...
'Callback',@(hObject,eventdata)Zoerbex_v5_source('edit6_Callback',hObject,eve
ntdata,guidata(hObject)),...
'Position',[3.8 3.84615384615385 10 2],...
'String','10',...
'Style','edit',...
'CreateFcn', {@local_CreateFcn,
@(hObject,eventdata)Zoerbex_v5_source('edit6_CreateFcn',hObject,eventdata,gui
data(hObject)), appdata} ,...
'Tag','edit6');

appdata = [];
appdata.lastValidTag = 'edit7';

h33 = uicontrol(...
'Parent',h19,...
'Units','characters',...
'BackgroundColor',[1 1 1],...
'Callback',@(hObject,eventdata)Zoerbex_v5_source('edit7_Callback',hObject,eve
ntdata,guidata(hObject)),...
'Position',[19.8 3.84615384615385 10 2],...
'String','10',...
'Style','edit',...
'CreateFcn', {@local_CreateFcn,
@(hObject,eventdata)Zoerbex_v5_source('edit7_CreateFcn',hObject,eventdata,gui
data(hObject)), appdata} ,...
'Tag','edit7');

appdata = [];
appdata.lastValidTag = 'edit8';
```

```
h34 = uicontrol(...
'Parent',h19,...
'Units','characters',...
'BackgroundColor',[1 1 1],...
'Callback',@(hObject,eventdata)Zoerbex_v5_source('edit8_Callback',hObject,eve
ntdata,guidata(hObject)),...
'Position',[3.8 0.846153846153846 10 2],...
'String','1',...
'Style','edit',...
'CreateFcn', {@local_CreateFcn,
@(hObject,eventdata)Zoerbex_v5_source('edit8_CreateFcn',hObject,eventdata,gui
data(hObject)), appdata} ,...
'Tag','edit8');

appdata = [];
appdata.lastValidTag = 'edit9';

h35 = uicontrol(...
'Parent',h19,...
'Units','characters',...
'BackgroundColor',[1 1 1],...
'Callback',@(hObject,eventdata)Zoerbex_v5_source('edit9_Callback',hObject,eve
ntdata,guidata(hObject)),...
'Position',[19.8 0.846153846153846 10 2],...
'String','1',...
'Style','edit',...
'CreateFcn', {@local_CreateFcn,
@(hObject,eventdata)Zoerbex_v5_source('edit9_CreateFcn',hObject,eventdata,gui
data(hObject)), appdata} ,...
'Tag','edit9');

appdata = [];
appdata.lastValidTag = 'text2';

h36 = uicontrol(...
'Parent',h19,...
'Units','characters',...
'BackgroundColor',[0.729411764705882 0.831372549019608 0.956862745098039],...
'CData',[],...
'Position',[3.8 11.9230769230769 10 1.76923076923077],...
'String','Peak 1',...
'Style','text',...
'Tag','text2',...
'UserData',[],...
'CreateFcn', {@local_CreateFcn, blanks(0), appdata} );

appdata = [];
appdata.lastValidTag = 'text3';

h37 = uicontrol(...
'Parent',h19,...
'Units','characters',...
'BackgroundColor',[0.729411764705882 0.831372549019608 0.956862745098039],...
'CData',[],...
```

```
'Position',[19.8 11.9230769230769 10 1.76923076923077],...
'String','Peak 2',...
'Style','text',...
'Tag','text3',...
'UserData',[],...
'CreateFcn', {@local_CreateFcn, blanks(0), appdata} );

appdata = [];
appdata.lastValidTag = 'text4';

h38 = uicontrol(...
'Parent',h19,...
'Units','characters',...
'BackgroundColor',[0.729411764705882 0.831372549019608 0.956862745098039],...
'CData',[],...
'Position',[31.9 9.61538461538462 18 1.76923076923077],...
'String','Center Frequency',...
'Style','text',...
'Tag','text4',...
'UserData',[],...
'CreateFcn', {@local_CreateFcn, blanks(0), appdata} );

appdata = [];
appdata.lastValidTag = 'text5';

h39 = uicontrol(...
'Parent',h19,...
'Units','characters',...
'BackgroundColor',[0.729411764705882 0.831372549019608 0.956862745098039],...
'CData',[],...
'Position',[31.9 6.61538461538462 18 1.76923076923077],...
'String','Lorentzian Width',...
'Style','text',...
'Tag','text5',...
'UserData',[],...
'CreateFcn', {@local_CreateFcn, blanks(0), appdata} );

appdata = [];
appdata.lastValidTag = 'text6';

h40 = uicontrol(...
'Parent',h19,...
'Units','characters',...
'BackgroundColor',[0.729411764705882 0.831372549019608 0.956862745098039],...
'CData',[],...
'Position',[31.9 3.61538461538462 18 1.76923076923077],...
'String','Gaussian Width',...
'Style','text',...
'Tag','text6',...
'UserData',[],...
'CreateFcn', {@local_CreateFcn, blanks(0), appdata} );

appdata = [];
appdata.lastValidTag = 'text7';
```

```
h41 = uicontrol(...
'Parent',h19,...
'Units','characters',...
'BackgroundColor',[0.729411764705882 0.831372549019608 0.956862745098039],...
'CData',[],...
'Position',[31.9 0.615384615384615 18 1.76923076923077],...
'String','Population',...
'Style','text',...
'Tag','text7',...
'UserData',[],...
'CreateFcn', {@local_CreateFcn, blanks(0), appdata} );


hsingleton = h1;


% --- Set application data first then calling the CreateFcn.
function local_CreateFcn(hObject, eventdata, createfcn, appdata)

if ~isempty(appdata)
   names = fieldnames(appdata);
   for i=1:length(names)
       name = char(names(i));
       setappdata(hObject, name, getfield(appdata,name));
   end
end

if ~isempty(createfcn)
   if isa(createfcn,'function_handle')
       createfcn(hObject, eventdata);
   else
       eval(createfcn);
   end
end


% --- Handles default GUIDE GUI creation and callback dispatch
function varargout = gui_mainfcn(gui_State, varargin)

gui_StateFields =  {'gui_Name'
    'gui_Singleton'
    'gui_OpeningFcn'
    'gui_OutputFcn'
    'gui_LayoutFcn'
    'gui_Callback'};
gui_Mfile = '';
for i=1:length(gui_StateFields)
    if ~isfield(gui_State, gui_StateFields{i})
        error('MATLAB:gui_mainfcn:FieldNotFound', 'Could not find field %s in
the gui_State struct in GUI M-file %s', gui_StateFields{i}, gui_Mfile);
    elseif isequal(gui_StateFields{i}, 'gui_Name')
        gui_Mfile = [gui_State.(gui_StateFields{i}), '.m'];
    end
```

```
end

numargin = length(varargin);

if numargin == 0
    % ZOERBEX_V5_SOURCE
    % create the GUI only if we are not in the process of loading it
    % already
    gui_Create = true;
elseif local_isInvokeActiveXCallback(gui_State, varargin{:})
    % ZOERBEX_V5_SOURCE(ACTIVEX,...)
    vin{1} = gui_State.gui_Name;
    vin{2} = [get(varargin{1}.Peer, 'Tag'), '_', varargin{end}];
    vin{3} = varargin{1};
    vin{4} = varargin{end-1};
    vin{5} = guidata(varargin{1}.Peer);
    feval(vin{:});
    return;
elseif local_isInvokeHGCallback(gui_State, varargin{:})
    % ZOERBEX_V5_SOURCE('CALLBACK',hObject,eventData,handles,...)
    gui_Create = false;
else
    % ZOERBEX_V5_SOURCE(...)
    % create the GUI and hand varargin to the openingfcn
    gui_Create = true;
end

if ~gui_Create
    % In design time, we need to mark all components possibly created in
    % the coming callback evaluation as non-serializable. This way, they
    % will not be brought into GUIDE and not be saved in the figure file
    % when running/saving the GUI from GUIDE.
    designEval = false;
    if (numargin>1 && ishghandle(varargin{2}))
        fig = varargin{2};
        while ~isempty(fig) && ~isa(handle(fig),'figure')
            fig = get(fig,'parent');
        end

        designEval = isappdata(0,'CreatingGUIDEFigure') ||
isprop(fig,'__GUIDEFigure');
    end

    if designEval
        beforeChildren = findall(fig);
    end

    % evaluate the callback now
    varargin{1} = gui_State.gui_Callback;
    if nargout
        [varargout{1:nargout}] = feval(varargin{:});
    else
        feval(varargin{:});
    end
```

```
    % Set serializable of objects created in the above callback to off in
    % design time. Need to check whether figure handle is still valid in
    % case the figure is deleted during the callback dispatching.
    if designEval && ishandle(fig)
        set(setdiff(findall(fig),beforeChildren), 'Serializable','off');
    end
else
    if gui_State.gui_Singleton
        gui_SingletonOpt = 'reuse';
    else
        gui_SingletonOpt = 'new';
    end

    % Check user passing 'visible' P/V pair first so that its value can be
    % used by oepnfig to prevent flickering
    gui_Visible = 'auto';
    gui_VisibleInput = '';
    for index=1:2:length(varargin)
        if length(varargin) == index || ~ischar(varargin{index})
            break;
        end

        % Recognize 'visible' P/V pair
        len1 = min(length('visible'),length(varargin{index}));
        len2 = min(length('off'),length(varargin{index+1}));
        if ischar(varargin{index+1}) &&
strncmpi(varargin{index},'visible',len1) && len2 > 1
            if strncmpi(varargin{index+1},'off',len2)
                gui_Visible = 'invisible';
                gui_VisibleInput = 'off';
            elseif strncmpi(varargin{index+1},'on',len2)
                gui_Visible = 'visible';
                gui_VisibleInput = 'on';
            end
        end
    end

    % Open fig file with stored settings.  Note: This executes all component
    % specific CreateFunctions with an empty HANDLES structure.


    % Do feval on layout code in m-file if it exists
    gui_Exported = ~isempty(gui_State.gui_LayoutFcn);
    % this application data is used to indicate the running mode of a GUIDE
    % GUI to distinguish it from the design mode of the GUI in GUIDE. it is
    % only used by actxproxy at this time.
    setappdata(0,genvarname(['OpenGuiWhenRunning_', gui_State.gui_Name]),1);
    if gui_Exported
        gui_hFigure = feval(gui_State.gui_LayoutFcn, gui_SingletonOpt);

        % make figure invisible here so that the visibility of figure is
        % consistent in OpeningFcn in the exported GUI case
        if isempty(gui_VisibleInput)
```

```
            gui_VisibleInput = get(gui_hFigure,'Visible');
        end
        set(gui_hFigure,'Visible','off')

        % openfig (called by local_openfig below) does this for guis without
        % the LayoutFcn. Be sure to do it here so guis show up on screen.
        movegui(gui_hFigure,'onscreen');
    else
        gui_hFigure = local_openfig(gui_State.gui_Name, gui_SingletonOpt,
gui_Visible);
        % If the figure has InGUIInitialization it was not completely created
        % on the last pass.  Delete this handle and try again.
        if isappdata(gui_hFigure, 'InGUIInitialization')
            delete(gui_hFigure);
            gui_hFigure = local_openfig(gui_State.gui_Name, gui_SingletonOpt,
gui_Visible);
        end
    end
    if isappdata(0, genvarname(['OpenGuiWhenRunning_', gui_State.gui_Name]))
        rmappdata(0,genvarname(['OpenGuiWhenRunning_', gui_State.gui_Name]));
    end

    % Set flag to indicate starting GUI initialization
    setappdata(gui_hFigure,'InGUIInitialization',1);

    % Fetch GUIDE Application options
    gui_Options = getappdata(gui_hFigure,'GUIDEOptions');
    % Singleton setting in the GUI M-file takes priority if different
    gui_Options.singleton = gui_State.gui_Singleton;

    if ~isappdata(gui_hFigure,'GUIOnScreen')
        % Adjust background color
        if gui_Options.syscolorfig
            set(gui_hFigure,'Color',
get(0,'DefaultUicontrolBackgroundColor'));
        end

        % Generate HANDLES structure and store with GUIDATA. If there is
        % user set GUI data already, keep that also.
        data = guidata(gui_hFigure);
        handles = guihandles(gui_hFigure);
        if ~isempty(handles)
            if isempty(data)
                data = handles;
            else
                names = fieldnames(handles);
                for k=1:length(names)
                    data.(char(names(k)))=handles.(char(names(k)));
                end
            end
        end
        guidata(gui_hFigure, data);
    end
```

```
    % Apply input P/V pairs other than 'visible'
    for index=1:2:length(varargin)
        if length(varargin) == index || ~ischar(varargin{index})
            break;
        end

        len1 = min(length('visible'),length(varargin{index}));
        if ~strncmpi(varargin{index},'visible',len1)
            try set(gui_hFigure, varargin{index}, varargin{index+1}), catch
break, end
        end
    end

    % If handle visibility is set to 'callback', turn it on until finished
    % with OpeningFcn
    gui_HandleVisibility = get(gui_hFigure,'HandleVisibility');
    if strcmp(gui_HandleVisibility, 'callback')
        set(gui_hFigure,'HandleVisibility', 'on');
    end

    feval(gui_State.gui_OpeningFcn, gui_hFigure, [], guidata(gui_hFigure),
varargin{:});

    if isscalar(gui_hFigure) && ishandle(gui_hFigure)
        % Handle the default callbacks of predefined toolbar tools in this
        % GUI, if any
        guidemfile('restoreToolbarToolPredefinedCallback',gui_hFigure);

        % Update handle visibility
        set(gui_hFigure,'HandleVisibility', gui_HandleVisibility);

        % Call openfig again to pick up the saved visibility or apply the
        % one passed in from the P/V pairs
        if ~gui_Exported
            gui_hFigure = local_openfig(gui_State.gui_Name,
'reuse',gui_Visible);
        elseif ~isempty(gui_VisibleInput)
            set(gui_hFigure,'Visible',gui_VisibleInput);
        end
        if strcmpi(get(gui_hFigure, 'Visible'), 'on')
            figure(gui_hFigure);

            if gui_Options.singleton
                setappdata(gui_hFigure,'GUIOnScreen', 1);
            end
        end

        % Done with GUI initialization
        if isappdata(gui_hFigure,'InGUIInitialization')
            rmappdata(gui_hFigure,'InGUIInitialization');
        end

        % If handle visibility is set to 'callback', turn it on until
        % finished with OutputFcn
```

```
        gui_HandleVisibility = get(gui_hFigure,'HandleVisibility');
        if strcmp(gui_HandleVisibility, 'callback')
            set(gui_hFigure,'HandleVisibility', 'on');
        end
        gui_Handles = guidata(gui_hFigure);
    else
        gui_Handles = [];
    end

    if nargout
        [varargout{1:nargout}] = feval(gui_State.gui_OutputFcn, gui_hFigure,
[], gui_Handles);
    else
        feval(gui_State.gui_OutputFcn, gui_hFigure, [], gui_Handles);
    end

    if isscalar(gui_hFigure) && ishandle(gui_hFigure)
        set(gui_hFigure,'HandleVisibility', gui_HandleVisibility);
    end
end

function gui_hFigure = local_openfig(name, singleton, visible)

% openfig with three arguments was new from R13. Try to call that first, if
% failed, try the old openfig.
if nargin('openfig') == 2
    % OPENFIG did not accept 3rd input argument until R13,
    % toggle default figure visible to prevent the figure
    % from showing up too soon.
    gui_OldDefaultVisible = get(0,'defaultFigureVisible');
    set(0,'defaultFigureVisible','off');
    gui_hFigure = openfig(name, singleton);
    set(0,'defaultFigureVisible',gui_OldDefaultVisible);
else
    gui_hFigure = openfig(name, singleton, visible);
end

function result = local_isInvokeActiveXCallback(gui_State, varargin)

try
    result = ispc && iscom(varargin{1}) ...
             && isequal(varargin{1},gcbo);
catch
    result = false;
end

function result = local_isInvokeHGCallback(gui_State, varargin)

try
    fhandle = functions(gui_State.gui_Callback);
    result = ~isempty(findstr(gui_State.gui_Name,fhandle.file)) || ...
             (ischar(varargin{1}) ...
             && isequal(ishandle(varargin{2}), 1) ...
```

```
            && (~isempty(strfind(varargin{1},[get(varargin{2}, 'Tag'),
'_'])) || ...
                ~isempty(strfind(varargin{1}, '_CreateFcn'))) );
catch
    result = false;
end
```

Zoerbex Version 5 for Command Line:

```
%Command Line Version of Zoerbex_v5
%
%Zoerbex was written by M.C. Zoerb in Spring 2011 at the UC Berkeley
%College of Chemistry in the research group of C.B. Harris.
%
%This program is based on the math from Grevels et al. J. Am. Chem. Soc.
%(1998), 120, 10423-10433.
%This program takes inputs of peak parameters and exchange time
%constant and simulates the vibrational lineshape due to exchange between
%two sites.
%
%Some code for the fft section was adapted from examples
%on www.blinkdagger.com
%

clear;

% ----------------------------------------------------
% --- Input Section ---
% ----------------------------------------------------

disp('Peak inputs are center frequency, Lorentzian width,');
disp('Gaussian width, and Intensity factor.');

% --- time constant ---
tau = input('What is the exchange time constant in ps?  ');
if isempty(tau)
    tau = 10000 ;
end

% --- peak 1 inputs ---
w1 = input('What is the center frequency of peak 1?  ');
if isempty(w1)
    w1 = 1900 ;
end
L1 = input('What is Lorentzian width peak 1?  ');
if isempty(L1)
    L1 = 10 ;
end
G1 = input('What is Gaussian width peak 1?  ');
if isempty(G1)
    G1 = 10 ;
end
p1 = input('What is the population for peak 1?  ');
if isempty(p1)
    p1 = 1 ;
end

% --- peak 2 inputs ---
w2 = input('What is the center frequency of peak 2?  ');
```

```
if isempty(w2)
    w2 = 1950 ;
end
L2 = input('What is Lorentzian width peak 2?  ');
if isempty(L2)
    L2 = 10 ;
end
G2 = input('What is Gaussian width peak 2?  ');
if isempty(G2)
    G2 = 10 ;
end
p2 = input('What is the population for peak 2?  ');
if isempty(p2)
    p2 = 1 ;
end

% ------------------------------------------------------
% --- End Input Section ---
% ------------------------------------------------------


% Convert parameters from wavenumbers to Hertz
w1_Hz = w1*100*3*10^8 ;
w2_Hz = w2*100*3*10^8 ;
L1_Hz = L1*100*3*10^8*pi ; % pi is the empirical correction factor for
Lorentzian FWHM
L2_Hz = L2*100*3*10^8*pi ;
G1_Hz = G1*100*3*10^8*(8/3) ; % (8/3) is the empirical correction factor for
Gaussian FWHM
G2_Hz = G2*100*3*10^8*(8/3) ;

% Convert time constant to rate
kex = 1/(tau*10^-12);


% Exchange matrix
K = kex*[-1 1; 1 -1];

% Center frequencies and Lorentzian linewidths
A = [ (-1i*2*pi*w1_Hz + L1_Hz - K(1,1)) -K(1,2) ;
     -K(2,1) (-1i*2*pi*w2_Hz + L2_Hz - K(2,2)) ];
[S,Lam] = eig(A,'nobalance') ;

% Gaussian linewidths
G = [G1_Hz^(2) 0 ; 0 G2_Hz^(2)];
Sinv = inv(S) ;
Gprime = S\G*S ;

% Generate correlation functions
% Preallocation
q = 10001;
Gcorr_11 = zeros(1,q);
Gcorr_22 = zeros(1,q);
```

```
for k = 1:q
    Fs = 10^14;
    %t = (1/Fs)*(k-1) ;
    Gcorr_11(k) = exp(-Lam(1,1)*((1/Fs)*(k-1)) - (Gprime(1,1)*((1/Fs)*(k-
1)).^2)./2 );
    Gcorr_22(k) = exp(-Lam(2,2)*((1/Fs)*(k-1)) - (Gprime(2,2)*((1/Fs)*(k-
1)).^2)./2 );
end

%--- Beginning of fft section
N = (q*100);
if mod(N,2)==0
    k=-N/2:N/2-1; % N even
else
    k=-(N-1)/2:(N-1)/2; % N odd
end
T=N/Fs;
freq=k/T;

Iw_1a=fftshift(fft(Gcorr_11,N)/Fs);

Iw_2a=fftshift(fft(Gcorr_22,N)/Fs);
%--- end of fft section

% Multiplicative terms for populations
one = [1 ; 1];
p = [p1*2*(w1+w2)/2/(1.05*10^-34);
     p2*2*(w1+w2)/2/(1.05*10^-34)] ;
pdagger = ctranspose(p) ;
pdS = pdagger*S ;
Sinvone = S\one;

% Defining each of the complete lineshape components and summing them for
% the total lineshape
Iw_11_1 = pdS(1,1)*Iw_1a*Sinvone(1,1) ;
Iw_22_1 = pdS(1,1)*Iw_2a*Sinvone(1,1) ;
Iw_11_2 = pdS(1,2)*Iw_1a*Sinvone(2,1) ;
Iw_22_2 = pdS(1,2)*Iw_2a*Sinvone(2,1) ;
Iw_11 = Iw_11_1 + Iw_11_2;
Iw_22 = Iw_22_1 + Iw_22_2;
scale = [p(1)*S(1,1)*Sinv(1,1) + p(1)*S(1,1)*Sinv(1,2) +
p(2)*S(2,1)*Sinv(1,1) + p(2)*S(2,1)*Sinv(1,2) ;
    p(1)*S(1,2)*Sinv(2,1) + p(1)*S(1,2)*Sinv(2,2) + p(2)*S(2,2)*Sinv(2,1) +
p(2)*S(2,2)*Sinv(2,2)];
Iw_1 = Iw_11*scale(1);
Iw_2 = Iw_22*scale(2);
Iw = real(Iw_1 + Iw_2);

% Correcting the fft shift to actual values
[~,zed_index]=min(abs(freq));
freq_Hz1 = freq(zed_index:length(freq));
freq_Hz2 = freq(1:zed_index-1);
freq_Hz2_rev = freq_Hz2(end:-1:1);
freq_Hz2_ind = abs(freq_Hz2_rev) + freq(length(freq));
```

```
freq_Hz = [freq_Hz1 freq_Hz2_ind];
Iw_hshift1 = Iw(zed_index:length(freq));
Iw_hshift2 = Iw(1:zed_index-1);
Iw_hshift = [Iw_hshift1 Iw_hshift2];
freq_wave = freq_Hz./(3*10^10);

% Setting the baseline to zero and normalizing the spectrum to 1
Iw_vshift = Iw_hshift - min(Iw_hshift);
Iw_norm = Iw_vshift ./ max(Iw_vshift);

% Defining the Baseline
xlim1=w1-65;
xlim2=w2+65;
xlim1a=w1-100;
xlim2a=w2+100;
xbase=xlim1a:xlim2a;
baseline=zeros(1,length(xbase));

% Plot Parameters
hold on;
plot(freq_wave,Iw_norm,'color','k','LineWidth',1.5);
plot(xbase,baseline,'color','k','LineWidth',1.5)
xlim([xlim1 xlim2]);
ylim([-0.1 1.1]);
title('Zoerbex Infrared Spectrum Simulation');
xlabel('wavenumber (cm^-^1)');
ylabel('Normalized Absorbance');
hold off;
```